the 44th crystallographic course at
Ettore Majorana Centre, Erice, Italy
June 2 to 12, 2011

MAX PLANCK GESELLSCHAFT

Pushing the limits of Modern Powder Diffraction[1]

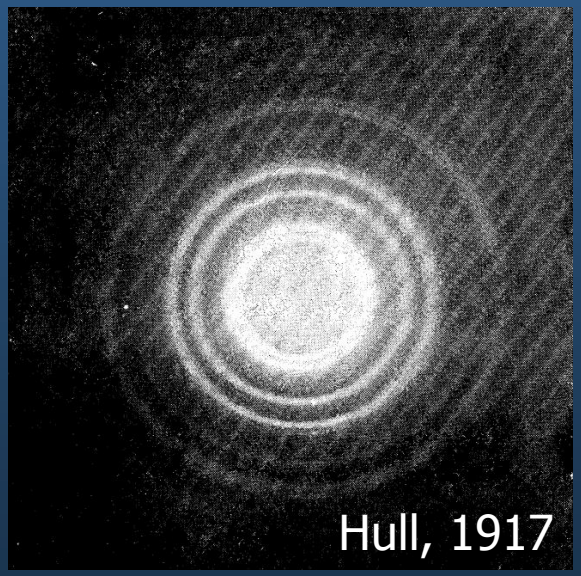
Hull, 1917


Von Dreele, 2007

R. E. Dinnebier
Max-Planck Institute for Solid State Research, Stuttgart, Germany

[1] As a reminder: „Yesterday today was tomorrow, but tomorrow today will be yesterday "

Content

- Instrumentation 1917
- Instrumentation 2011
- Exploring 2D powder patterns
- Parametric Rietveld refinement
- MEM + CF

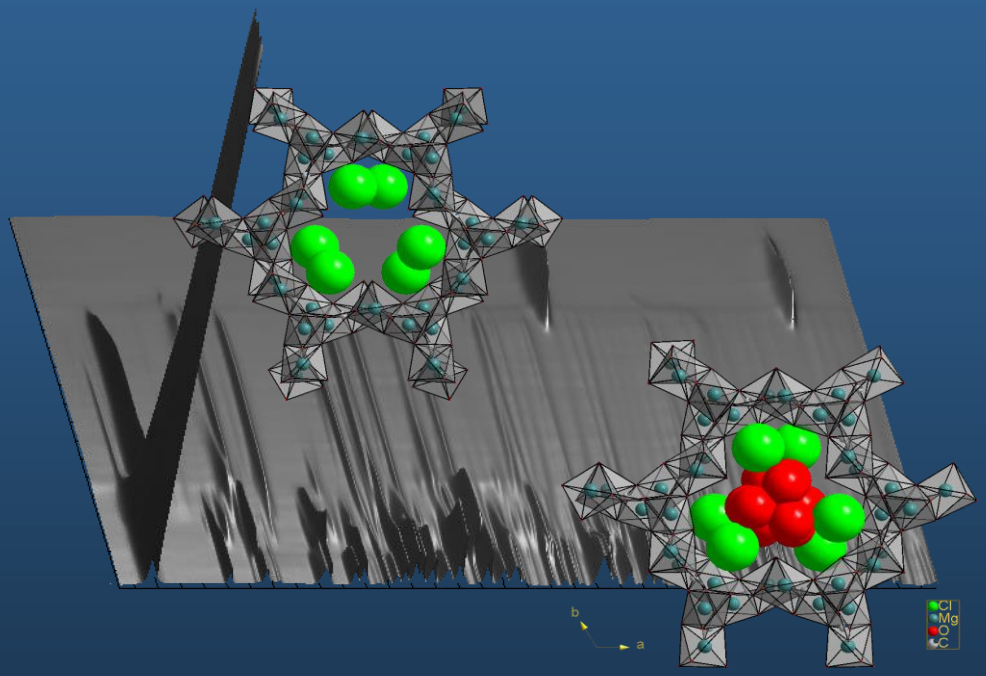

The pioneers of powder diffraction 1916/1917

Peter J.W. Debye

Paul Scherrer

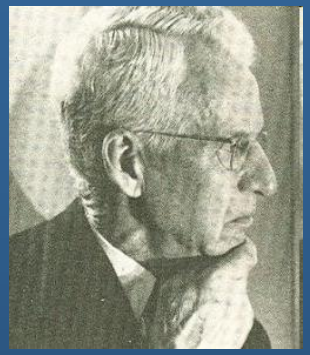

Albert W. Hull

OUTLINE OF METHOD.

The method consists in sending a narrow beam of monochromatic X-rays (Fig. 2) through a disordered mass of small crystals of the substance to be investigated, and photographing the diffraction pattern produced. Disorder, as regards orientation of the small crystals, is essential. It is at-

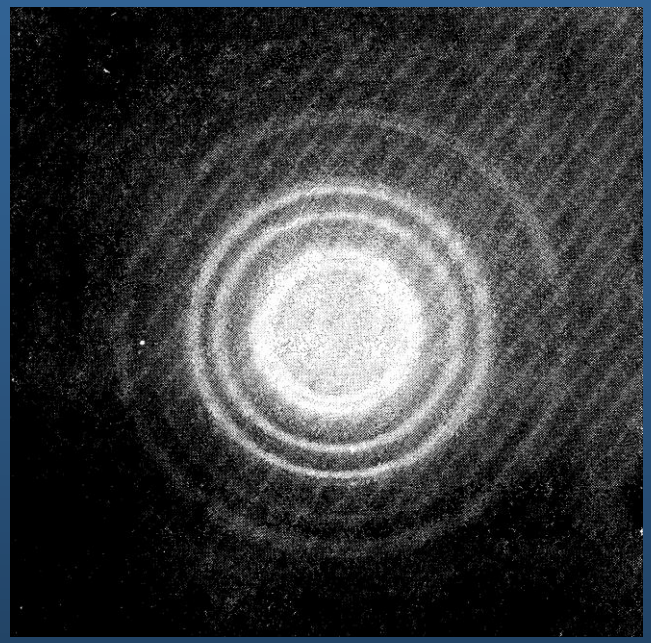

Al

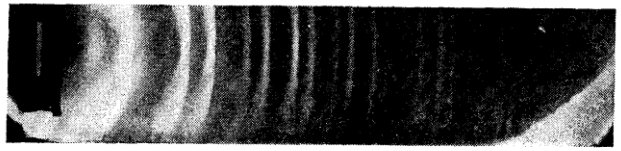

FIG. 8. Silicon.

Si

Debye, P.;Scherrer, P. (1916), Interferenzen an regellos orientierten Teilchen im Roentgenlicht, Physikalische Zeitschrift 17, 277-283
Hull, A. W. (1917), A New Method of X-Ray Crystal Analysis, Phys. Rev. 10, 661 - 696

Crystal structure from '*in situ*' powder diffraction: The beginning…

An early ‚in-situ‘ powder xray diffraction experiment on the structure of α-N_2

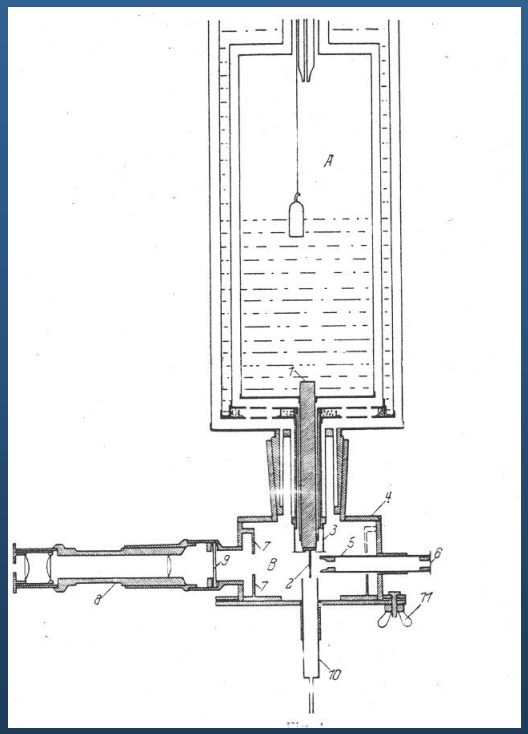

Schematic drawing of the used cryo-camera

Fig. 2.

Debye-Scherrer film of α-N_2 at 34K

Exposure time: 18h

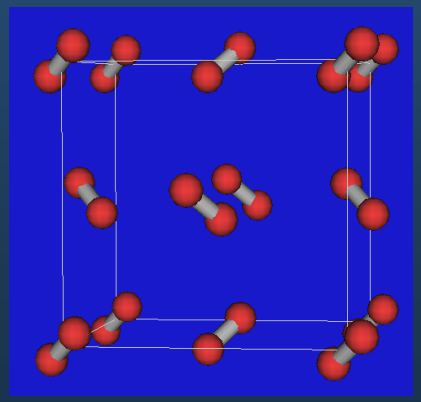

α-N_2 *Pa*-3

VEGARD, L. (1929). *Z. Phys.* 58, 497-501.

The next big step: towards higher resolution

André GUINIER

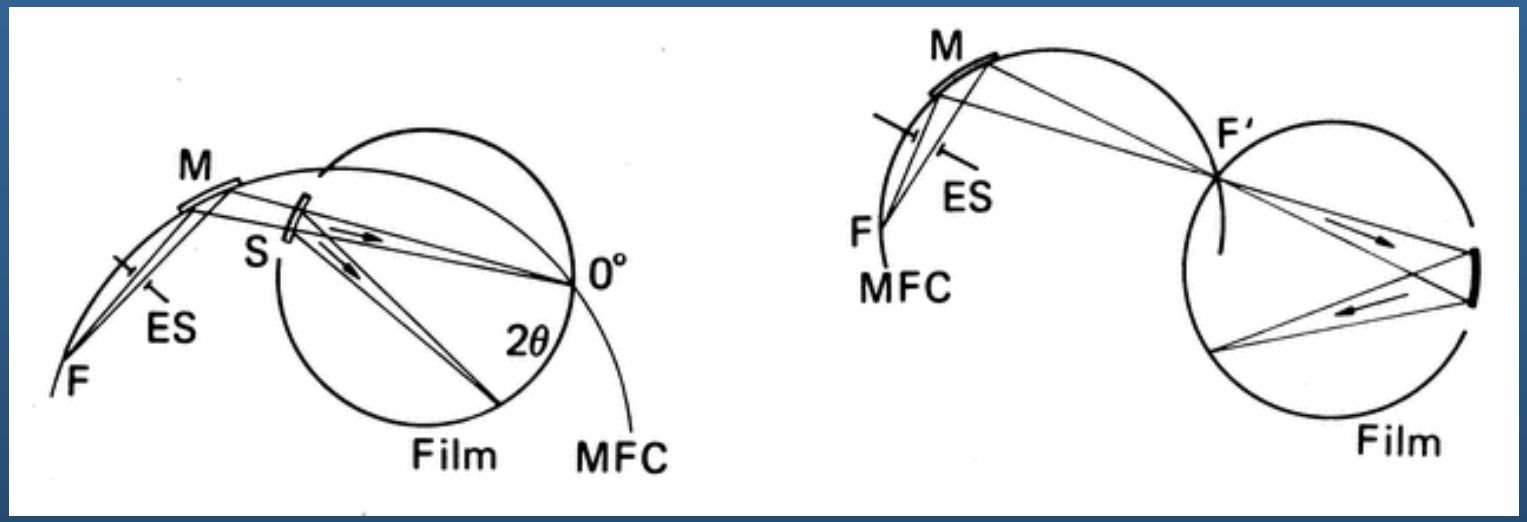

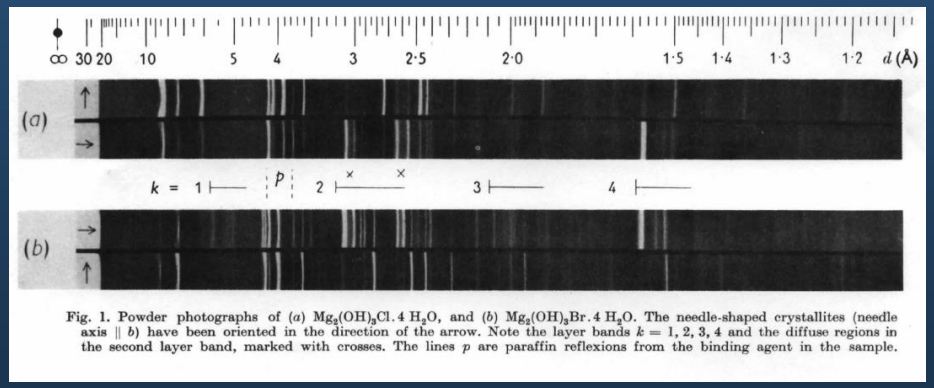

Fig. 1. Powder photographs of (a) $Mg_2(OH)_3Cl.4\,H_2O$, and (b) $Mg_2(OH)_3Br.4\,H_2O$. The needle-shaped crystallites (needle axis ∥ b) have been oriented in the direction of the arrow. Note the layer bands $k = 1, 2, 3, 4$ and the diffuse regions in the second layer band, marked with crosses. The lines p are paraffin reflexions from the binding agent in the sample.

Guinier, A. (1937). Arrangement for obtaining intense diffraction diagrams of crystalline powders with monochromatic radiation. C. R. Acad. Sci. 204, 1115–1116.

The first “modern” powder diffractometer

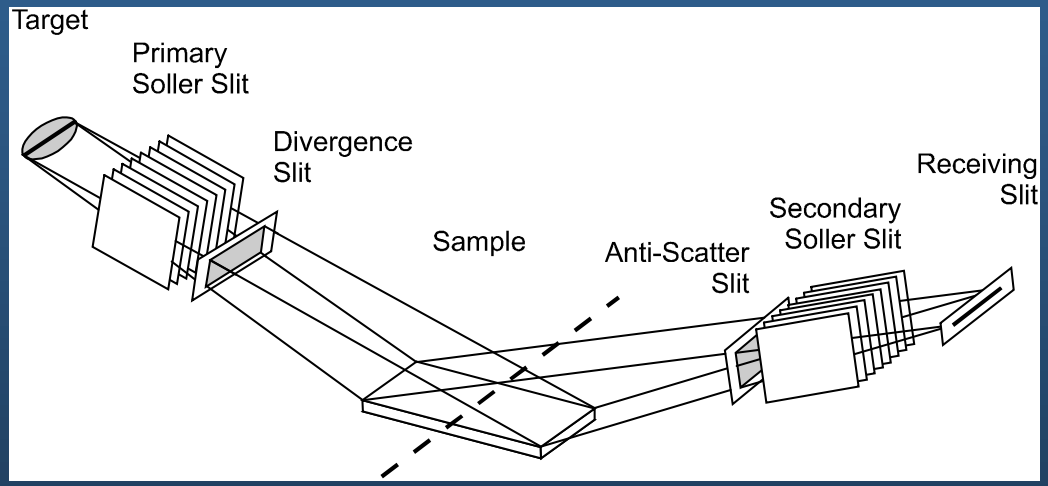

Norelco powder, X-ray goniometers. First installed in 1949 at the Geophysical Laboratory
(Design patented by William Parrish in 1947)

Standard Bragg-Brentano geometry

Modern laboratory powder diffractometers

MAX PLANCK GESELLSCHAFT

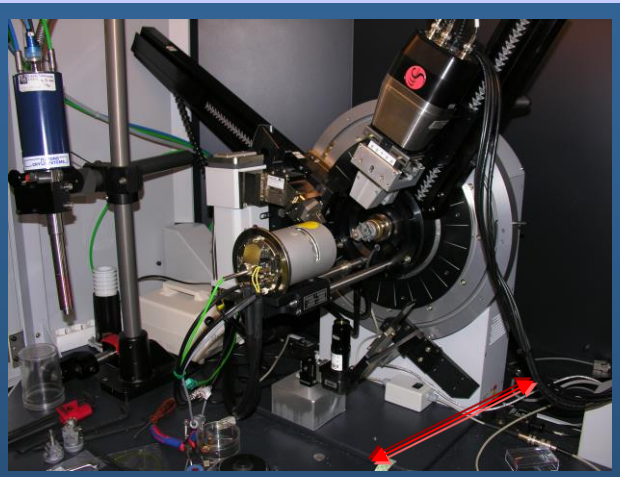

Bruker D8-Advance, Våntag PSD

Stoe-Stadi-P with 140° IP-PSD

PANalytical, X'pert PRO with Accelerator

Stoe-Stadi-P, 6° PSD‘s and Mythen

High speed, high resolution PSD‘s in Debye-Scherrer geometry

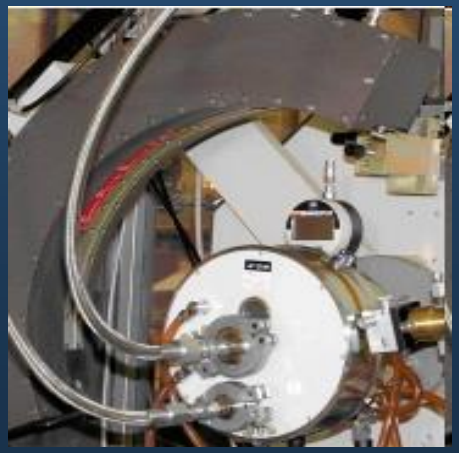

Inel CPS120 with 120° PSD

Modern powder diffractomters at synchrotron beamlines

MAX PLANCK GESELLSCHAFT

Multi-analyzer crystals or 2D detectors in Debye-Scherrer geometry

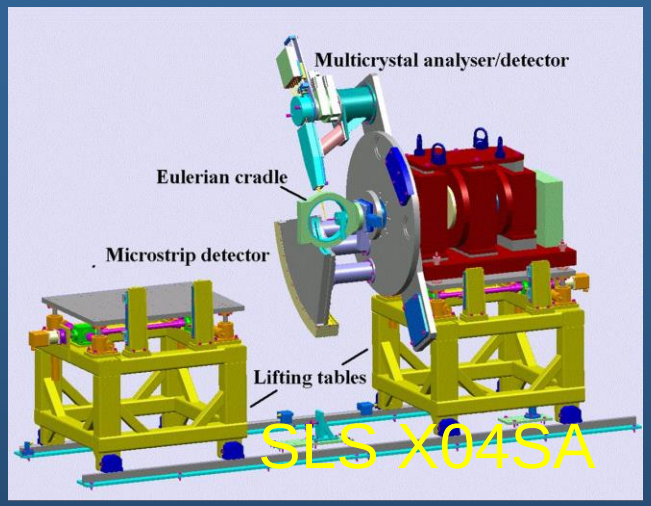

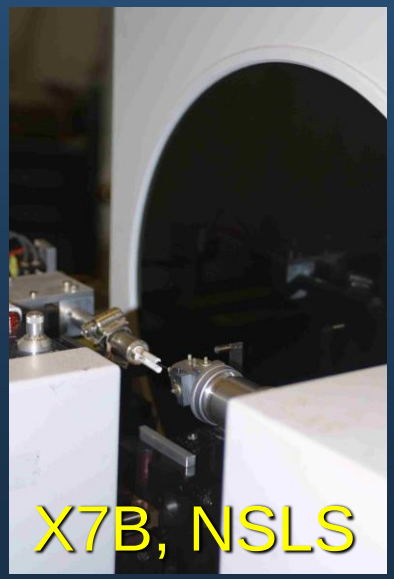

Back to the roots …
Why Debye-Scherrer geometry in the laboratory ?

MAX PLANCK GESELLSCHAFT

Advantages of the Debye-Scherrer method

- Less grain size effects
- Little preferred orientation
- Small amounts of material
- Handling of extremely sensitive samples
- Simple correction functions
- No overspill effect
- Simple line profile (→ fundamental paramters)
- Easy adaptation of reaction cells for non-ambient conditions, gas flow etc.
- Perfect for structure determination

Disadvantages of the Debye-Scherrer method

- Absorption (for Z > 20)
- High background
- Peak to background ratio

Solution → Using a high resolution Mo diffractometer with Ge(220) primary beam monochromator and a high efficiency detector

LaB_6 reference pattern of the Mo-$K_{\alpha 1}$ radiation high resolution Debye-Scherrer diffractometer

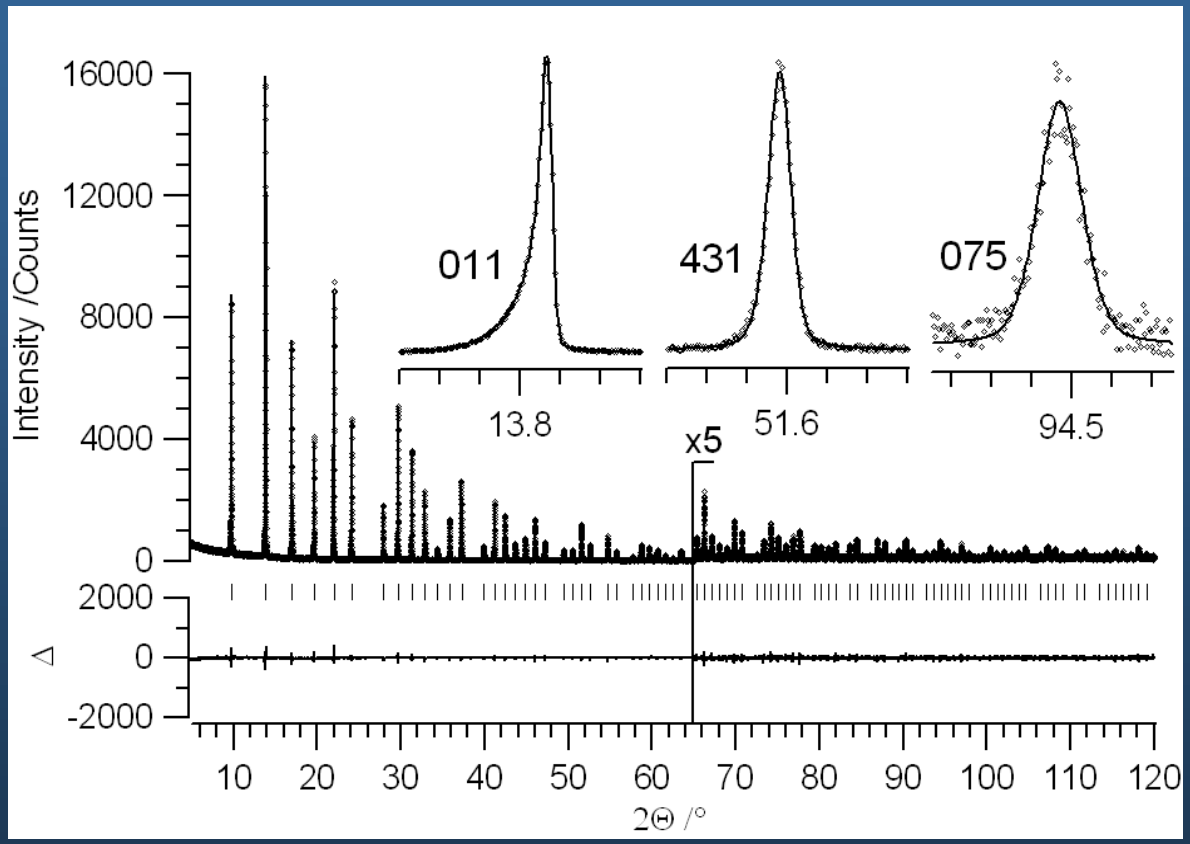

LaB_6 line profile standard measured with Mo-Ka1 radiation (Bruker D8 Advance with Ge(220) primary beam monochromator and Lynx-Eye detector with 0.5 mm thick solicon stripes, 17 h counting time)

- wavelengths distribution (Lorentzian)

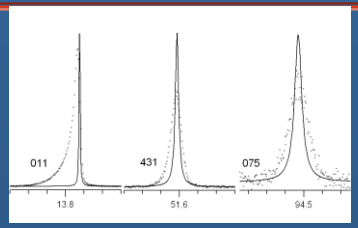

- Receiving slit width (Hat)

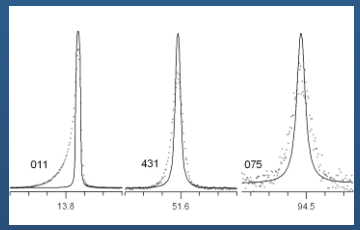

- Source, sample, slit lengths (exp.)

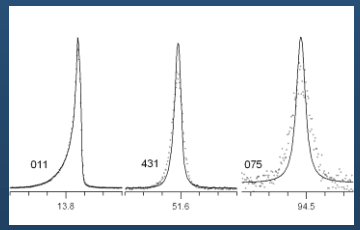

- Gaussian strain

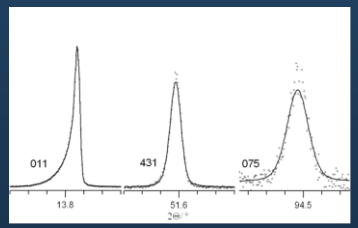

4 refined parameters only

Resolution in 2 θ < 0.04° 2 θ
Minimum d-spacing < 0.4 Å

Starting from an unknown chemical composition: a new nitridoosmate from lab data (Stoe-Stadi-P, Mo-$K_{\alpha 1}$)

MAX PLANCK GESELLSCHAFT

Known composition before simulated annealing: Ba/Os = 3:1 plus several nitrogen atoms

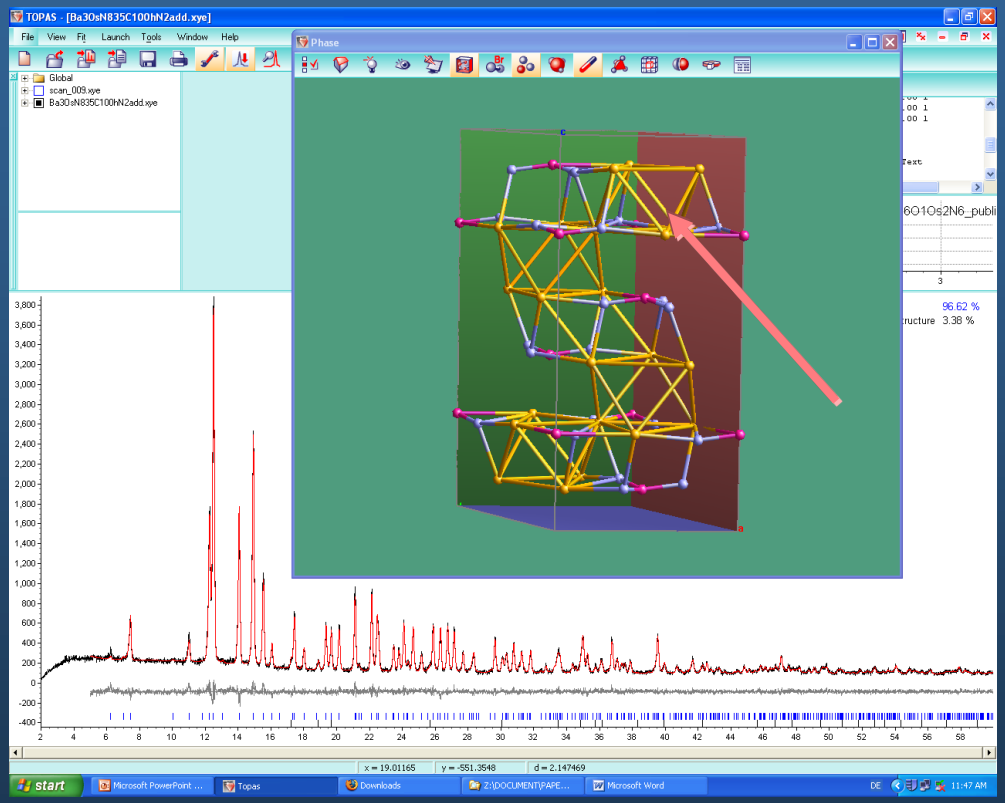

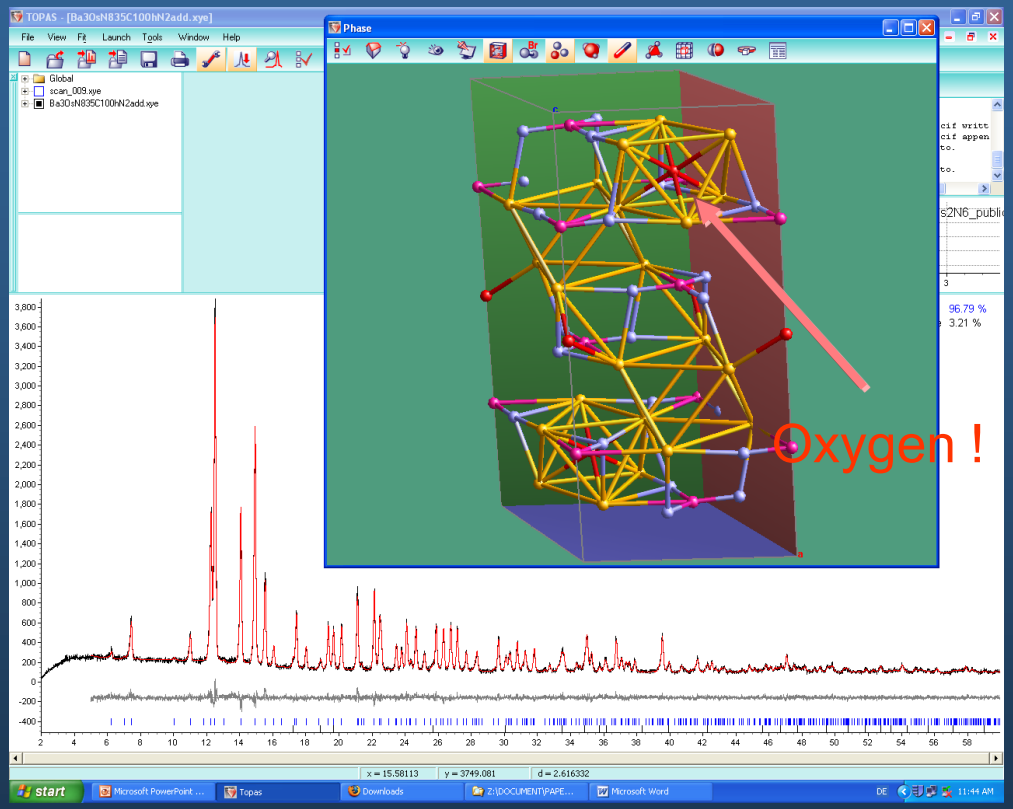

"Ba_3OsN_3"

R-wp 6.690 R-Bragg 1.95

$(Ba_6O)(OsN_3)_2$

R-wp 6.486 R-Bragg 1.67

C. Schmidt, U. Wedig, R.E. Dinnebier, M. Jansen , Synthesis, Crystal structure, Properties and Bonding of $Ba_6(O)(OsN_3)_2$, (2008), Chem. Asian J. 3, 1983 – 1990

Alternatively: $(Ba_6O)(OsN_3)_2$

"Ba_3OsN_3"

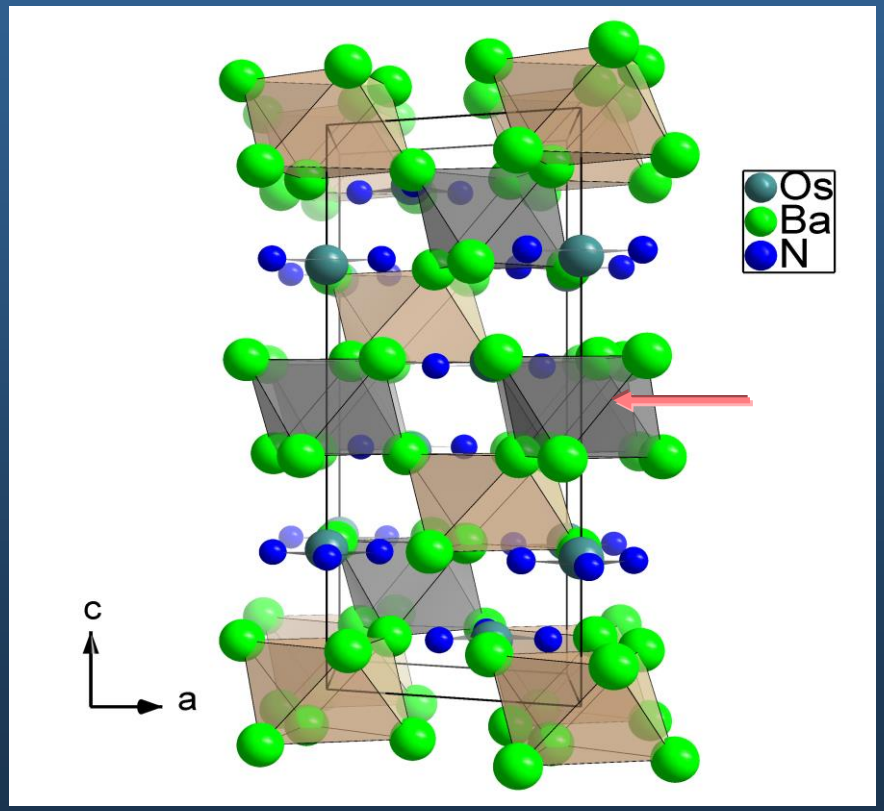

$(Ba_6O)(OsN_3)_2$

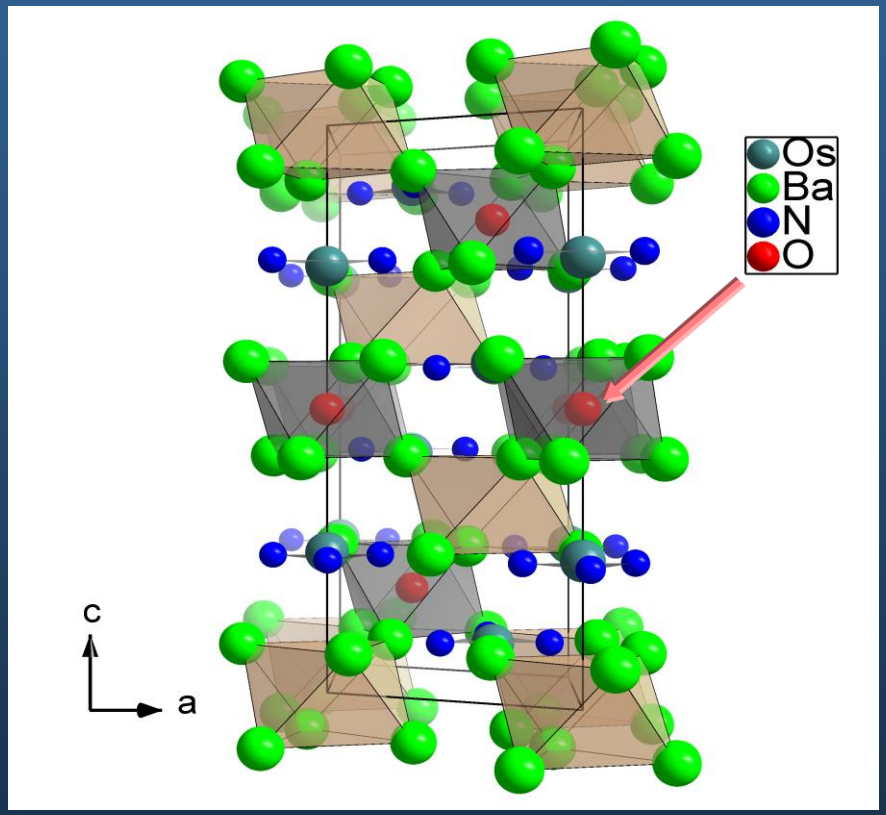

Ba_3FeN_3 exists !

CRYSTAL06 (DFT)-Calculations – Hybrid-Funktional B3PW

		exp.	calculated			
		$(Ba_6O)(OsN_3)_2$	$(Ba_6\square)(OsN_3)_2$	$(Ba_6O)(OsN_3)_2$	$(Ba_6N)(OsN_3)_2$	$(Ba_6O_2)\ (OsN_3)_2$
Position	3b	**O**	**-**	**O**	**N**	**O**
	3a	**-**	**-**	**-**	**-**	**O**
Lattice parameter / Å	*a*	**8.112**	**8.077**	**8.085**	**8.135**	**8.094**
	c	**17.390**	**17.348**	**17.414**	**17.599**	**17.359**
Distance / Å	Ba –3b	**2.73**	**2.82**	**2.71**	**2.70**	**2.80**
	Ba –3a	**2.91**	**2.82**	**2.92**	**2.96**	**2.80**
Binding energy / (kJ / mole)	O / N in 3a / 3b			**822**	**578**	**1586**
Partial charges/	$OsN_3^{-\delta}$		**-2.8 / +1.9**	**-2.6 / +1.6**	**-2.4 / +1.1**	**-2.4 / +1.0**
Spin charges	Ba		**+1.2 / -0.1**	**+1.3 / +0.1**	**+1.4 / +0.1**	**+1.4 / 0**
	Pos. 3b		**-0.7 / -0.6**	**-1.9 / 0**	**-2.8 / 0**	**-1.8 / 0**
	Pos. 3a		**-0.7 / -0.6**	**-0.5 / +0.5**	**-0.5 / +0.4**	**-1.8 / 0**

Calculations by Ulrich Wedig, MPI-FKF, Stuttgart

Data reduction & filtering: A high pressure phase of the NLO – compound BiB_3O_6 (BiBO)

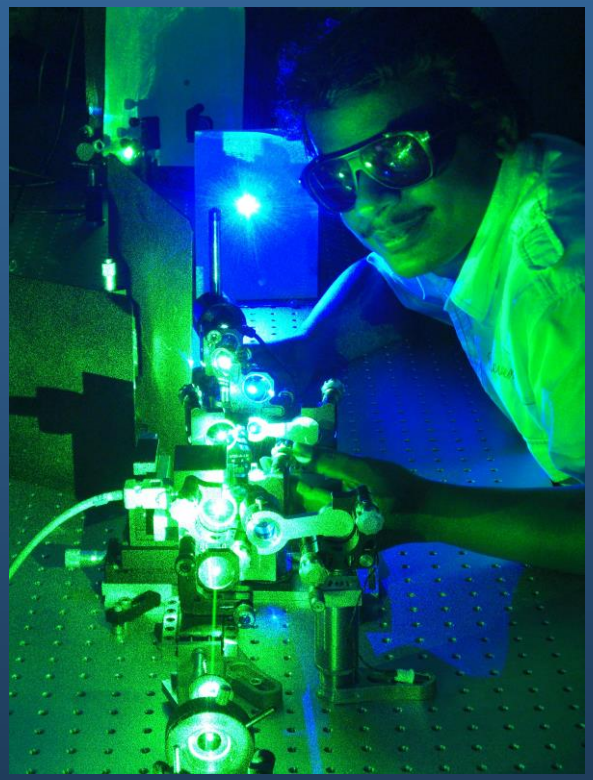

- Better conversion efficiency than BBO (β-BaB_2O_4) or LBO (LiB_3O_5)
- Better resistance to laser damage than KTP
- Tunable laser 240nm – 1000nm

R. E. Dinnebier,B. Hinrichsen, A. Lennie, and M. Jansen, The high pressure crystal structure of the NLO compound BiB_3O_6 from 2D powder diffraction data. (2009), Acta Cryst. B65, 1-10 (see also IUCr newsletter June 2009)

B. Hinrichsen, R. E. Dinnebier , M. Jansen, On the intensity distributions within Debye-Scherrer rings. What is different in high pressure experiments ? Part I: Theory & Part II: Application (2009), . *Kristallogr. Suppl. 30 (2009) 139-153*

Known phases of BiBO

α (*C*2)
NLO

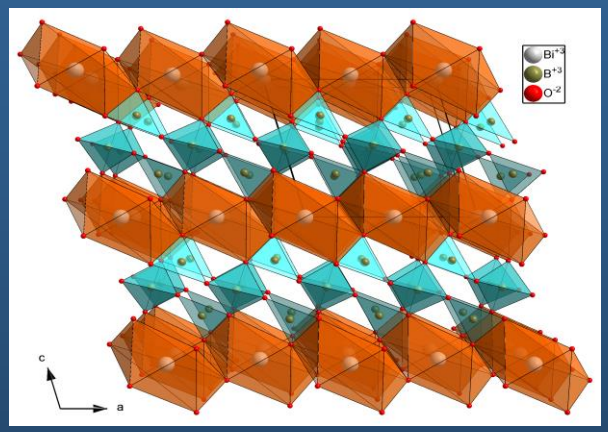

β ($P2_1/n$)

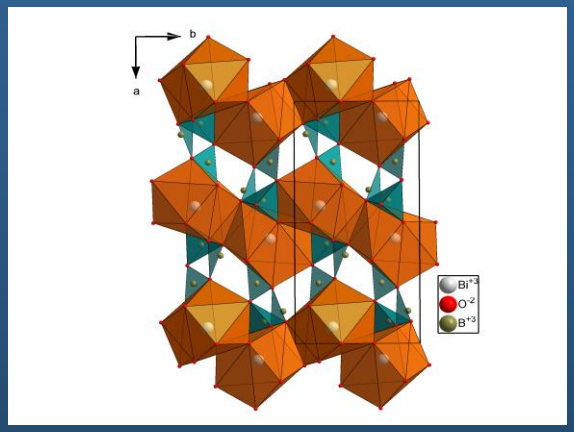

γ ($P2_1/n$)

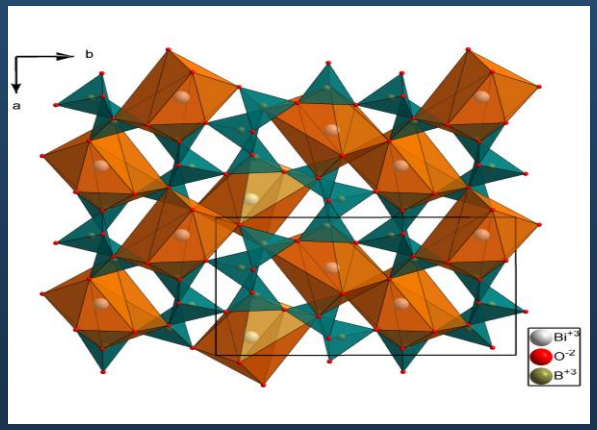

δ ($Pca2_1$)

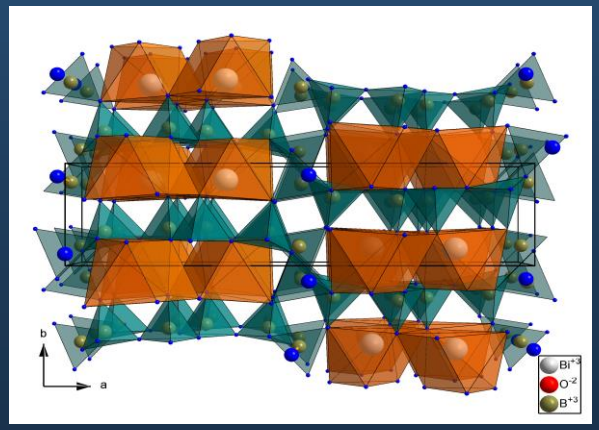

Raw data at high pressure…

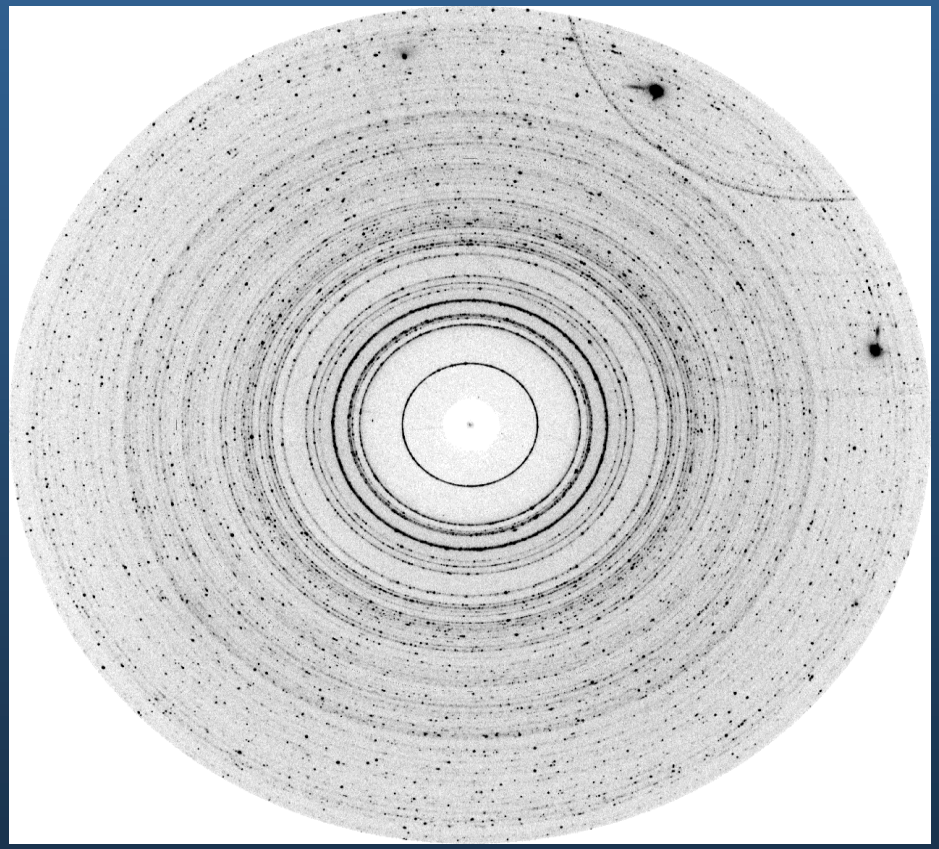

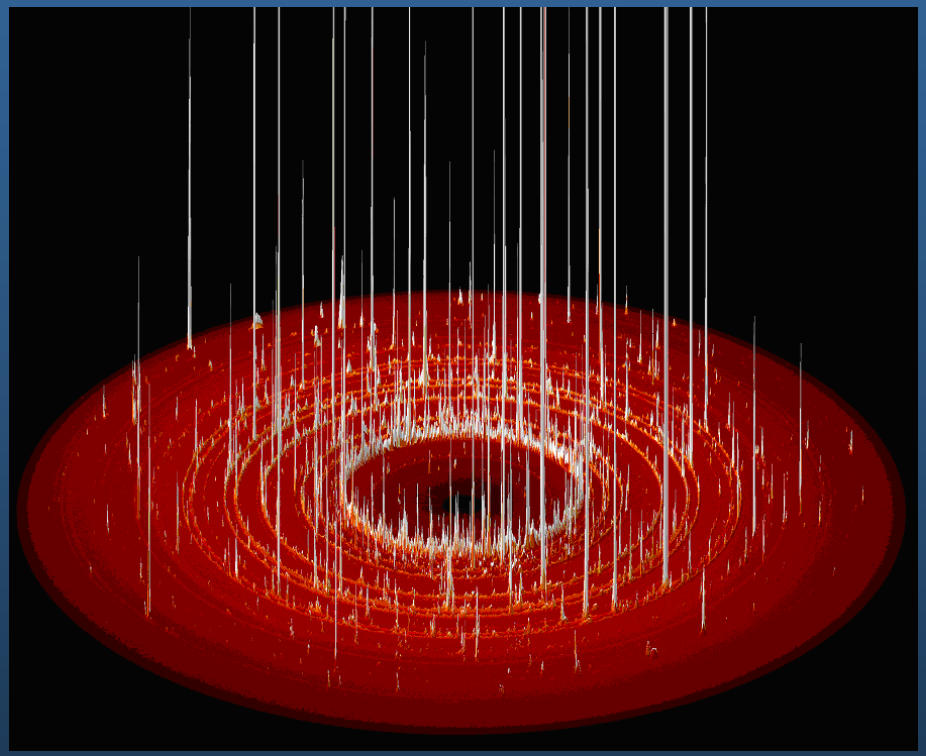

2D image plate powder diffraction data set of BiB_3O_6 at <u>high pressure</u>

How about counting statistics with 2D XRPD data ?

A very large number of equally sized and randomly oriented crystallites to the diffraction pattern would lead to an ideal binomial intensity distribution over the entire Bragg cone.

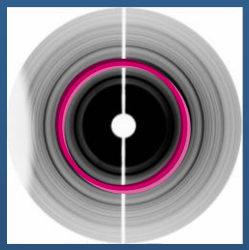

$$P_B(n|N) = \binom{N}{n} p^n q^{N-n} = \frac{N!}{n!(N-n)!} p^n (1-p)^{N-n}$$

probability P_B of exactly n successes out N trials where each trial has the probability of success p and probability of failure $q=1-p$

$n \to \infty$; p= const

Image plate

$$P_N(n) = \frac{1}{\sigma\sqrt{2\pi}} \exp\left[-\frac{(n-Np)^2}{2\sigma^2}\right]$$

Continuous Gaussian distribution

$n \to \infty$; p= 0; $Np = \nu > 0$

Counter

$$P_P(n) = \frac{\nu^n e^{-\nu}}{n!}$$

Discrete Poisson distribution

Intensity distribution in a bin

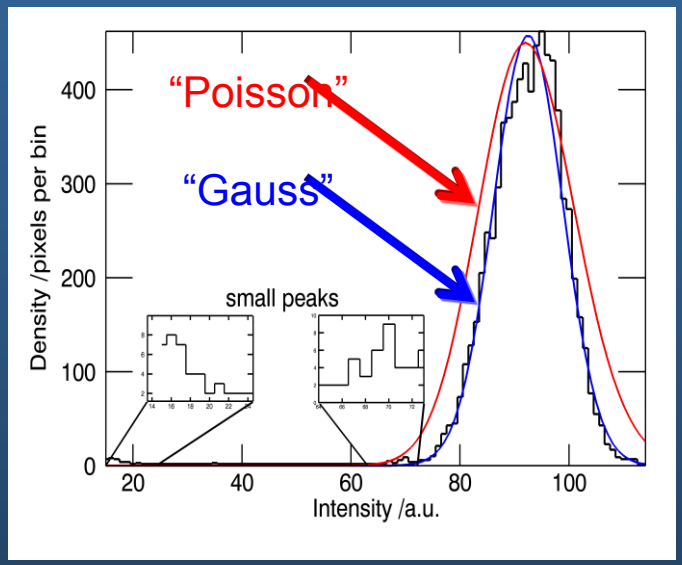

histogram of the intensities contributing to one bin* of air scattering intensity

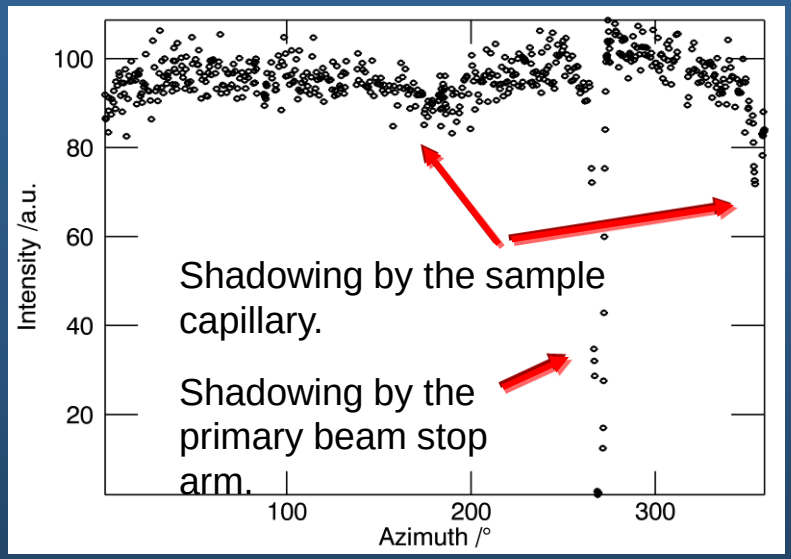

The distribution of the air scattering intensity as a function of the azimuth

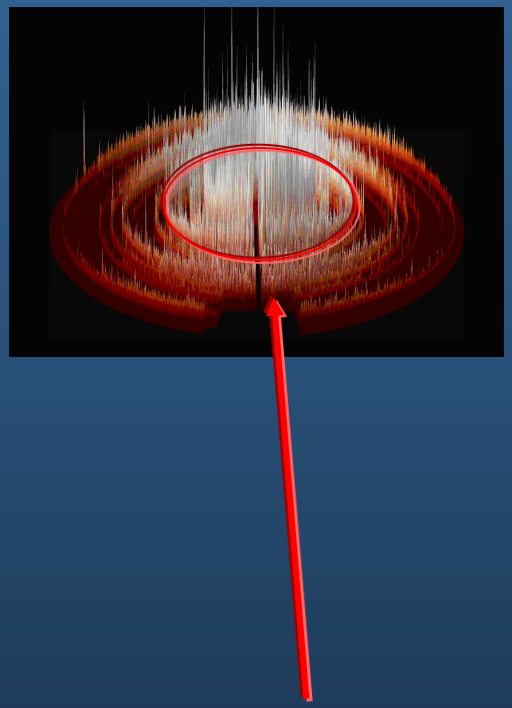

*A bin is a container into which pixels are grouped. It spans a 2D region of 2θ which is identical to the 2θ step width of the integrated pattern. The intensities of the pixels within a bin determine the corresponding intensity of a step in the integrated pattern.

The simpler the better … Fractile filtering

We propose a robust type of band pass filter based on *fractile statistics*.
A fraction x of the low intensity data and a fraction y of the high intensity data are removed:

$$I_{\min} + x\left(I_{\max} - I_{\min}\right) \geq I_{filtered} \geq I_{\min} + \left(1 - y\right)\left(I_{\max} - I_{\min}\right)$$

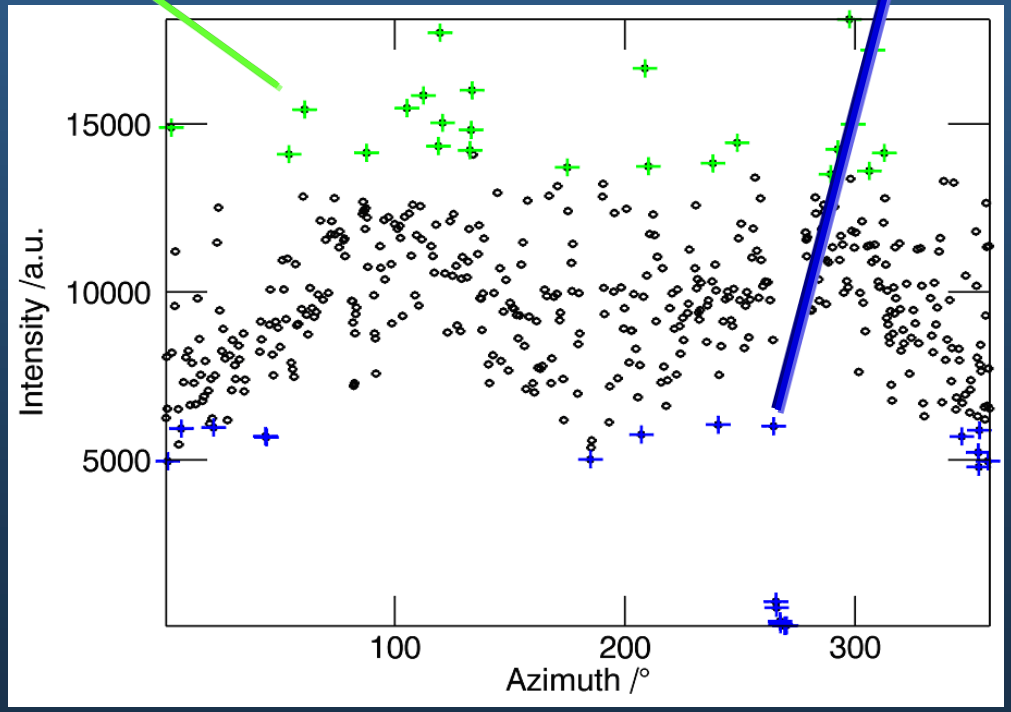

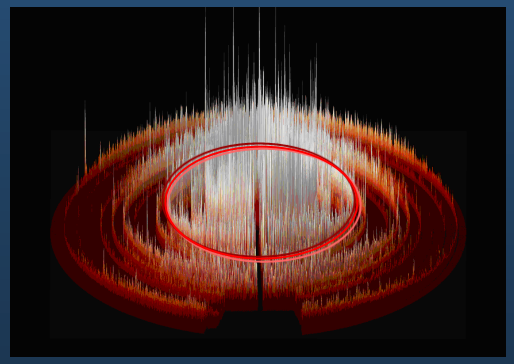

Fractile filtering on ideal data

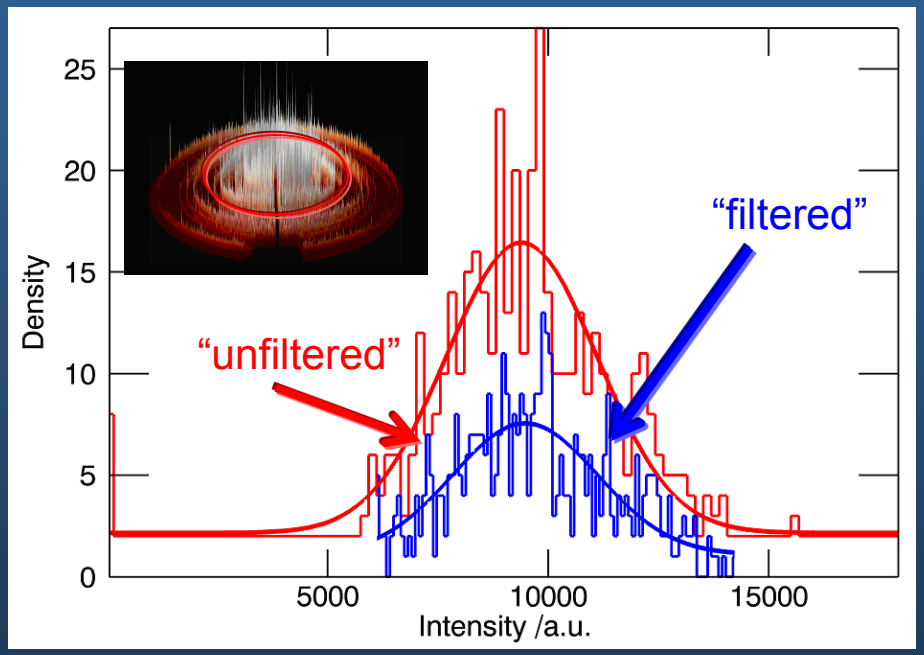

	Unfiltered data	Filtered data
Fit ("Gauss"):		
Mean	9399(41)	9481(40)
Variance	1713	1645
Data:		
Median	9760	9758
Mean	9764(51)	9793(43)
Variance	2639	1807

Effect of fractile filtering on the intensities of an almost ideal Bragg reflection as it would contribute to a two-theta bin.

The effect of filtering on high pressure XRPD data

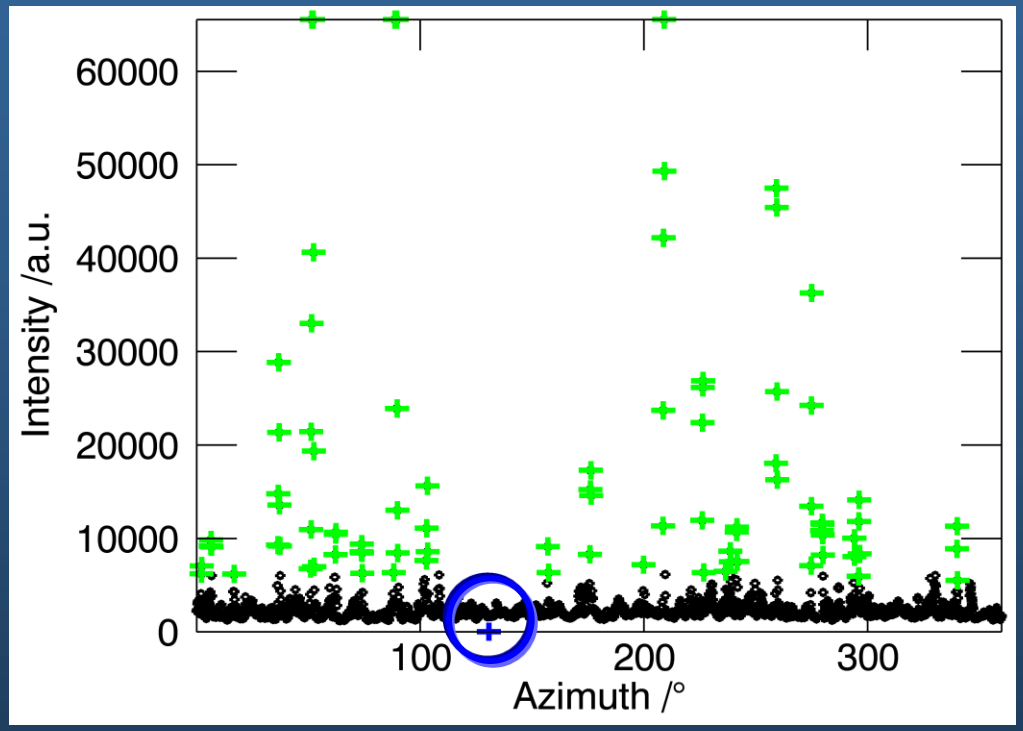

The intensity is shown as a function of the azimuth for a high pressure powder diffraction data set
(+) highest data fraction removed by the filter.
(+) lowest data fraction removed by the filter.

The azimuthal intensity distribution of a Bragg peak

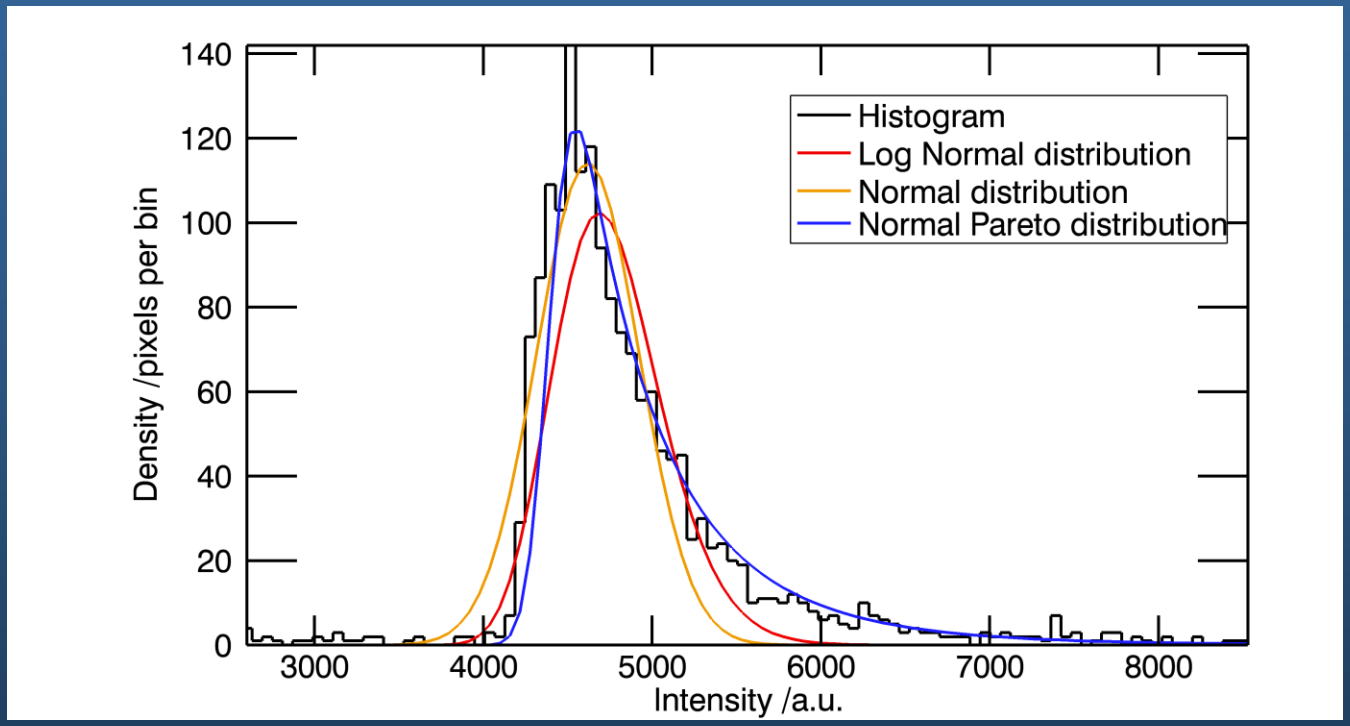

$$P_{Pareto}(x) = \begin{cases} 0 & \text{for } x < b \\ \dfrac{ab^a}{x^{a+1}} & \text{for } x \geq b \end{cases}$$

$$P_{NP}(x) = P_{normal}(x) \otimes P_{Pareto}(x)$$

Most promising description of the intensity distribution is the Pareto distribution *(80/20 rule)* convoluted with the normal distribution.

(At values of a>20, the Pareto distribution tends toward a Dirac delta function, thereby reducing a convoluted normal-Pareto (NP) function to the normal distribution of perfectly monodisperse grains)

Estimating the high intensity fraction to be filtered

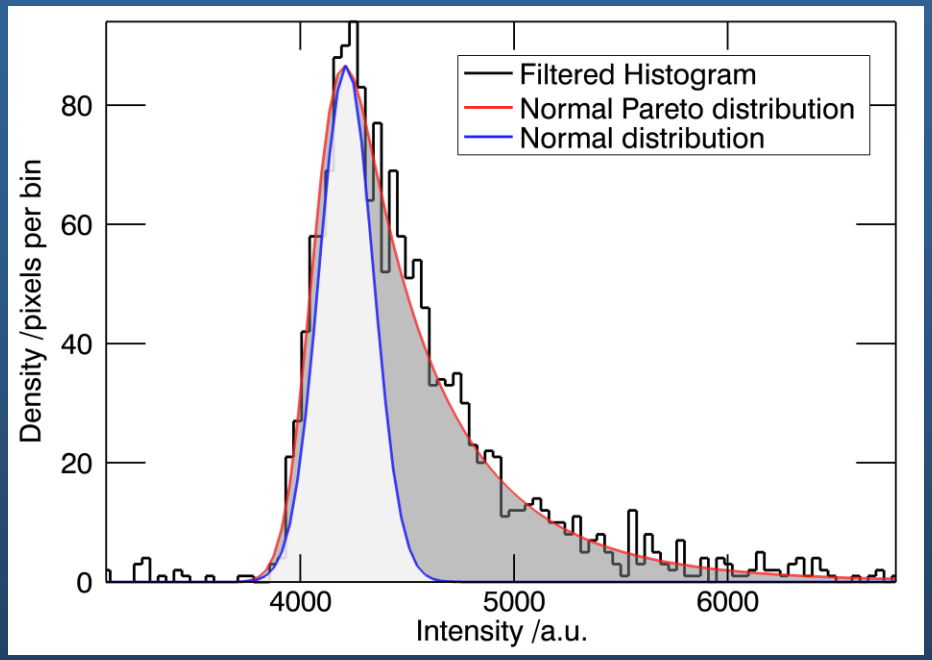

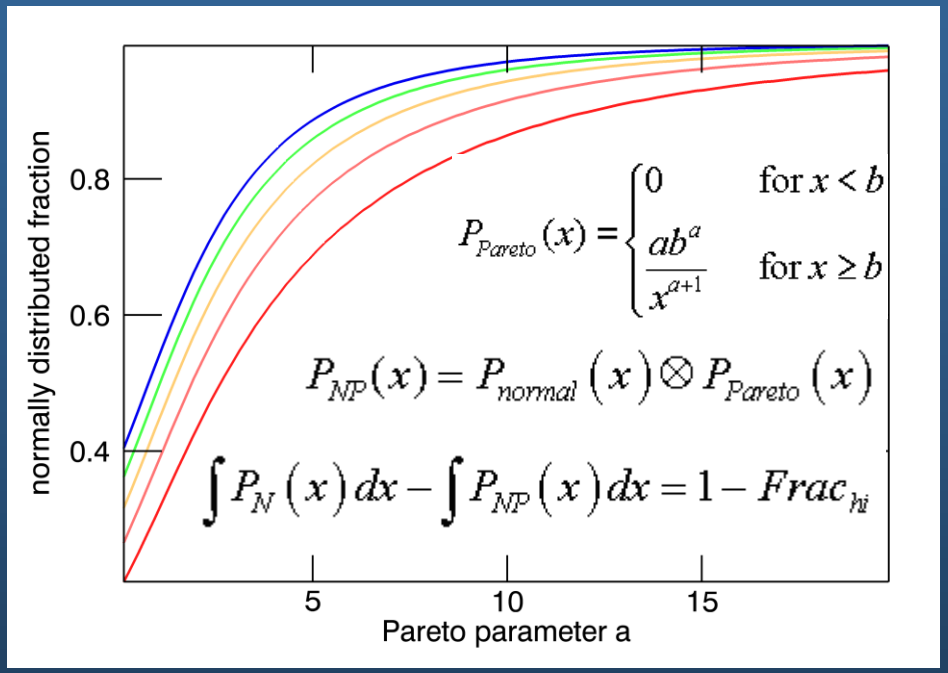

For high values of parameter *a* the normal fraction approaches 1 asymptotically.

<u>For a filter setting which would reduce the Pareto distribution to a roughly normal distribution (**1-normal fraction)** of the highest intensities should be removed</u>.

Finally, the filtered data…

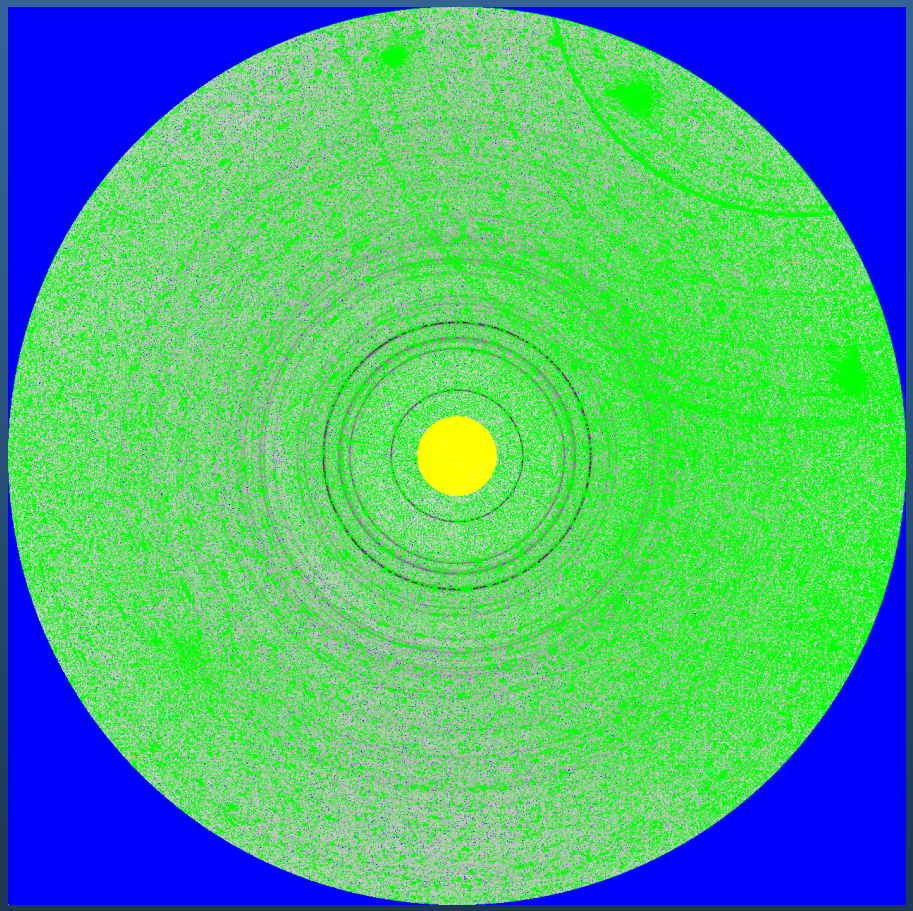

The effect of filtering on the diffraction image is shown in this figure. Intensities per integration bin:

Green mask → top 48%
Blue mask → bottom 2%
Yellow mask → beam stop

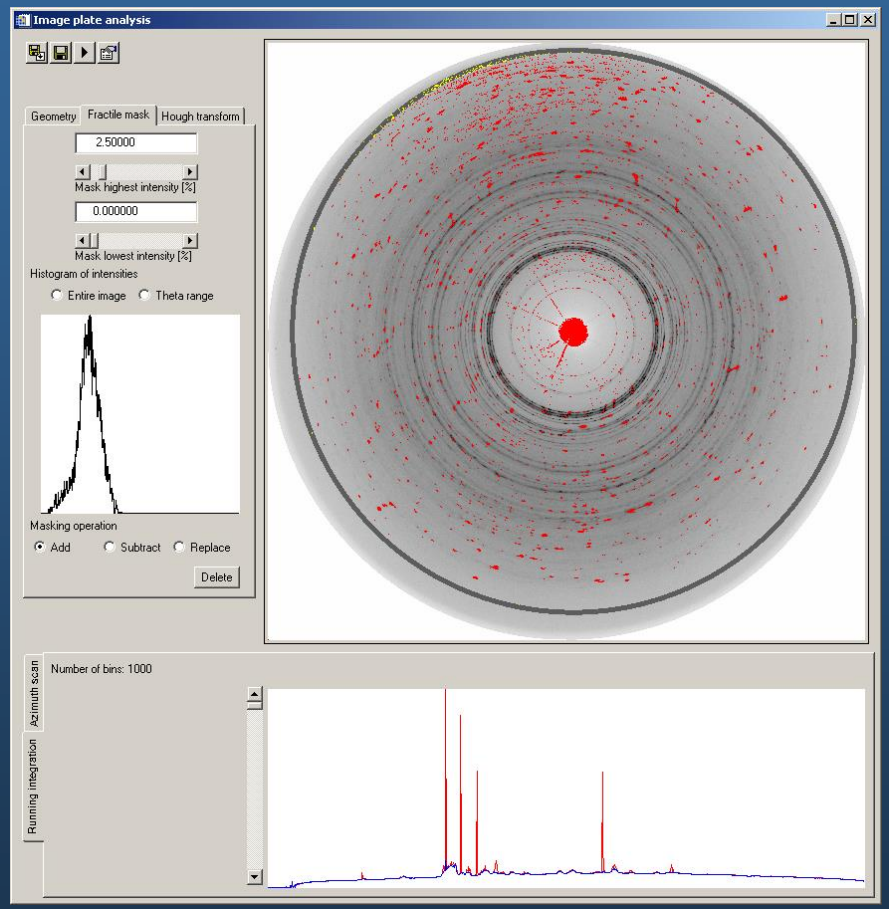

Screenshot of Powder3D-IP
http://www.fkf.mpg.de/xray/

The effect of filtering

Pattern

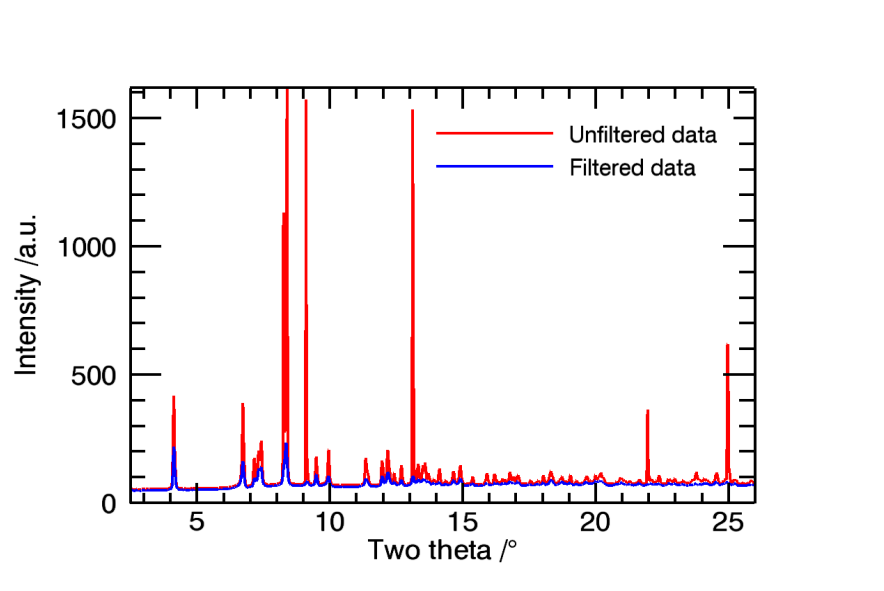

ESD's

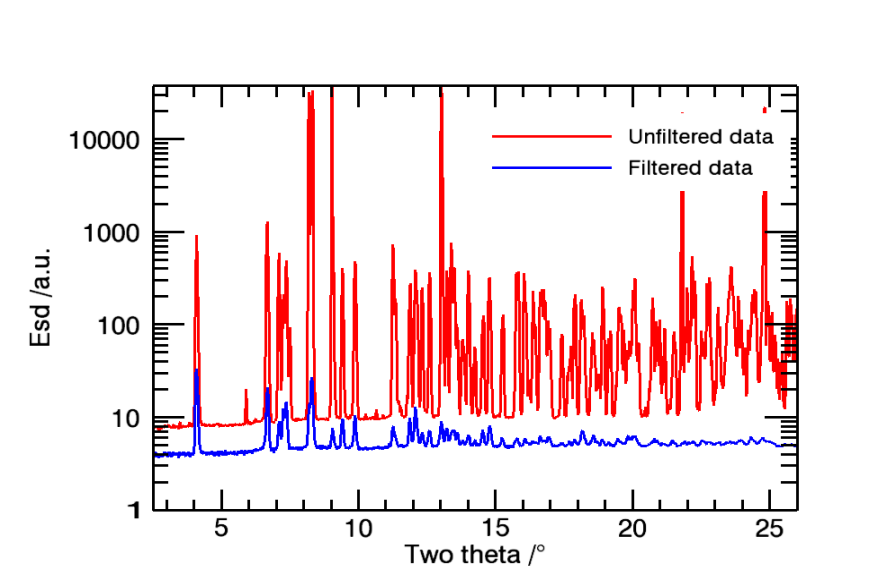

Red: integrated pattern (left) and standard deviation (right) of the unfiltered image
Blue: 48% of the highest intensities and 2% of the lowest intensities removed

Filtered diffraction patterns of BiBO at high pressure

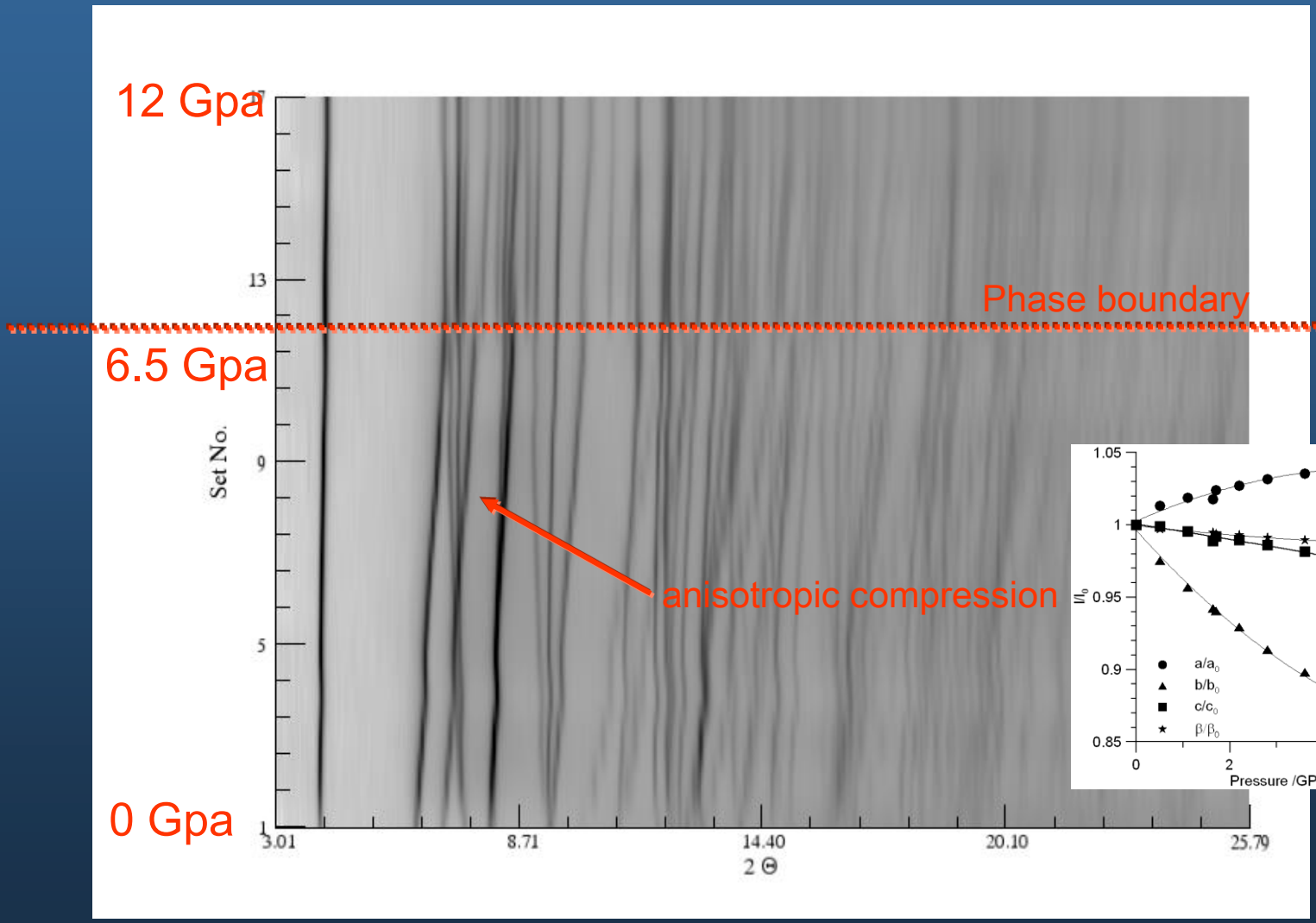

Simulated Guinier-plot of BiB_3O_6 in the pressure range from 0 to 12 GPa (using Powder3D)

Structure determination of ε-BiBO (TOPAS)

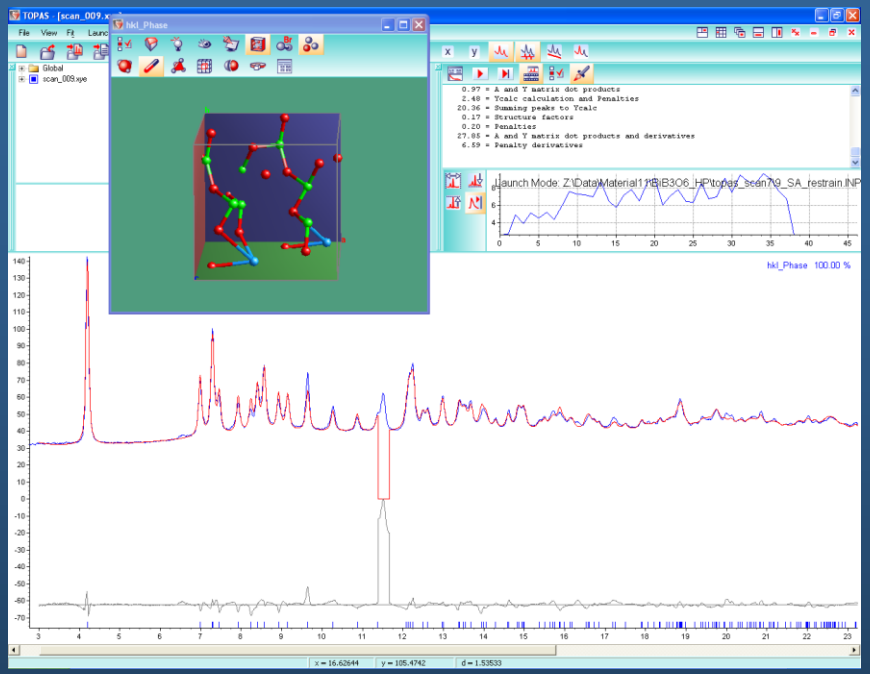

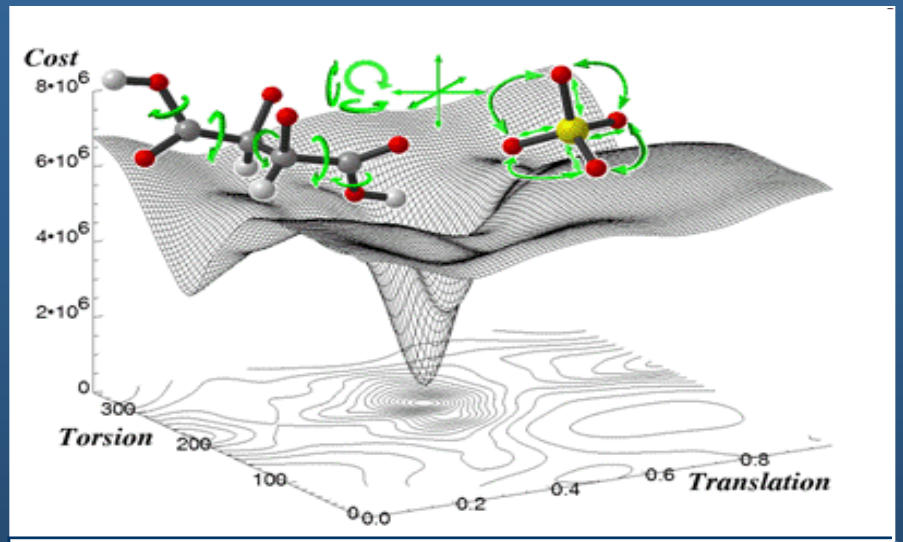

From: Radovan ČERNÝ, Chem. Met. Alloys 1(2008) 120-127,

The toolbox:

1. Global optimization (Simulated annealing)
2. Optimized cost function
3. Modified weighting scheme
4. Anti-bumping penalties
5. Distance restraints
6. Occupancy merging

3D hypersurface of the cost function for two parameters

$$\chi^2 = \sum_h \sum_k (I_h - c|F_h|^2)(V^{-1})_{hk}(I_k - c|F_k|^2)$$

W. I. F. David, On the equivalence of the Rietveld method and the correlated integrated intensities method in powder diffraction, J. Appl. Cryst. (2004). 37, 621-628.

How do the lone pairs react on pressure…

MAX PLANCK GESELLSCHAFT

α-BiBO

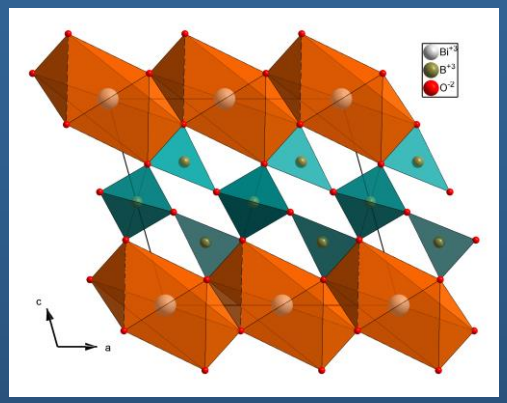

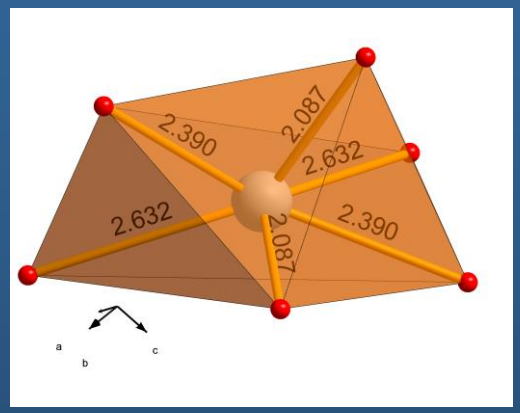

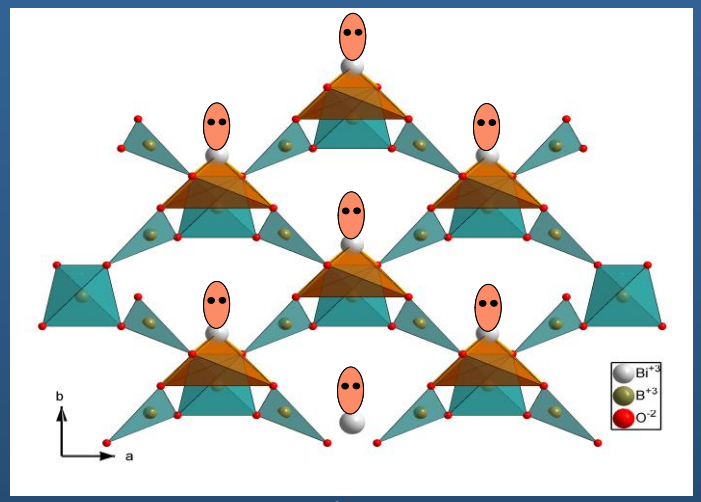

e-BiBO

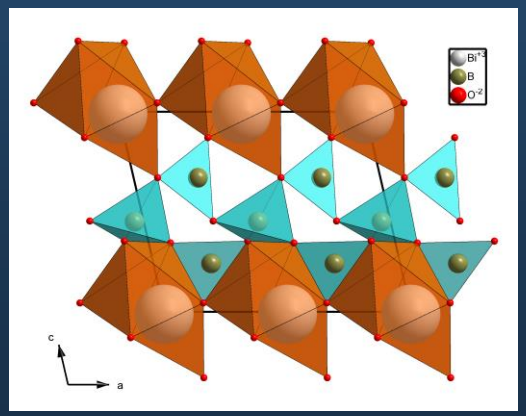

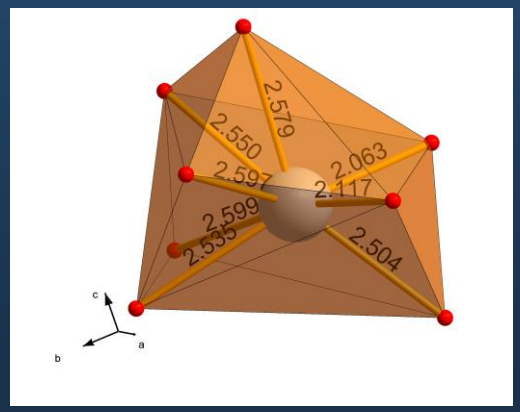

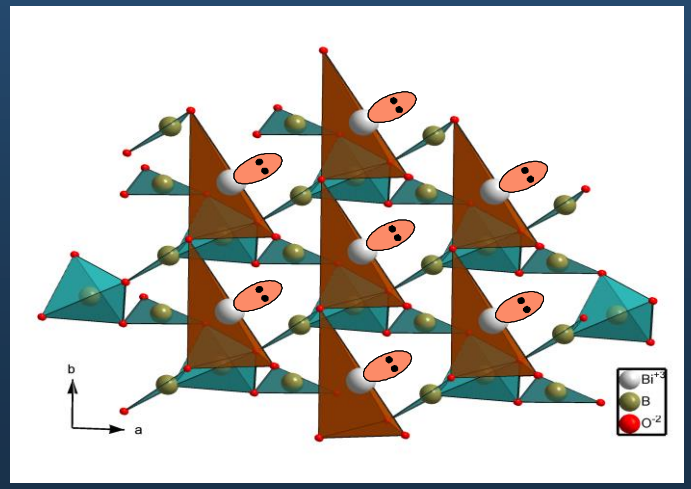

Direct access to the order parameter

MAX PLANCK GESELLSCHAFT

Parametric Rietveld refinement using spontaneous strain, symmetry modes and polyhedral tilting

as a function of external variables

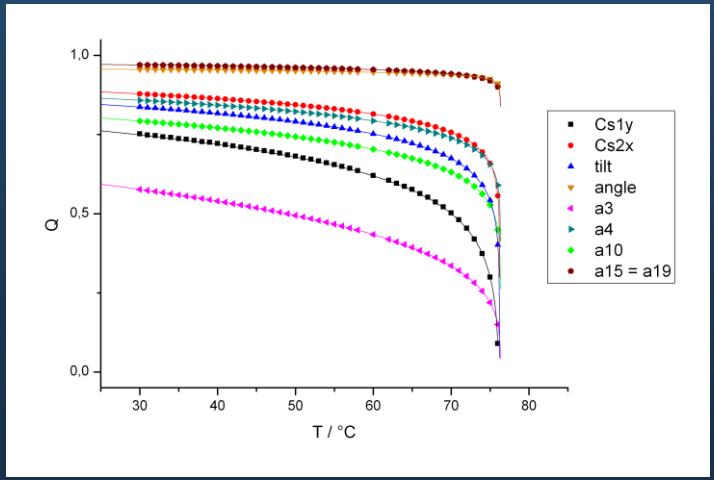

Sequential ←→ parametric Rietveld refinement

MAX PLANCK GESELLSCHAFT

Sequential Rietveld refinement:
Each parameter in each pattern is refined individually

$$y_{calc}\left(2\theta_{pattern(1)}\right) = function\left(p_{(1),1}, p_{(1),2}, \ldots, p_{(1),m}\right)$$
$$\ldots$$
$$y_{calc}\left(2\theta_{pattern(n)}\right) = function\left(p_{(n),1}, p_{(n),1}, \ldots, p_{(n),1}\right)$$

Parametric Rietveld refinement:
Some parameters in each pattern are functions of external variable(s)

$$y_{calc}\left(2\theta_{pattern(1)}\right) = function\left(p_{(1),1}, p_2 = f(T_1, T_2, ..T_t), \ldots, p_{(1),m}\right)$$
$$\ldots$$
$$y_{calc}\left(2\theta_{pattern(n)}\right) = function\left(p_{(n),1}, p_{(n),2} = f(T_1, T_2, ..T_t), \ldots, p_{(n),1}\right)$$

Minimization for each powder pattern independently

$$Min = \sum_i \left(w_i\left(y_{calc}(2\theta_i) - y_{obs}(2\theta_i)\right)^2\right)$$

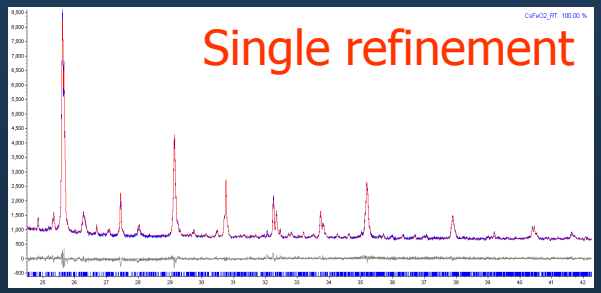

Minimization over all powder patterns simultaneously

$$Min = \sum_{pattern=1}^{n} \left(\sum_i \left(w_i\left(y_{calc}(2\theta_{pattern,i}) - y_{obs}(2\theta_{pattern,i})\right)^2\right)\right)$$

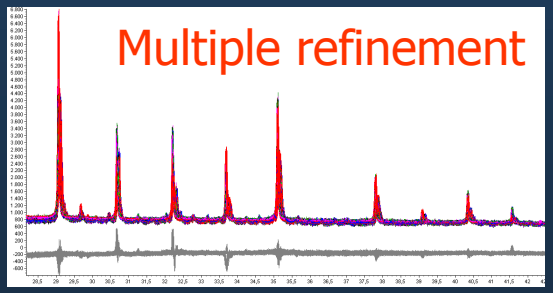

Advantages of „parametric Rietveld refinement"

MAX PLANCK GESELLSCHAFT

The idea:
The evolution of parameters in Rietveld refinement is described by functions in dependence on external variables (temperature, time, pressure, ...). The parameters of these functions are treated as global parameters and are subjected to „*surface*" Rietveld refinement (all powder patterns are refined simultaneously).

Advantages:

- the correlation between parameters and the final standard uncertainty can be reduced
- physically meaningful constraints and restraints can be introduced easily
- non-crystallographic parameters can be refined (e. g rate constants, temperatures, …)

Pioneering paper: Stinton G. W. & Evans J. S. O. (2007), „Parametric Rietveld refinement", J. Appl. Cryst. 40, 87-95

Idea:
Parameterization of the order parameter in dependence on temperature

The order parameter

Many crystalline solids can be considered as distorted versions of a higher symmetry parent structure. This parent structure can either be virtual or real. A group-subgroup relation must exist between the structures. All symmetry elements of the low-symmetry phase are already present in the high symmetry phase.

A new thermodynamic variable is necessary to specify the thermodynamic state of the low symmetry phase: order parameter η

e.g. spontaneous strain,
critical stress,
birefringence, …

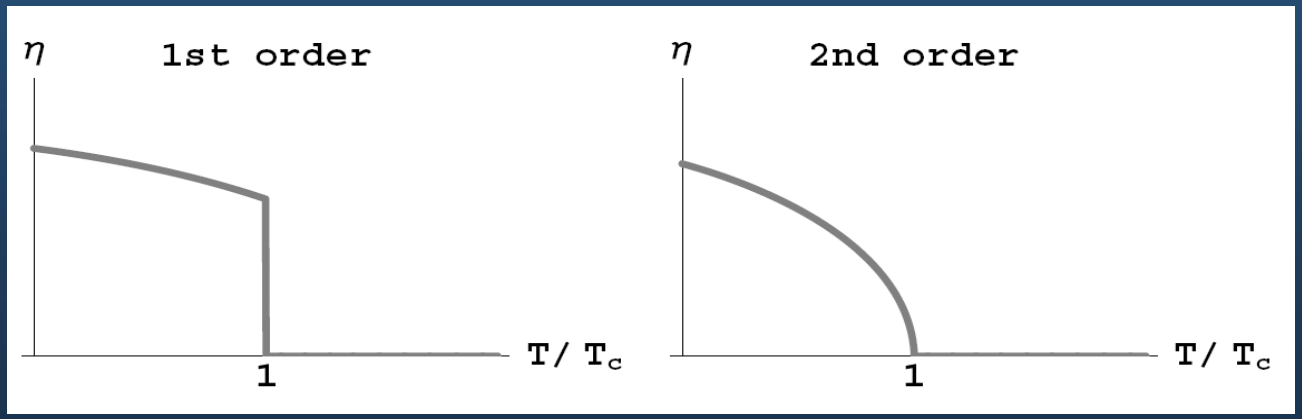

V. K. Wadhawan, Introduction to Ferroic Materials, (Gordon and Breach, Singapore, 2000).
E.K.H. Salje, Phase Transitions in Ferroelastic and Coelastic Crystals (Cambridge Univ. Press, Cambridge, 1993).

The order parameter in Landau theory

Landau theory is believed to decribe the main physical features of ferroelastic and co-elastic phase transitions.

Excess Gibbs (free) energy is the difference in Gibbs energy between both phases, stabilizing the low symmetry phase: $G_e = G_e(T,P,N,\eta)$

Equilibrium condition: $\partial G/\partial \eta = 0 \rightarrow G = G(T,P,N)$

Trivial solution $G(T) = 0$ *(for high temperature phase)*

All quantities are measured with respect to the high temperature phase as excess quantities

Landau assumed that the excess free energy (Landau potential) can be described in a Taylor series for small values of η. Assumption: polynomial form of G is a good approximation over an extended temperature interval and for large values of η.

$G = G0 + \alpha\eta + A\eta 2 + C\eta 3 + B\eta 4 + \ldots$ $G0, \alpha, A, B, C = f(P,T)$ $G0 \neq f(\eta)$

Power law behavior of the order parameter

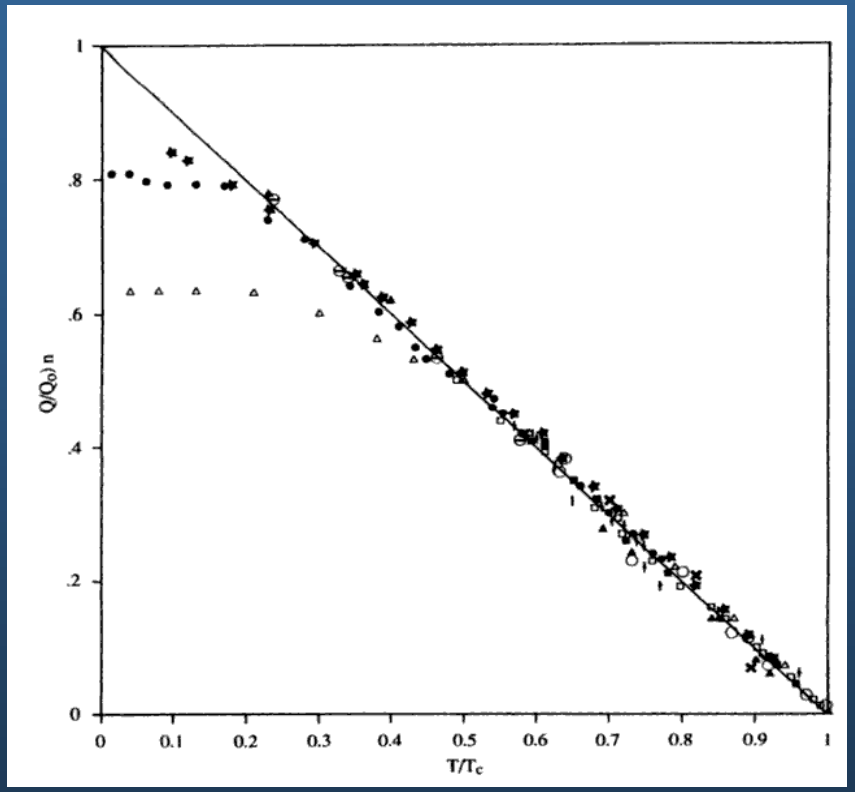

η/η(0K)

T/T_c

$\eta = \text{constant}\ (T_c - T)^{\beta}$

β = ½ (2nd order)

β = ¼ (tricritical)

Temperature evaluation of structural order parameters η for several 2nd order and tricritical phase transitions (from Salje, 1993)

Access to the order parameter via spontaneous strain

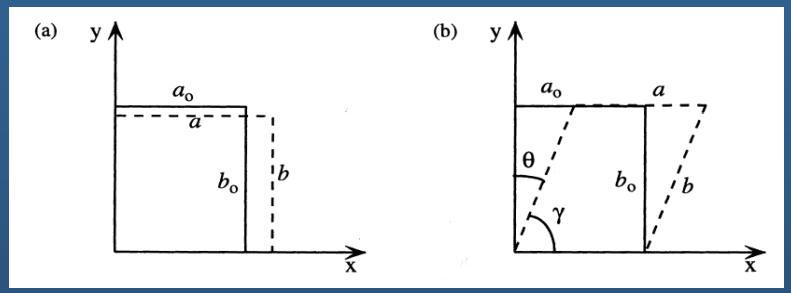

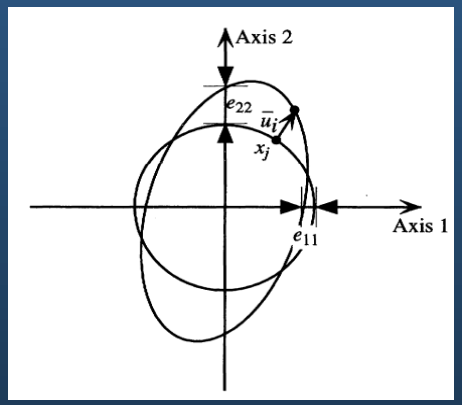

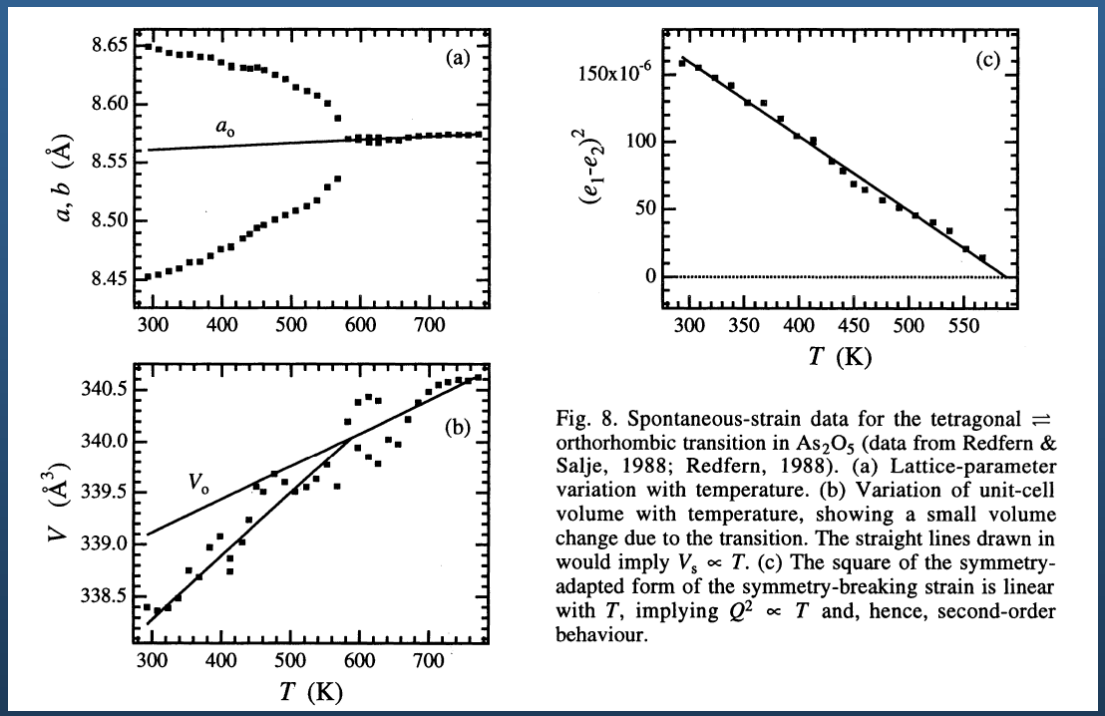

Fig. 8. Spontaneous-strain data for the tetragonal ⇌ orthorhombic transition in As_2O_5 (data from Redfern & Salje, 1988; Redfern, 1988). (a) Lattice-parameter variation with temperature. (b) Variation of unit-cell volume with temperature, showing a small volume change due to the transition. The straight lines drawn in would imply $V_s \propto T$. (c) The square of the symmetry-adapted form of the symmetry-breaking strain is linear with T, implying $Q^2 \propto T$ and, hence, second-order behaviour.

Carpenter, M.A., Salje, E.K.H. and Graeme-Barber, A. (1998) Spontaneous strain as a determinant of thermodynamic properties for phase transitions in minerals. Eur. J. Mineral., 10, 621–91

Access to the order parameter via symmetry/distortion modes

MAX PLANCK GESELLSCHAFT

Distorted Structure = High-symmetry Struct + "frozen" modes

distortion mode = Amplitude x polarization vector

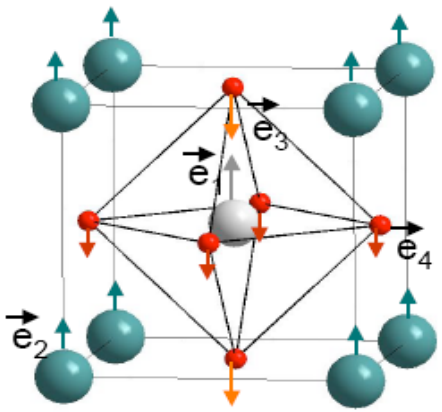

Description of a "mode":

$\vec{u}(\text{atoms}) = Q\,\vec{e}$

amplitude | polarization vector

$\mathbf{e} = (\vec{e}_1, \vec{e}_2, \vec{e}_3, \vec{e}_4)$

normalization: $|\vec{e}_1|^2 + |\vec{e}_2|^2 + |\vec{e}_3|^2 + 2\,|\vec{e}_4|^2 = 1$
(within a unit cell)

$$\mathbf{r}_j^{LS} = \mathbf{r}_j^{HS} + \sum_m c_m Q_m \boldsymbol{\varepsilon}(j|m)$$

Mois I. Aroyo, J. M. Perez-Mato and Danel Orobengoa, Universidad del Pais Vasco, Bilbao, Spain, THE BILBAO CRYSTALLOGRAPHIC SERVER: COMPUTER TOOLS FOR STRUCTURAL PHASE TRANSITIONS, lecture at "International School on the use and application of the Bilbao Crystallographic Server", 21-27 June 2009 Lekeitio (Spain)

The concept of polyhedral tilting, as an alternative way of describing distortions

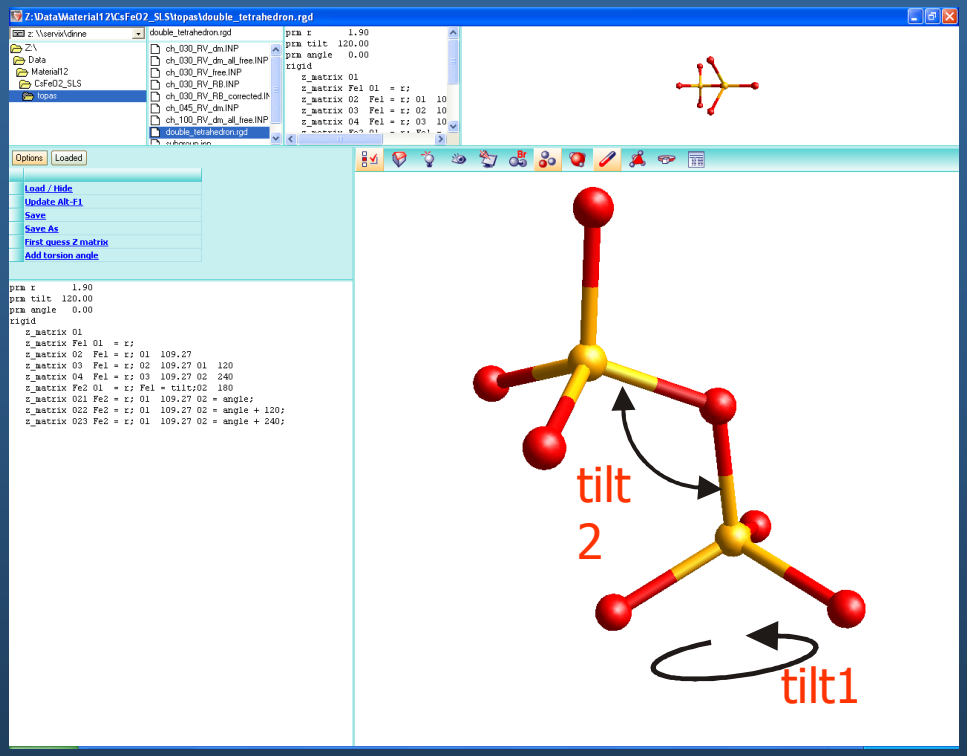


```
prm r       1.90
prm tilt1   120.00
prm tilt2     0.00
rigid
   z_matrix O1
   z_matrix Fe1 O1  = r;
   z_matrix O2  Fe1 = r; O1  109.27
   z_matrix O3  Fe1 = r; O2  109.27 O1  120
   z_matrix O4  Fe1 = r; O3  109.27 O2  240
   z_matrix Fe2 O1  = r; Fe1 = tilt1  ;O2  180
   z_matrix O21 Fe2 = r; O1  109.27 O2 = tilt2;
   z_matrix O22 Fe2 = r; O1  109.27 O2 = tilt2 + 120;
   z_matrix O23 Fe2 = r; O1  109.27 O2 = tilt2 + 240;
```

Double-tetrahedra-group with 3 internal deg. of freedom as main structural building unit :

- average Fe-O bond length
- tilt1 torsion angle between the tetrahedra
- tilt2 rotation angle of one tetrahedron with respect to the other

The concept of polyhedral tilting: Hazen, R.M. and L.W.Finger (1982) Comparative Crystal Chemistry: Temperature, Pressure, Composition and the Variation of Crystal Structure. London: J. Wiley & Sons, xv, 231 p.

Example I: $CsFeO_2$ (HT)

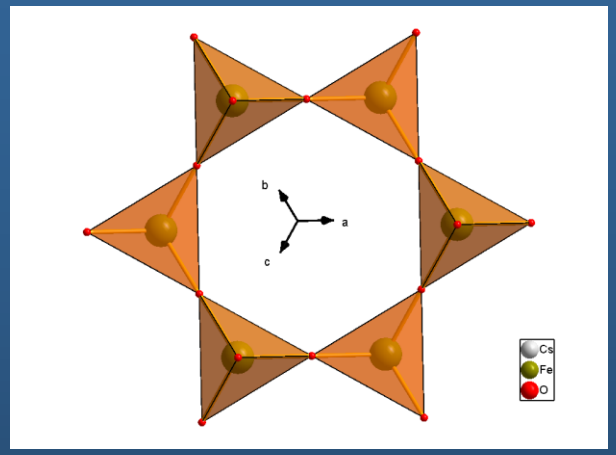

HT-phase

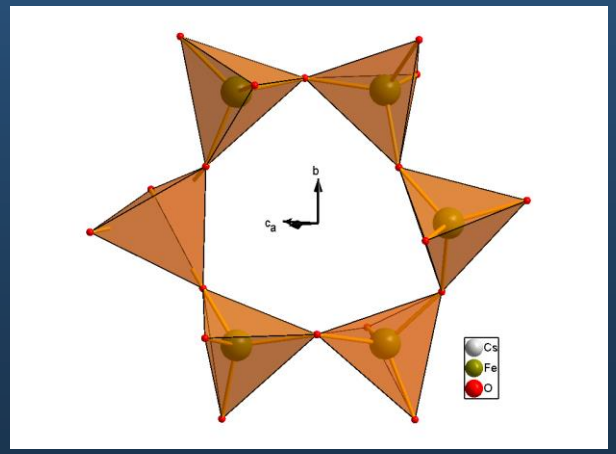

LT-phase

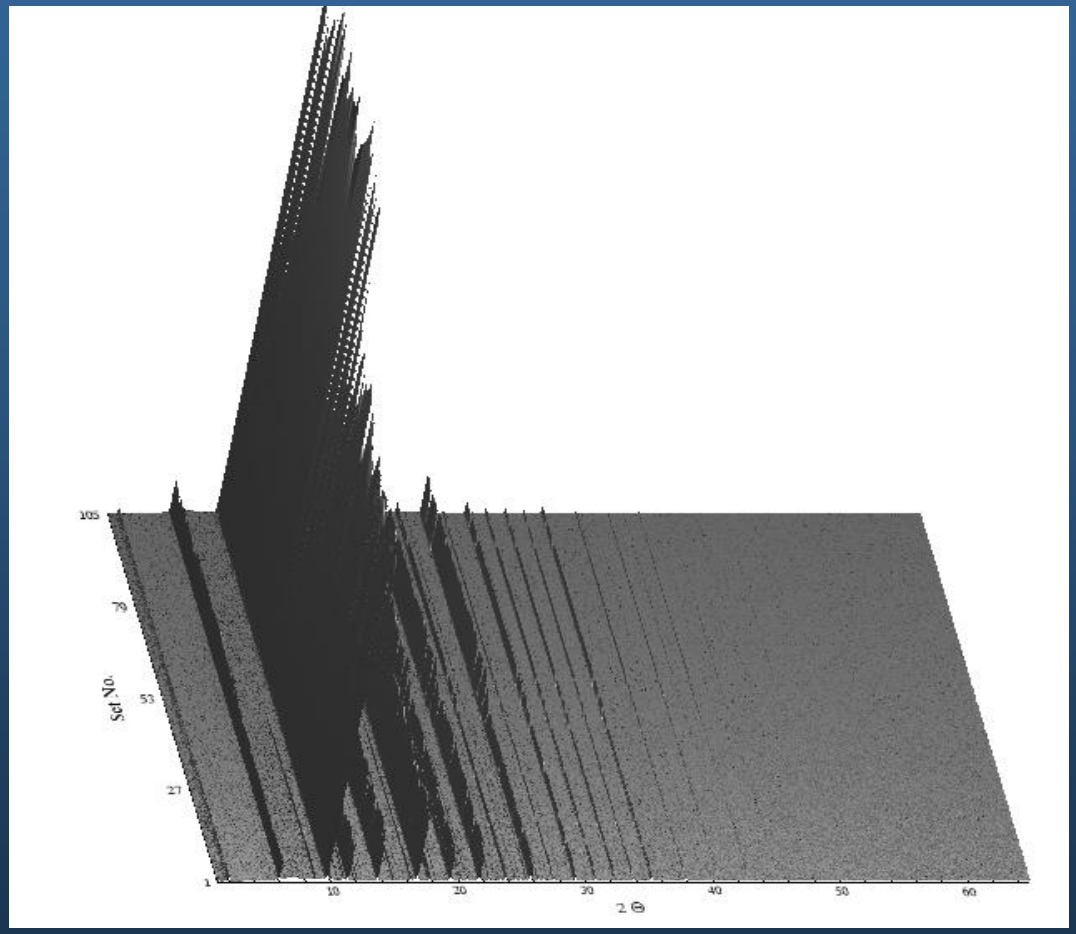

In-situ XRPD data of $CsFeO_2$, recorded at SLS with the 1D-Mythen-detector (4*10 seconds for each scan)

Structure of $RbFeO_2$, refined from a reticular pseudomerohedrally twinned crystal with six domains, J. Nuss, N. Z. Ali and M. Jansen, Acta Cryst. (2007). B63, 719-725

Aristotype: filled β-cristobalite structure

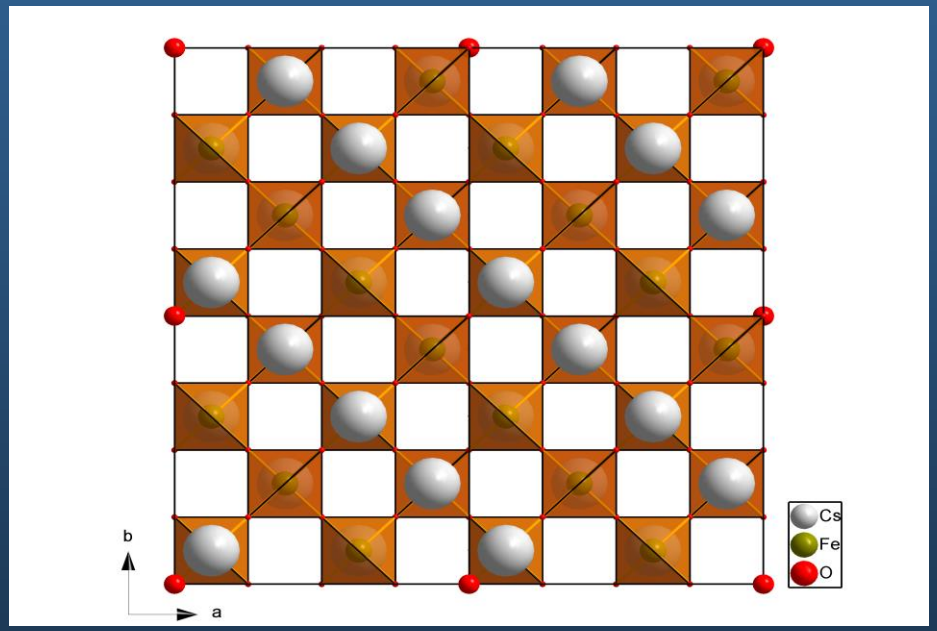

$CsFeO_2$ (HT)

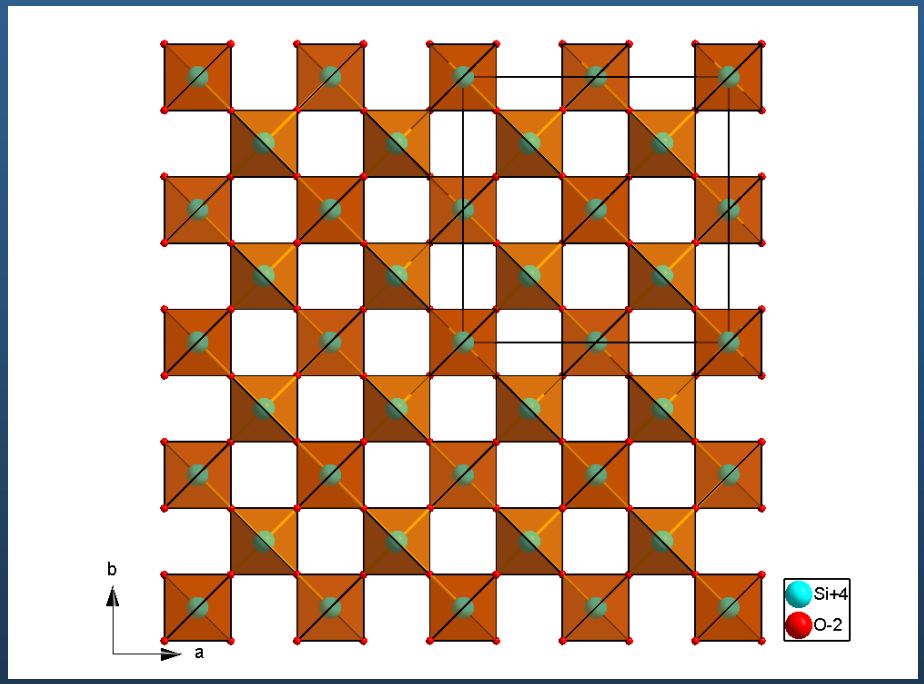

β-Cristobalite

Phase transformation of $CsFeO_2$

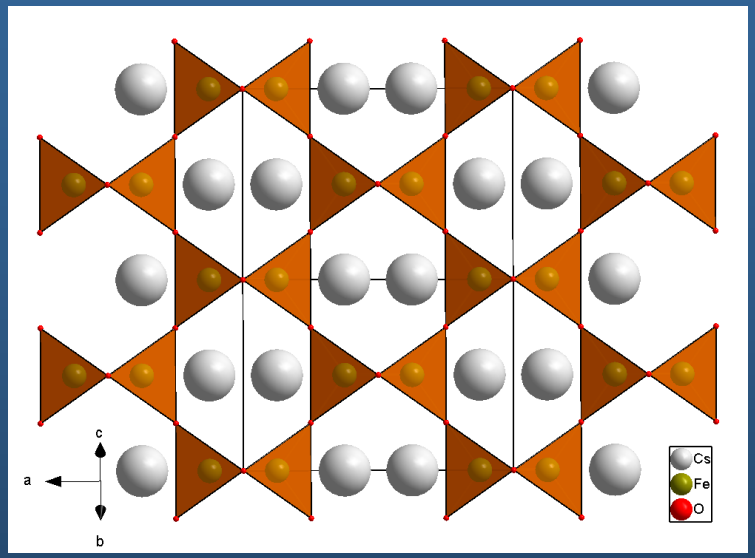

HT-phase
Fd-3m

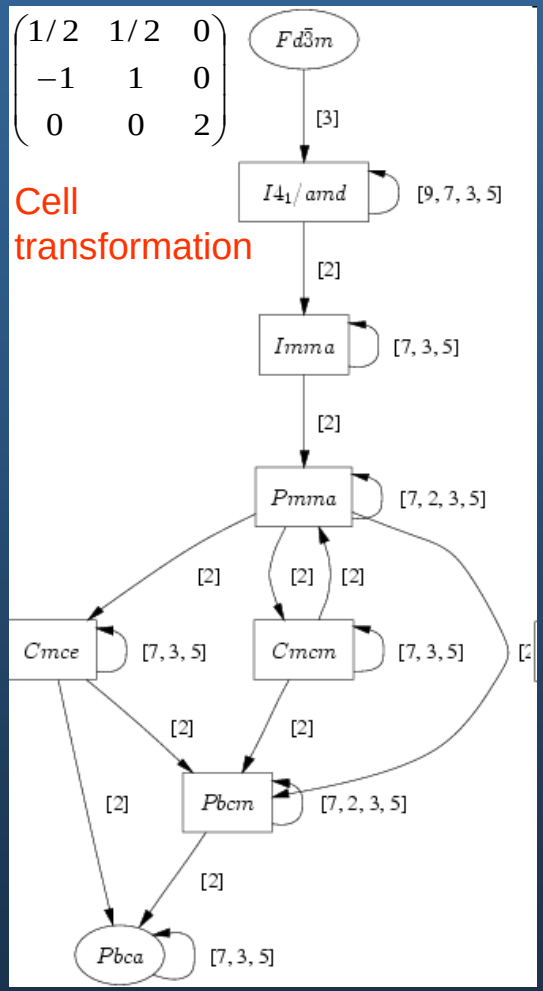

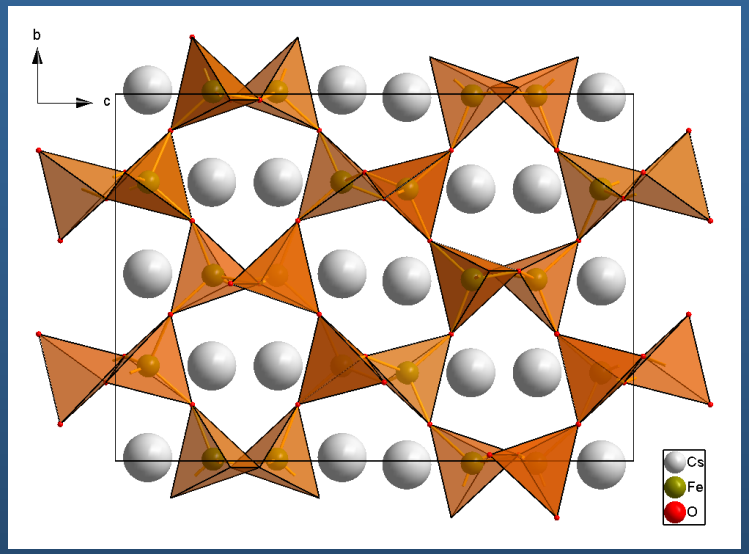

LT-phase
Pbca

Structural distortion mainly driven by
rotation of the Fe_2O_7 double tetrahedra & translation of Cs atoms

Distortion modes amplitudes of $CsFeO_2$

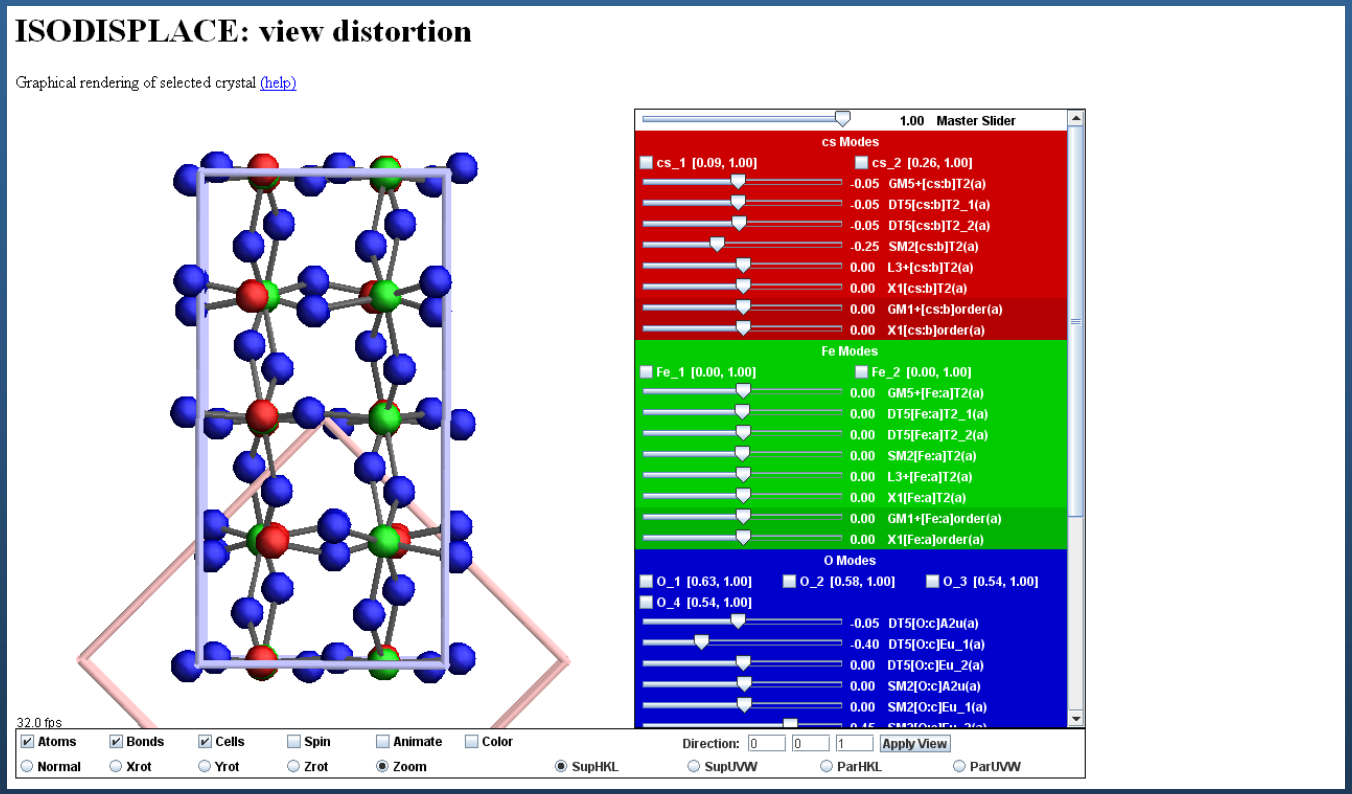

B. J. Campbell, H. T. Stokes, D. E. Tanner and D. M. Hatch, “ISODISPLACE: a web-based tool for exploring structural distortions”, J. Appl. Cryst. (2006). 39, 607-614

B. J. Campbell, J. S. O. Evans, F. Perselli, H. T. Stokes, "Rietveld refinement of structural distortion-mode amplitudes", IUCr Computing Commission Newsletter 8, 81-95 (2007).

M. Müller, R. E. Dinnebier, N. Z. Ali, B. J. Campbell and M. Jansen, Parameterized distortion modes versus rigid body Rietveld refinement, a case study of $CsFeO_2$, Materials Science Forum Vol. 651 (2010) pp 79-95.

(Main) distortion mode amplitudes of $CsFeO_2$

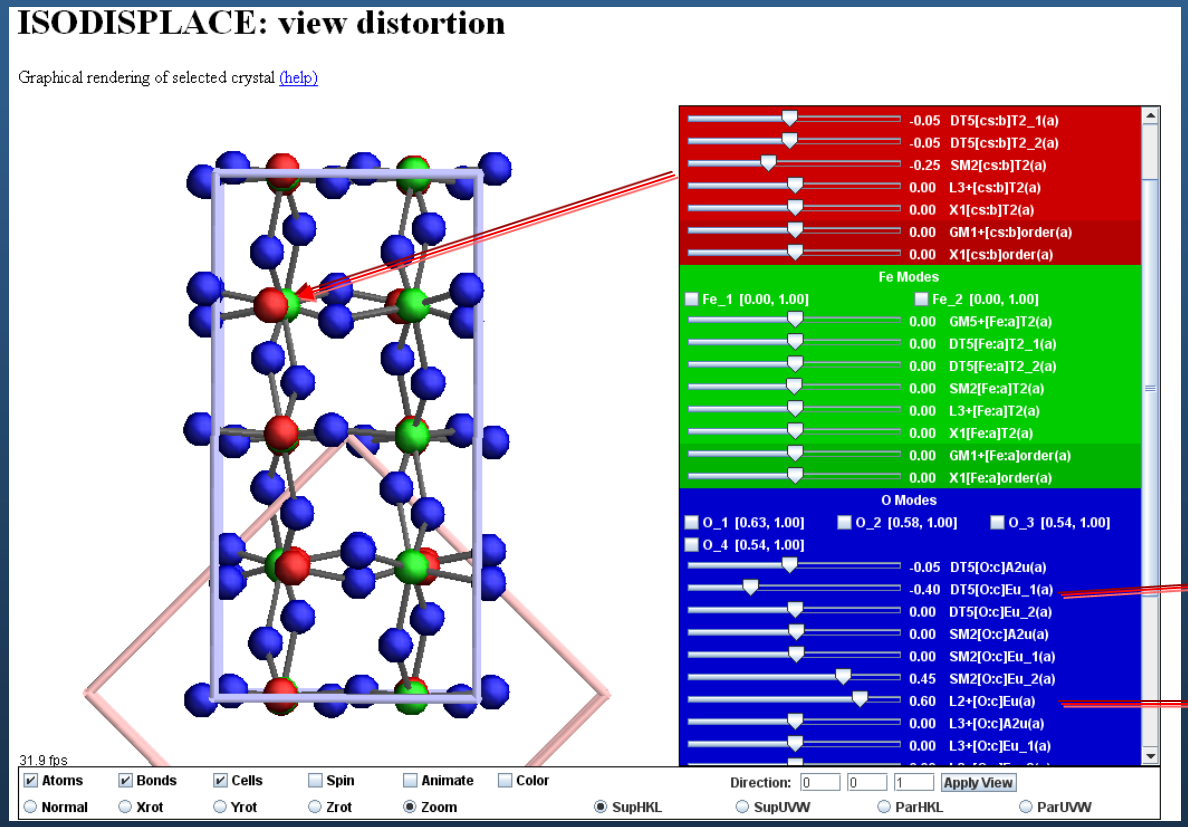

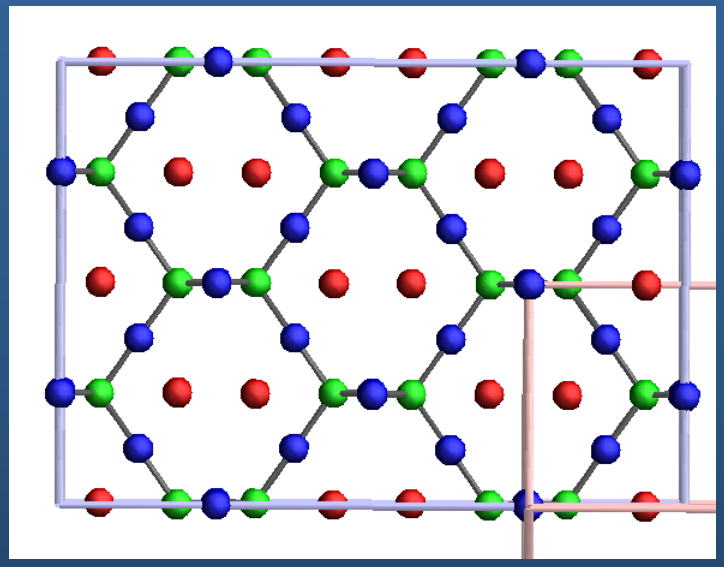

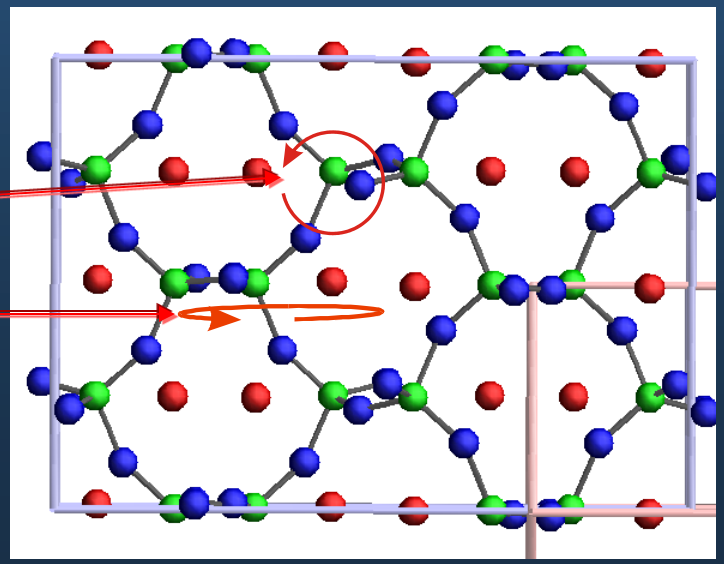

Difficulty: some modes are coupled !

Distortion modes & amplitudes for $CsFeO_2$

MAX PLANCK GESELLSCHAFT

1 Fd-3m[0,0,0]GM5+(a,0,0)[cs:b]T2(a) -0.0113(3)
2 Fd-3m[0,3/2,0]DT5(0,0,0,0,0,0,0,0,a,-0.414a,0.414a,a)[cs:b]T2_1(a) -0.0506(3)
3 Fd-3m[0,3/2,0]DT5(0,0,0,0,0,0,0,0,a,-0.414a,0.414a,a)[cs:b]T2_2(a) 0.1358(4)
4 Fd-3m[1/2,1/2,0]SM2(0,a,0,0,0,0,0,0,0,0,0,0)[cs:b]T2(a) -0.2839(4)
5 Fd-3m[1/2,1/2,1/2]L3+(0,0,0,0,a,-a,-a,a)[cs:b]T2(a) 0.0132(4)
6 Fd-3m[0,1,0]X1(0,a,0,0,0,0)[cs:b]T2(a) 0.0138(3)
7 Fd-3m[0,0,0]GM5+(a,0,0)[Fe:a]T2(a) -0.0020(5)
8 Fd-3m[0,3/2,0]DT5(0,0,0,0,0,0,0,0,a,-0.414a,0.414a,a)[Fe:a]T2_1(a) -0.1180(4)
9 Fd-3m[0,3/2,0]DT5(0,0,0,0,0,0,0,0,a,-0.414a,0.414a,a)[Fe:a]T2_2(a) 0.0168(4)
10 Fd-3m[1/2,1/2,0]SM2(0,a,0,0,0,0,0,0,0,0,0,0)[Fe:a]T2(a) -0.1948(5)
11 Fd-3m[1/2,1/2,1/2]L3+(0,0,0,0,a,-a,-a,a)[Fe:a]T2(a) -(
12 Fd-3m[0,1,0]X1(0,a,0,0,0,0)[Fe:a]T2(a) 0.0149(5)
13 Fd-3m[0,3/2,0]DT5(0,0,0,0,0,0,0,0,a,-0.414a,0.414a,
14 Fd-3m[0,3/2,0]DT5(0,0,0,0,0,0,0,0,a,-0.414a,0.414a,
15 Fd-3m[0,3/2,0]DT5(0,0,0,0,0,0,0,0,a,-0.414a,0.414a,
16 Fd-3m[1/2,1/2,0]SM2(0,a,0,0,0,0,0,0,0,0,0,0)[O:c]A2
17 Fd-3m[1/2,1/2,0]SM2(0,a,0,0,0,0,0,0,0,0,0,0)[O:c]Eu
18 Fd-3m[1/2,1/2,0]SM2(0,a,0,0,0,0,0,0,0,0,0,0)[O:c]Eu
19 Fd-3m[1/2,1/2,1/2]L2+(0,0,a,-a)[O:c]Eu(a) 0.611(2)
20 Fd-3m[1/2,1/2,1/2]L3+(0,0,0,0,a,-a,-a,a)[O:c]A2u(a) -
21 Fd-3m[1/2,1/2,1/2]L3+(0,0,0,0,a,-a,-a,a)[O:c]Eu_1(a)
22 Fd-3m[1/2,1/2,1/2]L3+(0,0,0,0,a,-a,-a,a)[O:c]Eu_2(a)
23 Fd-3m[0,1,0]X1(0,a,0,0,0,0)[O:c]A2u(a) 0.001(2)
24 Fd-3m[0,1,0]X1(0,a,0,0,0,0)[O:c]Eu(a) 0.046(2)

Multiple simultaneous Rietveld refinements

MAX PLANCK GESELLSCHAFT

Parameterization of lattice strains, distortion modes and polyhedral tilting in dependene on temperature by <u>multiple simultaneous Rietveld refinement</u>

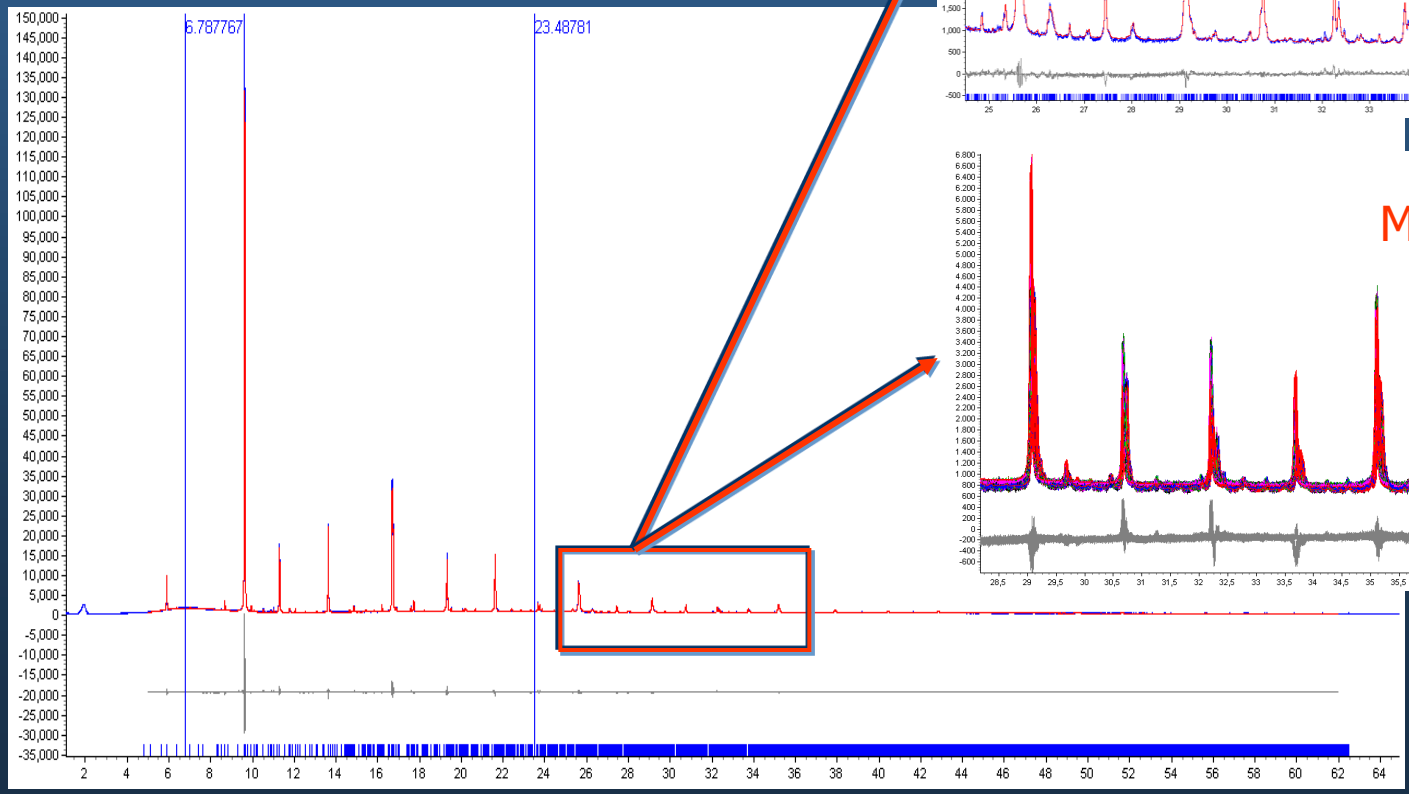

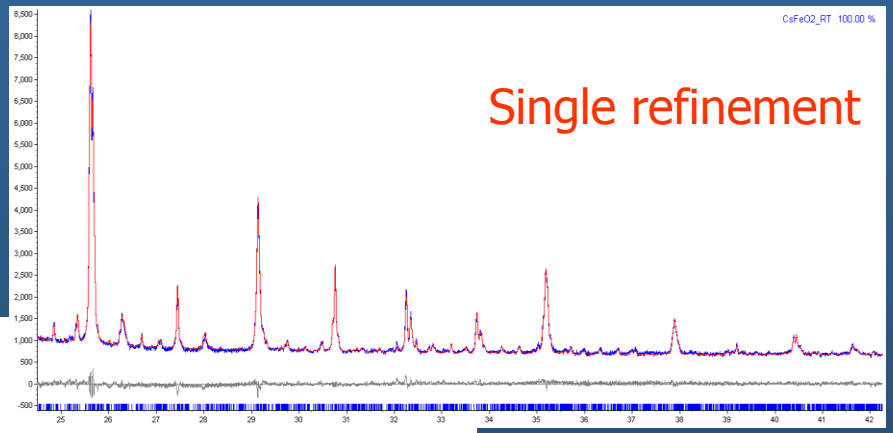

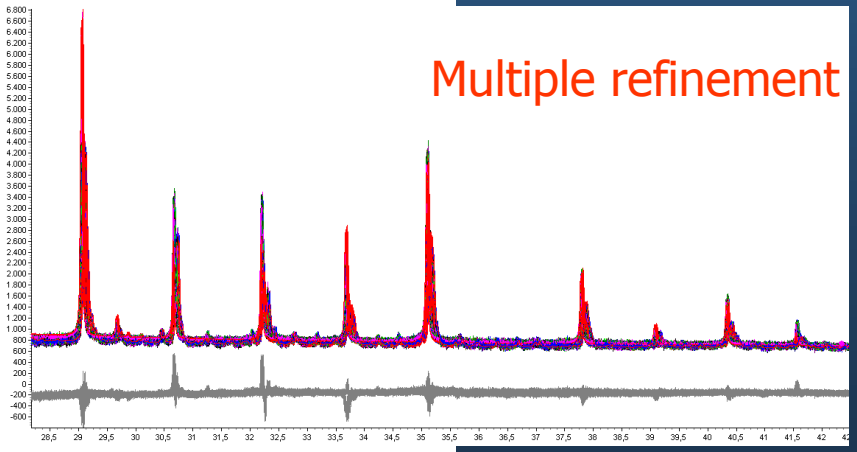

Parameterised strain modes in dependence on temperature

MAX PLANCK GESELLSCHAFT

Low symmetry orthorhombic phase (supercell)

$$e_{11s} = \frac{a_s}{a_{s0}} - 1 = \frac{a_s}{a_{p0}/\sqrt{2}} - 1$$

$$e_{22s} = \frac{b_s}{b_{s0}} - 1 = \frac{b_s}{\sqrt{2}a_{p0}} - 1$$

$$e_{33s} = \frac{c_s}{c_{s0}} = \frac{c_s}{2a_{p0}} - 1$$

High symmetry cubic phase

$$e_{11p} = e_{22p} = e_{33p} \quad \text{and} \quad e_{12p} = e_{23p} = e_{13p} = 0$$

$$e_{11p} = e_{22p} = \varepsilon_{\Gamma_1^+} - \frac{1}{2}\varepsilon_{\Gamma_3^+} = \frac{a_p}{a_{p0}} - 1 = \frac{b_p}{a_{p0}} - 1$$

$$e_{33p} = \varepsilon_{\Gamma_1^+} + \varepsilon_{\Gamma_3^+} = \frac{c_p}{a_{p0}} - 1$$

$$e_{12p} = e_{21p} = \frac{1}{2}\varepsilon_{\Gamma_5^+} = \frac{\pi}{2} - \gamma_p$$

$$e_{11s} = e_{11p} + e_{12p}$$

$$e_{22s} = e_{11p} - e_{12p}$$

$$e_{33s} = e_{33p}$$

relationship between the strain of the supercell and the cubic strain

$$\text{If } (\mathrm{T} < T_{crit}) \text{ then } \varepsilon_\Gamma(T) = f_\Gamma (T_{crit} - T)^{\beta_\Gamma}, \text{ else } \varepsilon_\Gamma = 0$$

Parameterised strain modes in dependence on temperature

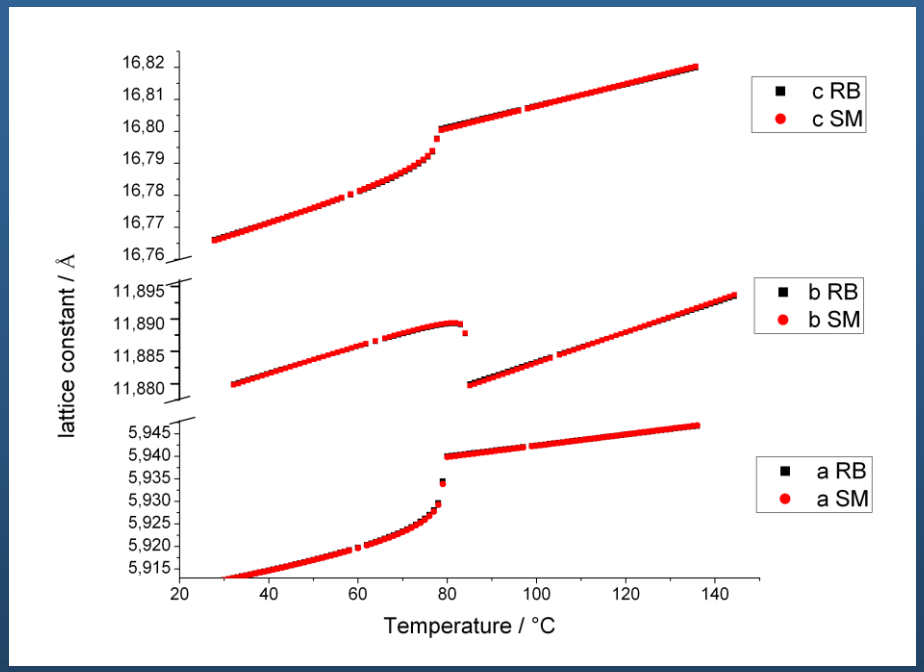

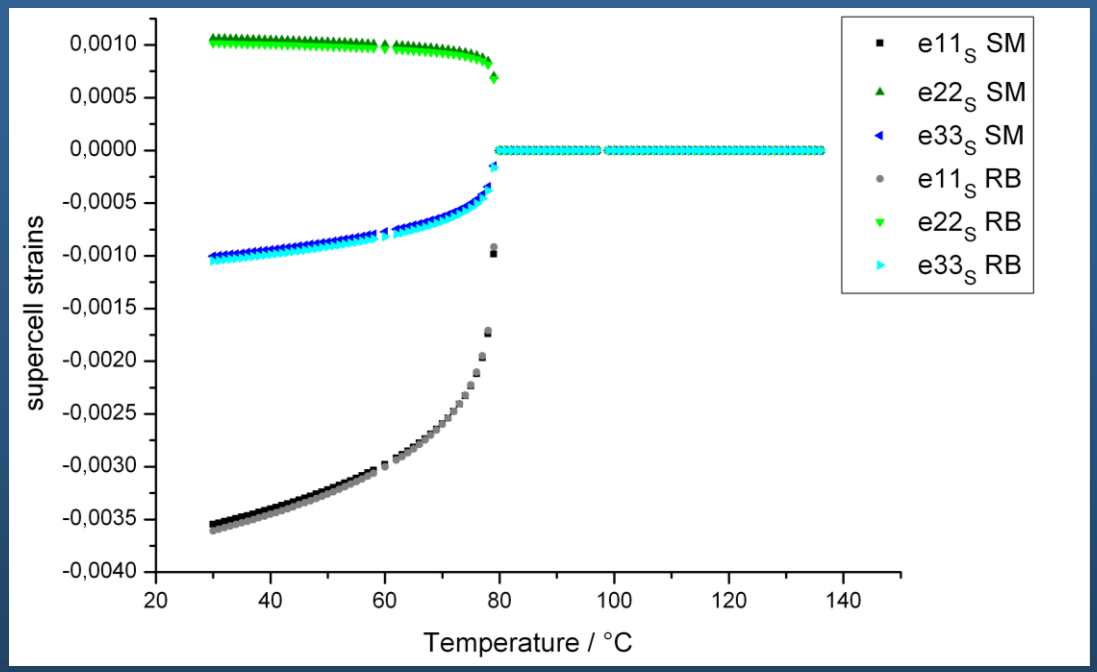

Temperature-dependent supercell parameters for $CsFeO_2$ as calculated from parametrically-refined power-law models of the strain parameters.

Temperature-dependent supercell strains for $CsFeO_2$ as calculated from their parametrically-refined power-law models

Order parameter η derived from parametric Rietveld refinement

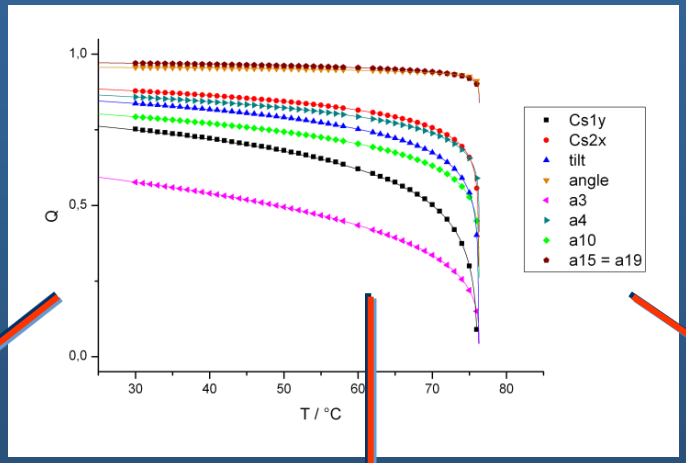

$$\eta = A(T_c - T)^{\beta}$$
$$\beta = [0.07..0.125]$$

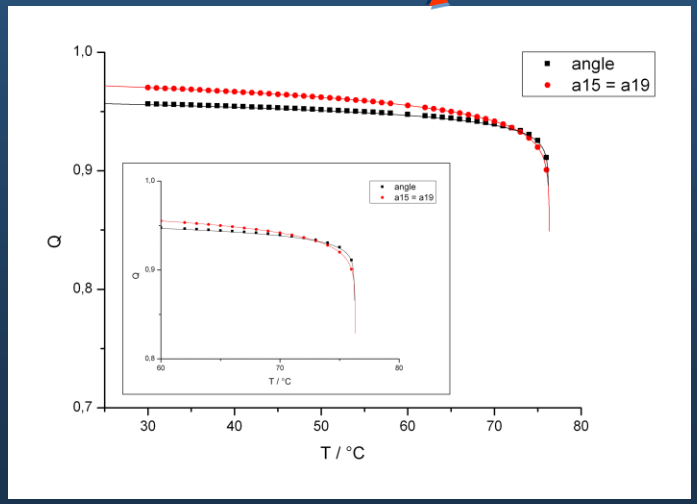

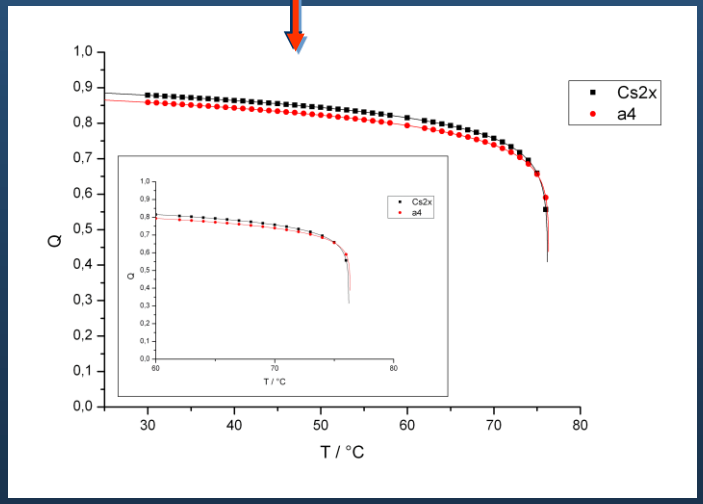

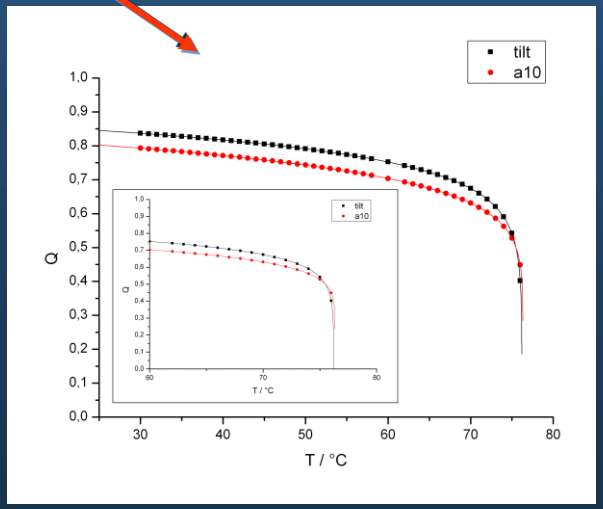

Parameterised distortion modes versus polyhedral tilting in dependence on temperature

Order parameter η derived from parametric Rietveld refinement

MAX PLANCK GESELLSCHAFT

distortion mode	critical exponent	rigid body	critical exponent
a3	0.27 (1)	Cs 1 y	0.21(1)
a4	0.08(1)	Cs 2 x	0.08(1)
a10	0.11 (1)	tilt-1	0.125(2)
a15 / a19	0.014(1)	tilt-2	0.009(1)
ε_1	0.125(6)	ε_1	0.12(1)
ε_2	0.03(1)	ε_2	0.03(1)
ε_3	0.16(1)	ε_3	0.15(1)
ε_S	0.23(1)	ε_S	0.23(1)

$$\eta = A(T_c - T)^{\beta}$$
$$\beta = [0.07..0.125]$$

Some results:

- order parameters derived from polyhedral tilting and distortion modes are equivalent.
- The spontaneous strain e_s is coupled linear-quadratic with the a10 distortion mode and the angle tilt-1: $e_s \sim \eta^2$
- The spontaneous strain e_s is coupled linear-cubic for a4 and Cs2x : $e_s \sim \eta^3$
- The phase transition is clearly of first order.

Example II: As_2O_5 (HP)

$$a = \sqrt[3]{V(P)} = \left[V_{0a} \left(1 + \frac{K'_a P}{K_{0a}} \right) \right]^{-\frac{1}{3K'_a}}$$

"Linear" Murnagham parameterisation of lattice parameters in dependence on high pressure.

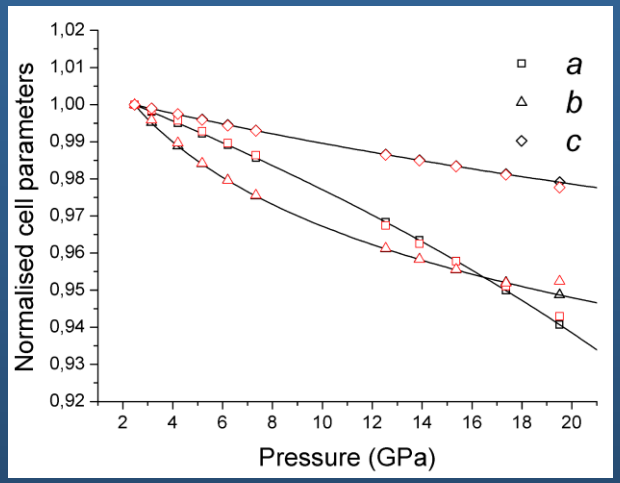

Comparison of relative unit cell parameters in dependence on pressure obtained by independent refinement (red) and by Murnaghan parameterisation (black).

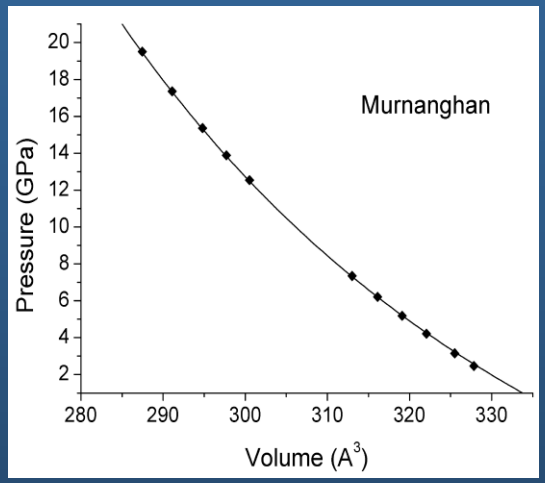

Resulting EoS from parameterised lattice parameters

Ivan Halasz, Robert E. Dinnebier, and Ross Angel, "Advantages of using parametric Rietveld refinement for the evaluation of powder diffraction patterns collected in dependence on pressure.", 2010, J. Appl. Cryst.

As_2O_5 (HP) polynomial parameterization of coordinates

$$a = A_0 + A_1 P + A_2 P^2 + A_3 \sqrt{P}$$

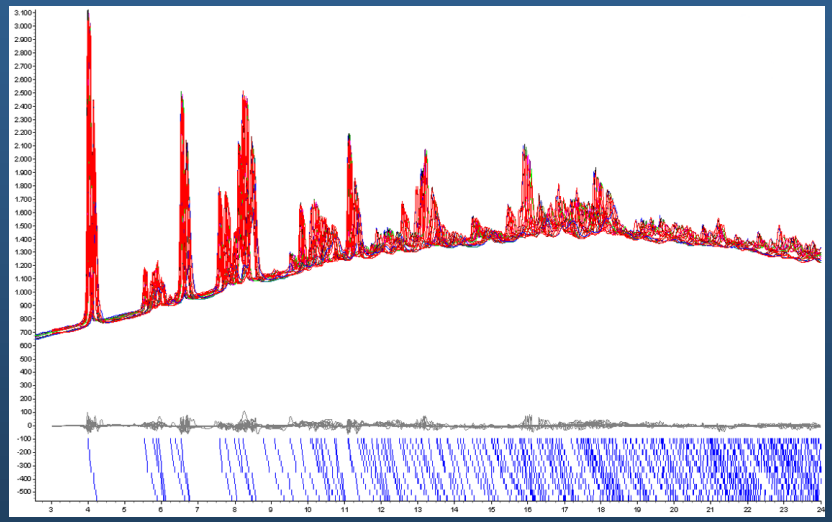

Joint plot of all the powder patters of As_2O_5 in dependence o pressure refined with polynomial parameterisation of coordinates

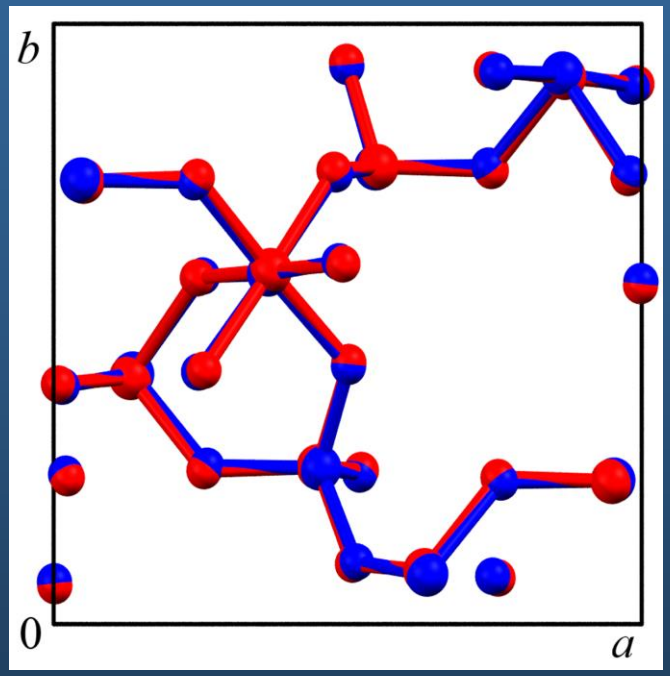

Overlapped projections of the crystal structures of As_2O_5 obtained by (red) independent refinement and (blue) refinement using polynomial parameterisation of coordinates at the pressure of 20 GPa.

Example III: $CuInSe_2$

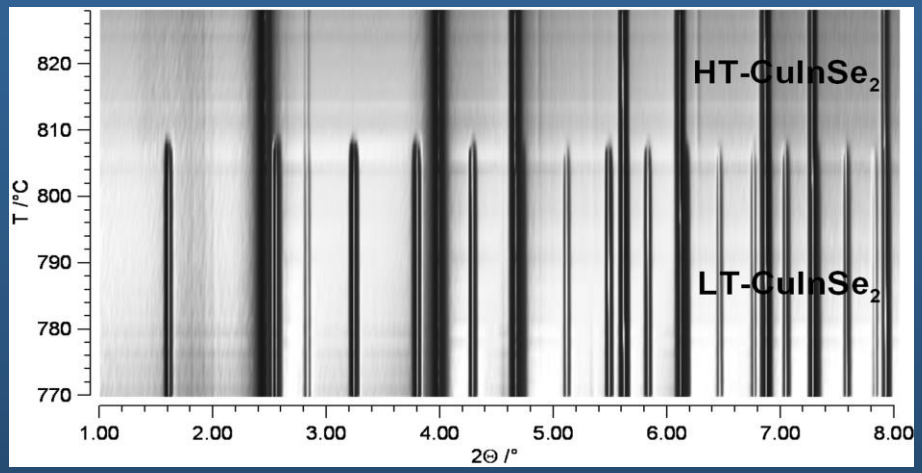

$F\bar{4}3m$

$I\bar{4}2d$

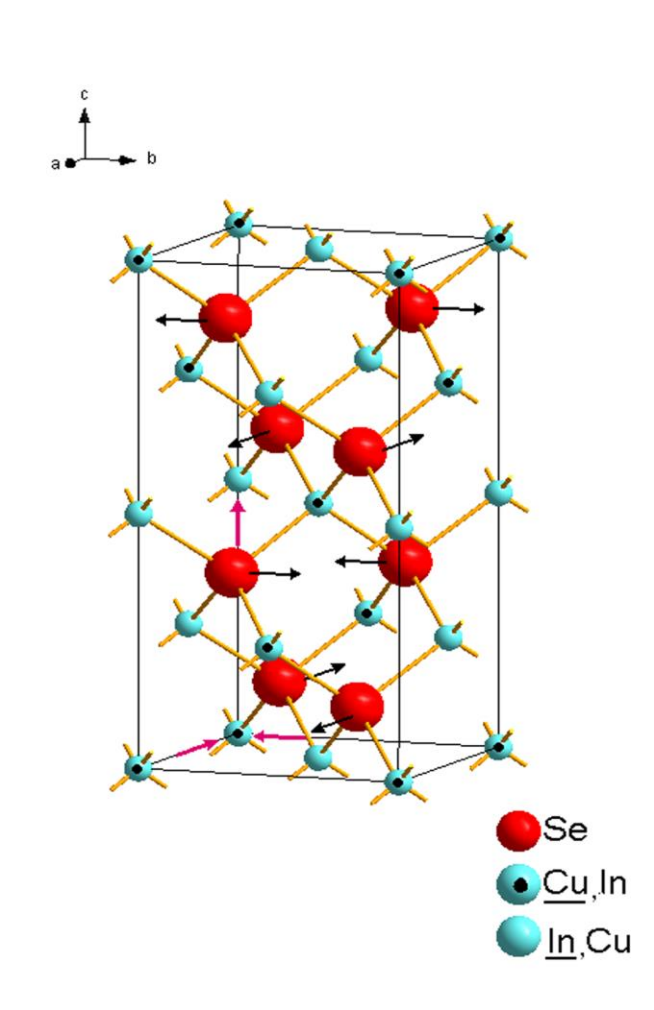

phase transition is driven by:

1) anti site ordering of copper and indium atoms
2) translation of slenium atoms

S. Schorr, G. Geandier, *Cryst. Res. Technol.*, **2006** 41(5), 450-467.

The modes

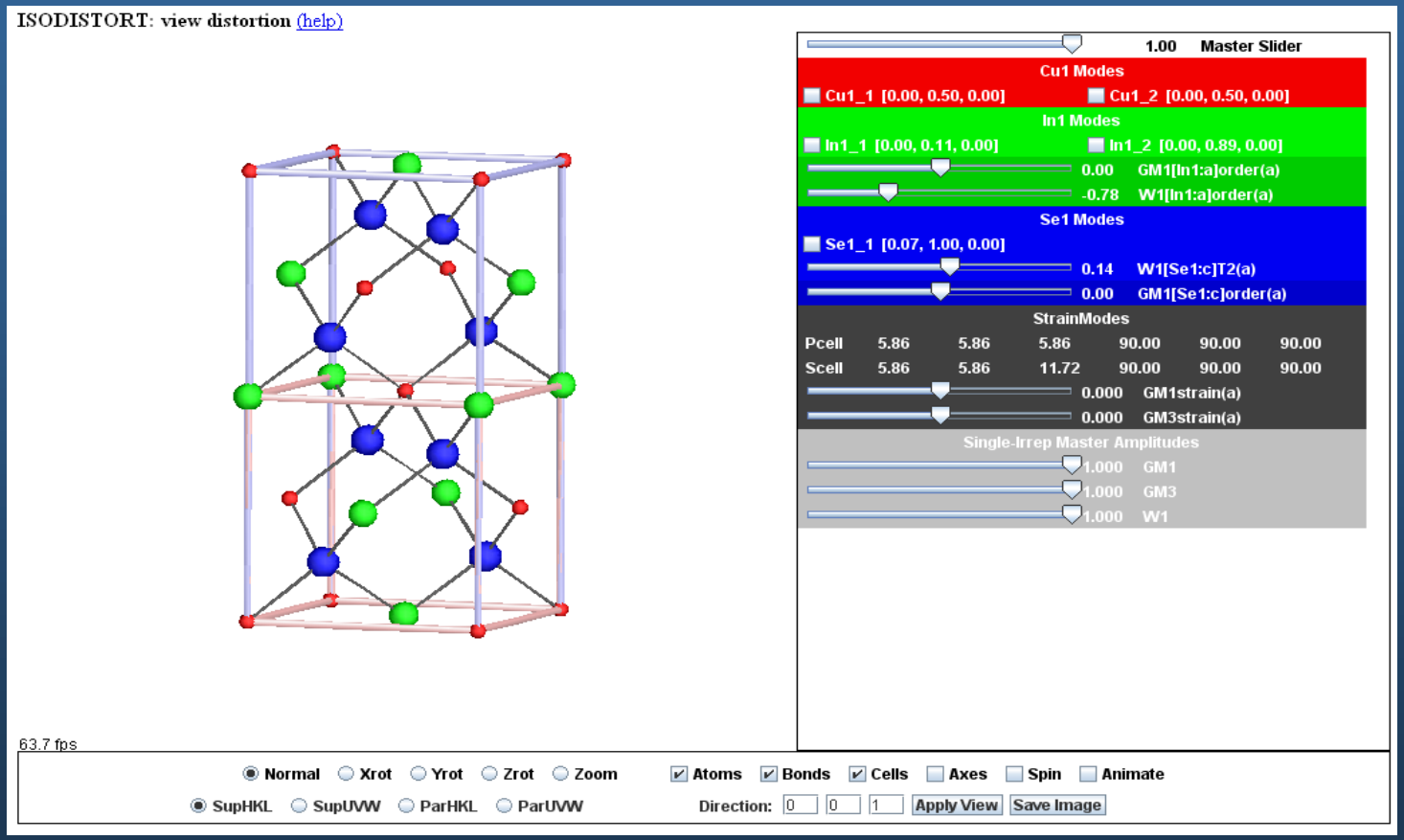

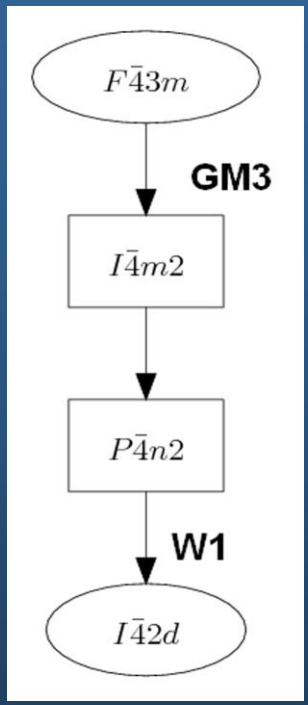

three different types of modes: strain, displacive, occupancy

ISODISTORT: Campbell B. J., Stokes H. T., Tanner D. E. and Hatch D. M. (2006). J. Appl. Cryst. **39**, 607-614
Subgroupgraph: S. Ivantchev, E. Kroumova, G. Madariaga, J. M. Perez-Mato, M. I. Aroyo, *J. Appl. Cryst.* **2000**, 33, 1190-1191.

Parameterization of strain, displacive, and occupancy modes

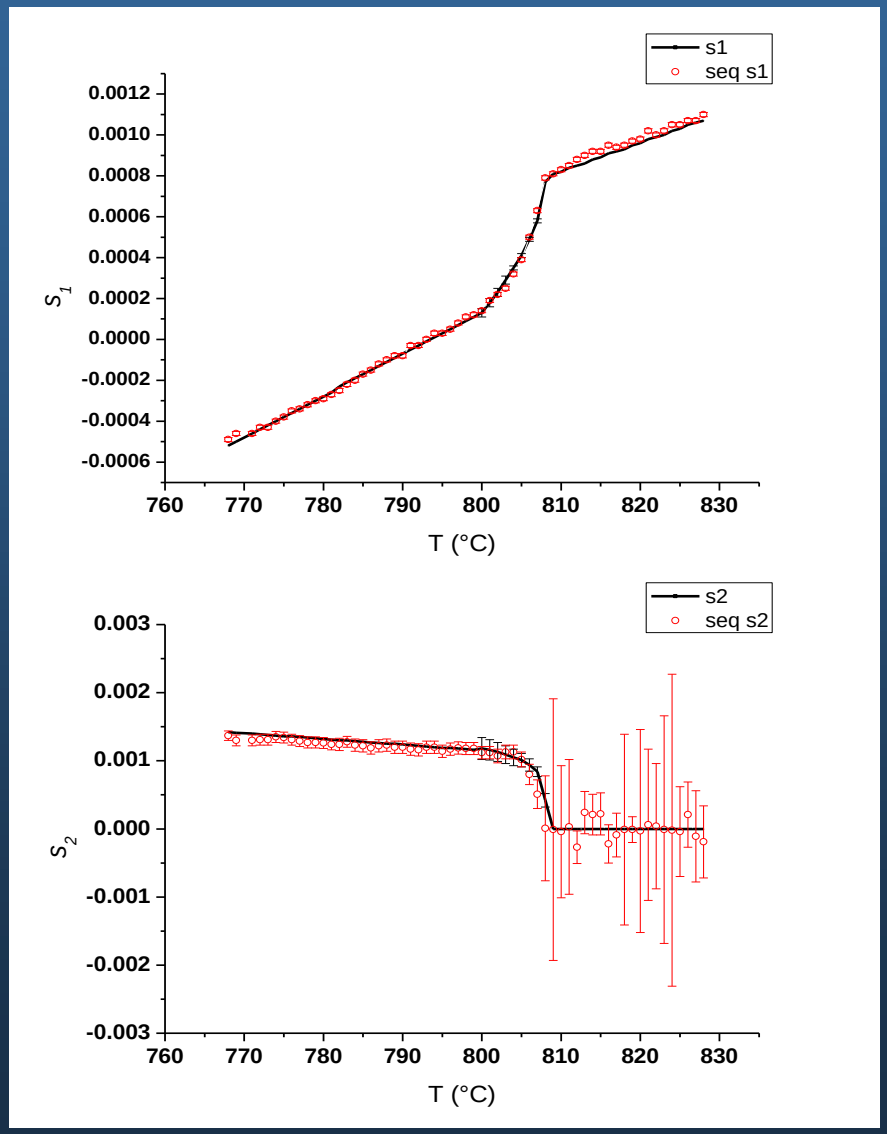

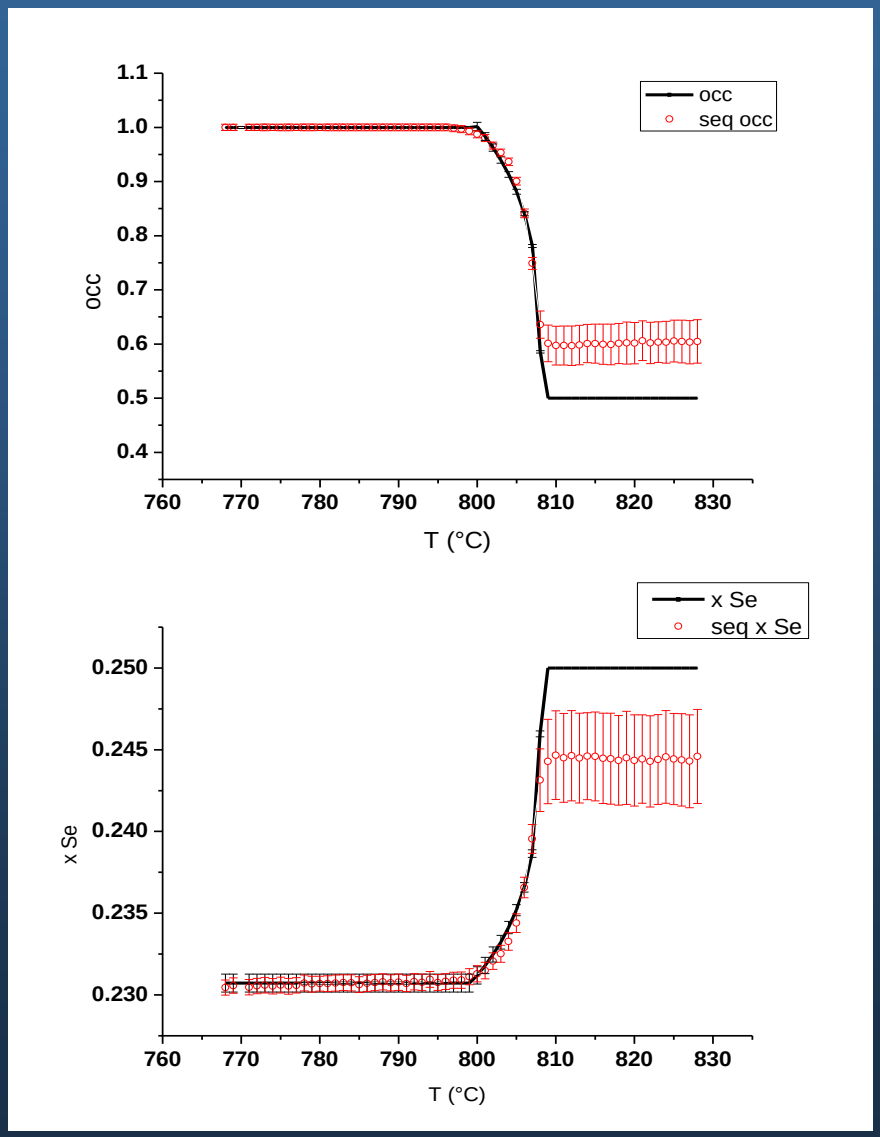

Some results of parametric refinement

mode	critical exponent	
a1	0.24(1)	tricritical displacive phase transition
s1	0.49(2)	linear quadratic coupling
s2	0.16(5)	maybe order-disorder transitions?
occupancy	0.28(1)	3D ordering phenomenon (Ising model)
temperature factor	**critical exponent**	
cations	0.24(1)	same as *a1*
anion	0.49(2)	same as *s1*

Þ phase transition combines an order-disorder (cation lattice) and a displacive (anion lattice) transition

Towards automation: Powder 3D[1] - Parametric

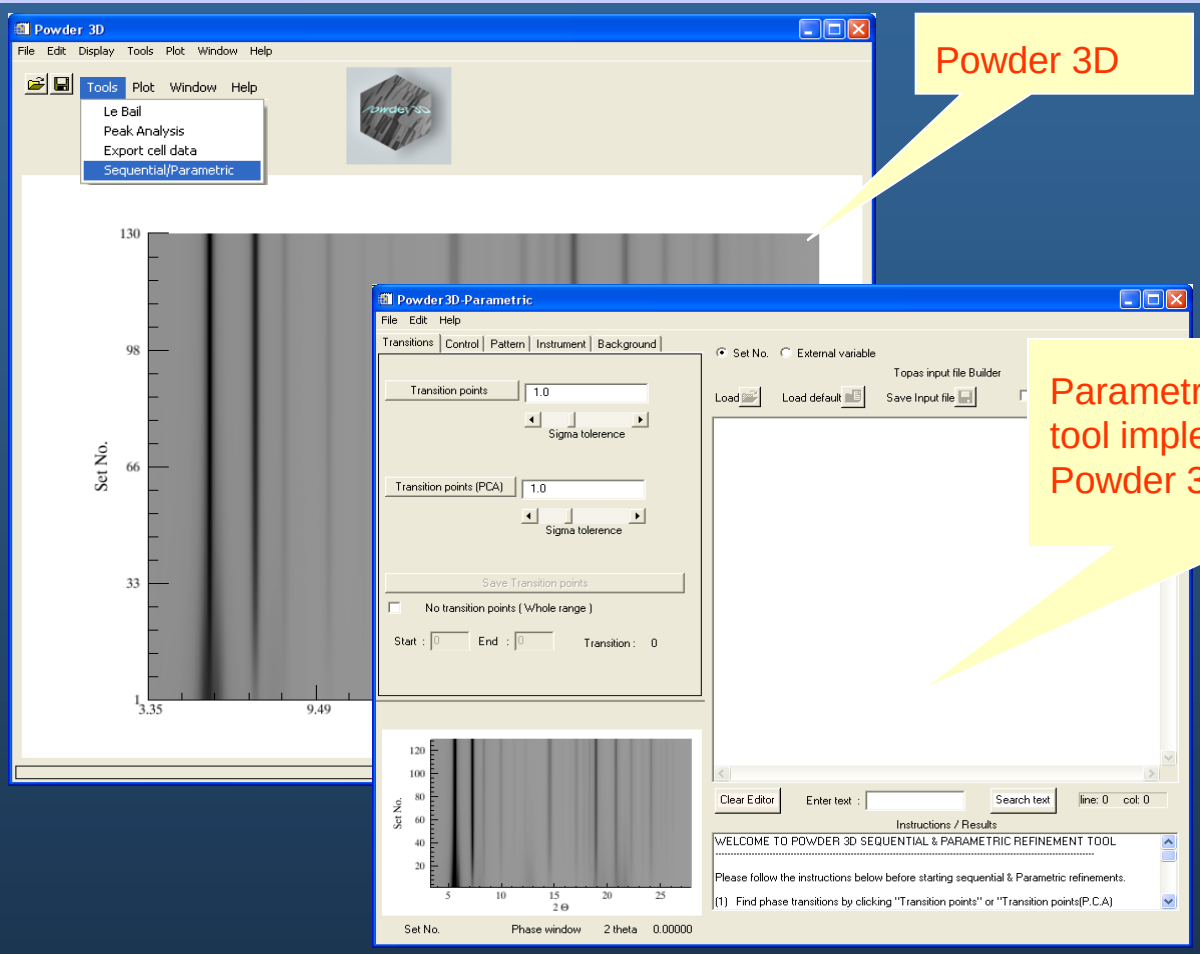

Powder 3D

Parametric refinement [2] tool implemented in Powder 3D

P. Rajiv, R. E. Dinnebier, M. Jansen, „Powder 3D Parametric"- A program for automated sequential and parametric Rietveld refinement using TOPAS, 2010, Mat. Science Forum

[1] B.Hinrichsen, R.E.Dinnebier and M. Jansen, *Z. Krist,* (2004) **23**, 231-236.
[2] .G.Stinton , J. Evans, *J. Appl. Cryst,* (2007) **40**, 87-95

Handling TOPAS input files with Powder3D-Parametric

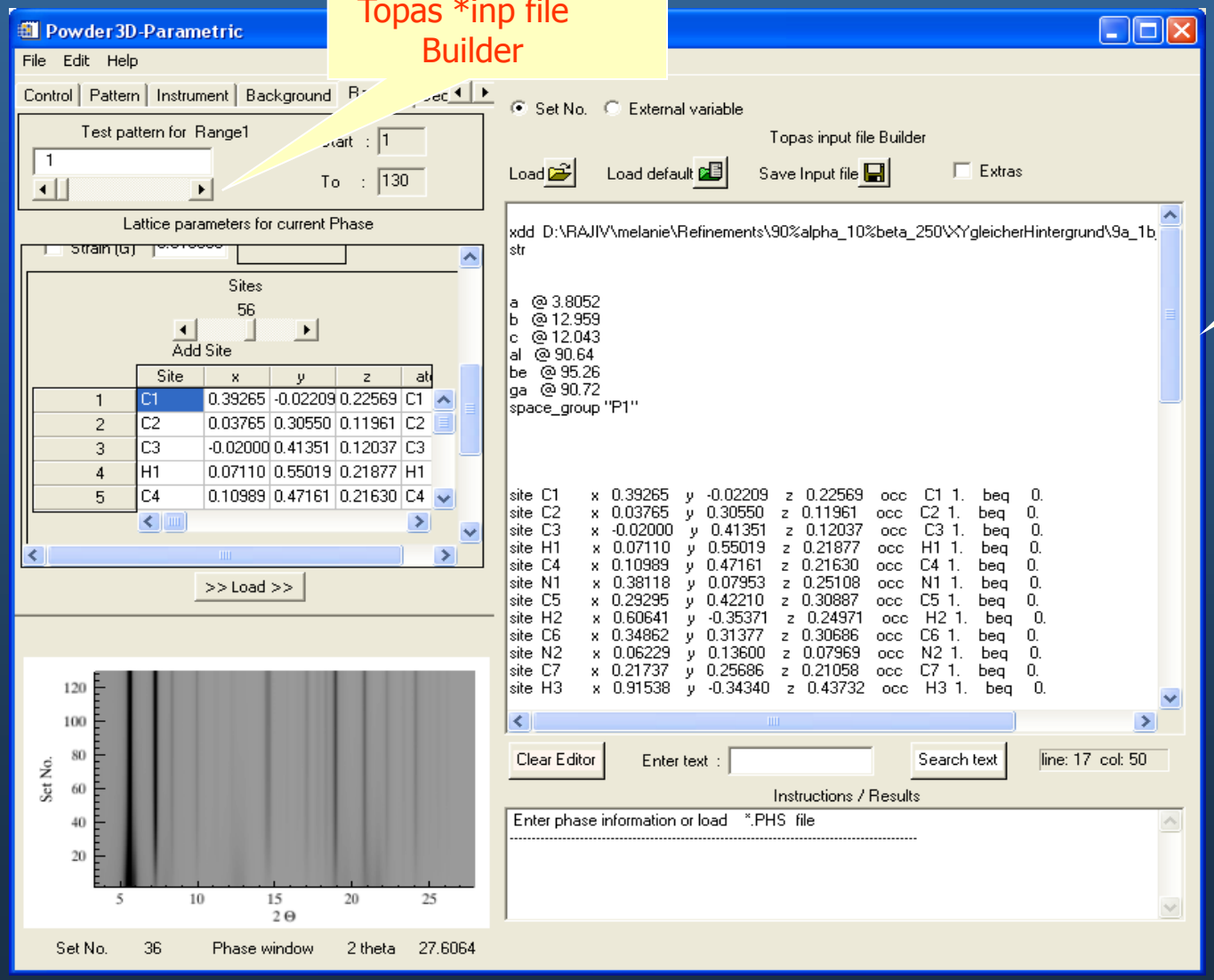

Sequential refinements with Powder3D-Parametric

MAX PLANCK GESELLSCHAFT

Sequentially refined parameters

Graphics

Applications
- Reaction kinetics
- Lattice parameters
- Distortion

Models:
Linear, quaratic, cubic, Avrami,..etc.

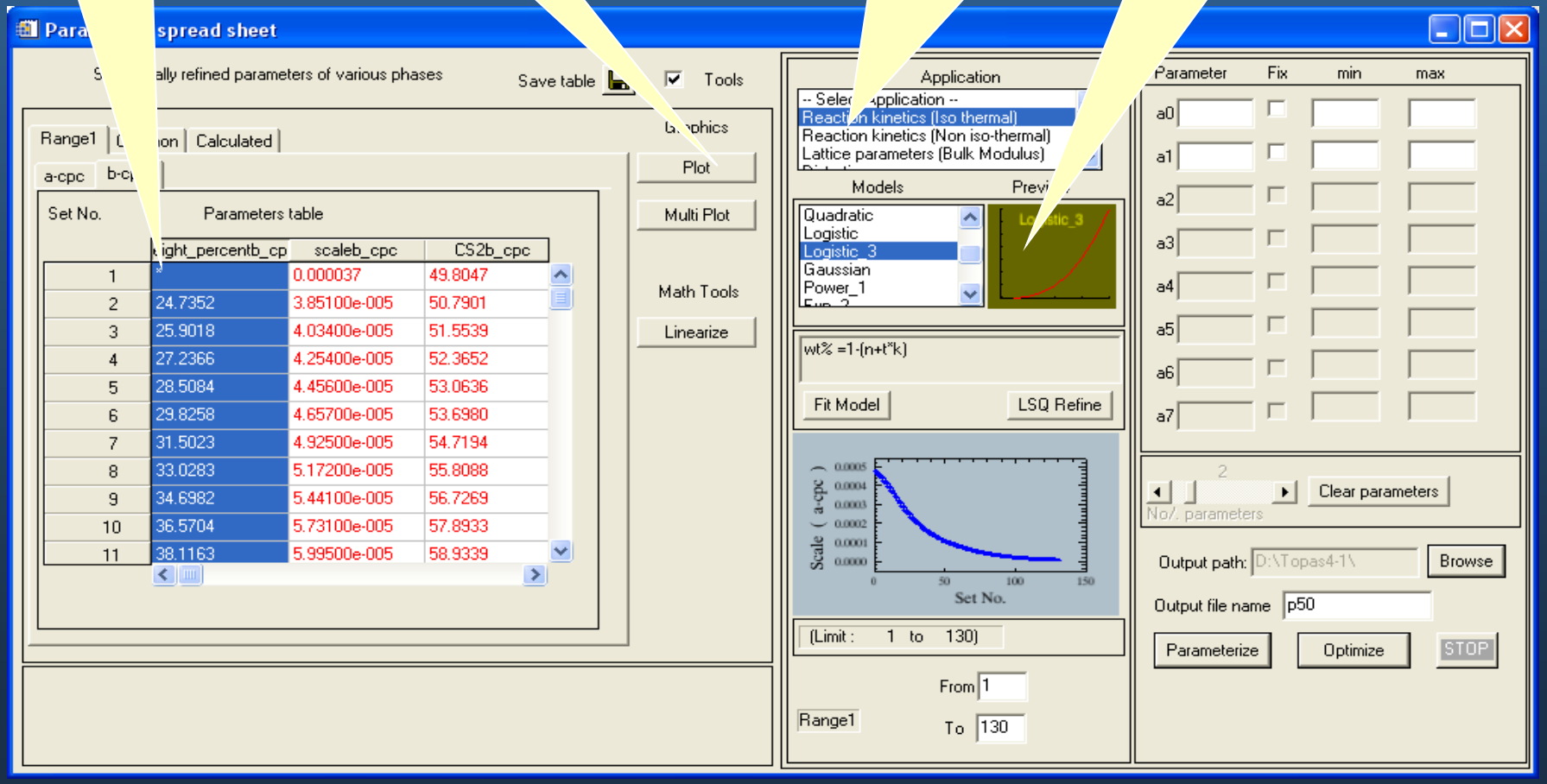

Parametric refinements of CuPc (isothermal) with Powder3D-Parametric

MAX PLANCK GESELLSCHAFT

90% alpha and 10% beta CUPC at 250°C

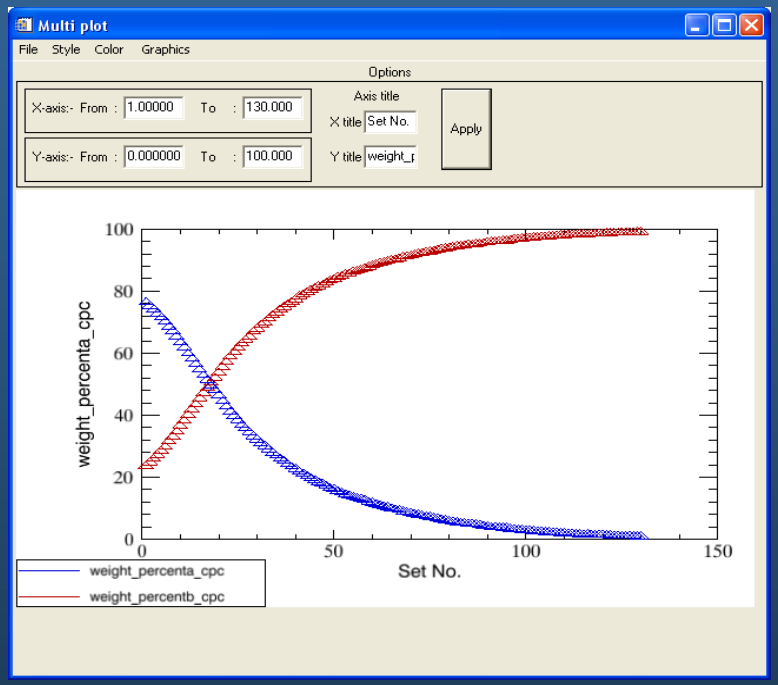

Weight fraction Vs Time at 250°C

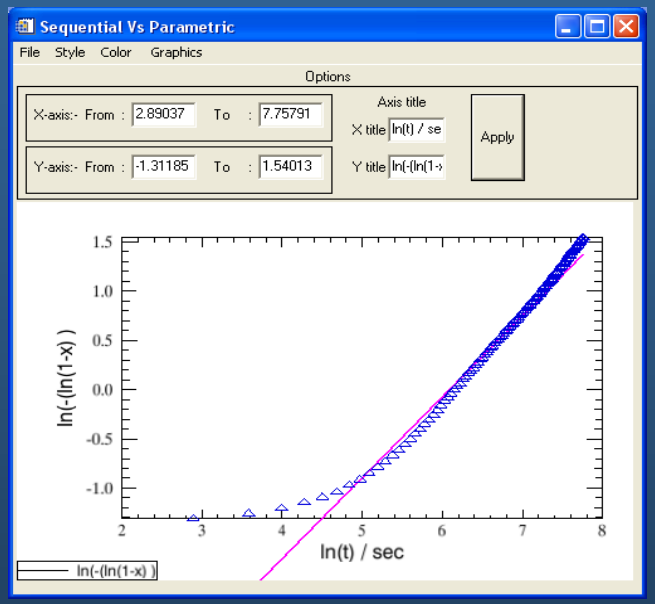

Patterns 1-130 of 130

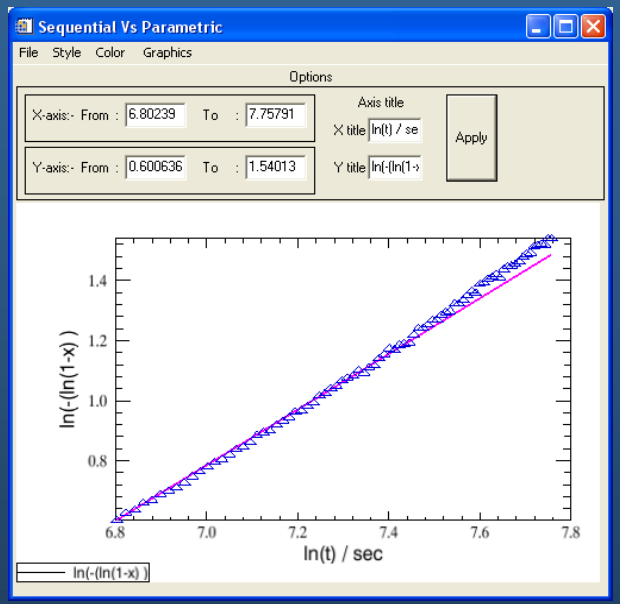

Patterns 50-130 of 130

Avrami paramameters for parametric refinements:

n = 0.82163 (1-130)
k = 0.00227

n = 0.92622 (50-130)
k =0.00213

sequential refinements for comparison:

n = 0.97
k = 0.00178

"True" disorder from XRPD by MEM and charge flipping

MAX PLANCK GESELLSCHAFT

The method of MEM

Entropy:

$$S = -\sum_{j=1}^{N} \rho_j \log\left(\frac{\rho_j}{\omega_j}\right)$$

N	number of pixels in the unit cell;
ρ_j	electron density in pixel *j*;
ω_j	initial value of the electron density or prior

Collins (1982)

The method of charge flipping with histogram matching

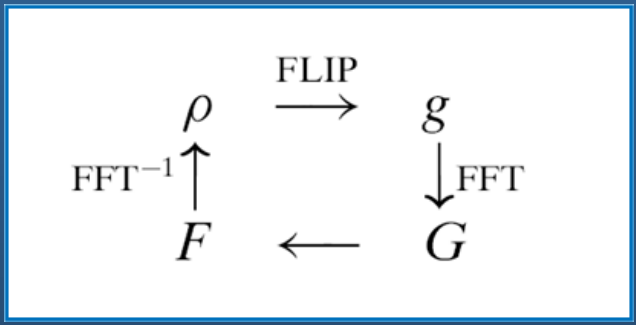

$$\rho(xyz) = \frac{1}{V}\sum_{hkl}|F_{hkl}|\cos(2\pi(hx+ky+lz)-\phi_{hkl})$$

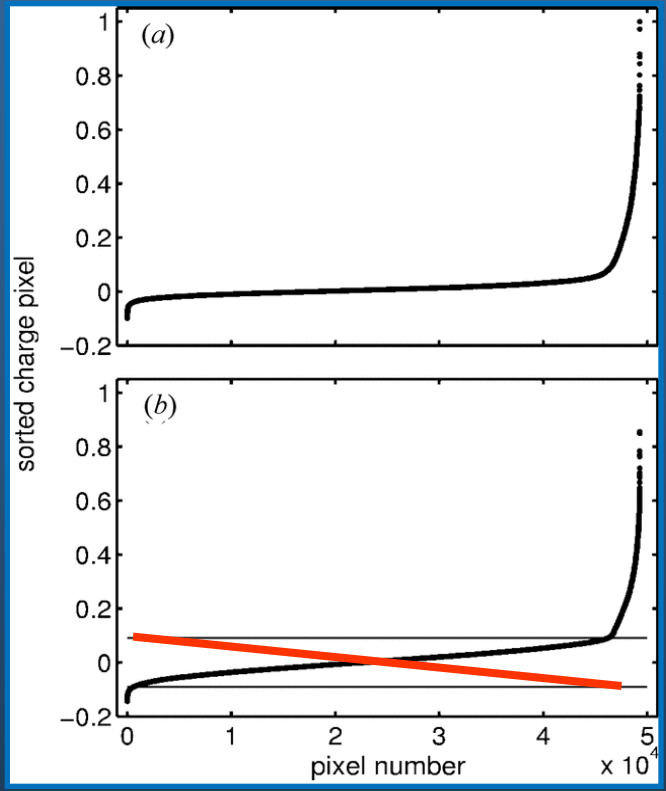

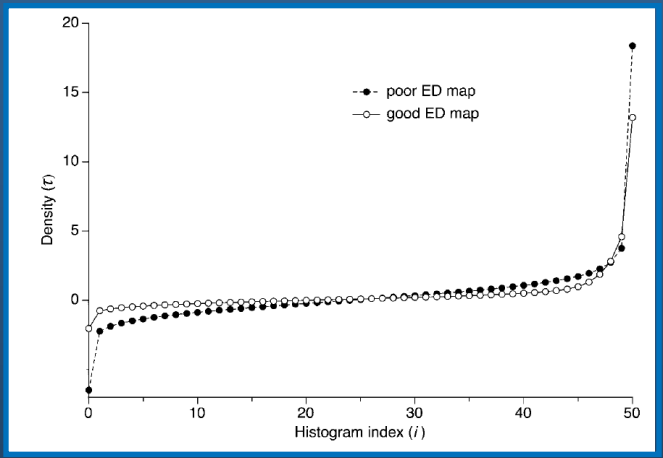

Oszlányi and Sütő Acta Cryst. (2004). A60, 134-141

Baerlocher, McCusker and Palatinus *Z.Krist.* (2007). **222** 47-53

The high temperature phases of rubidium oxalate by *in situ* powder diffraction

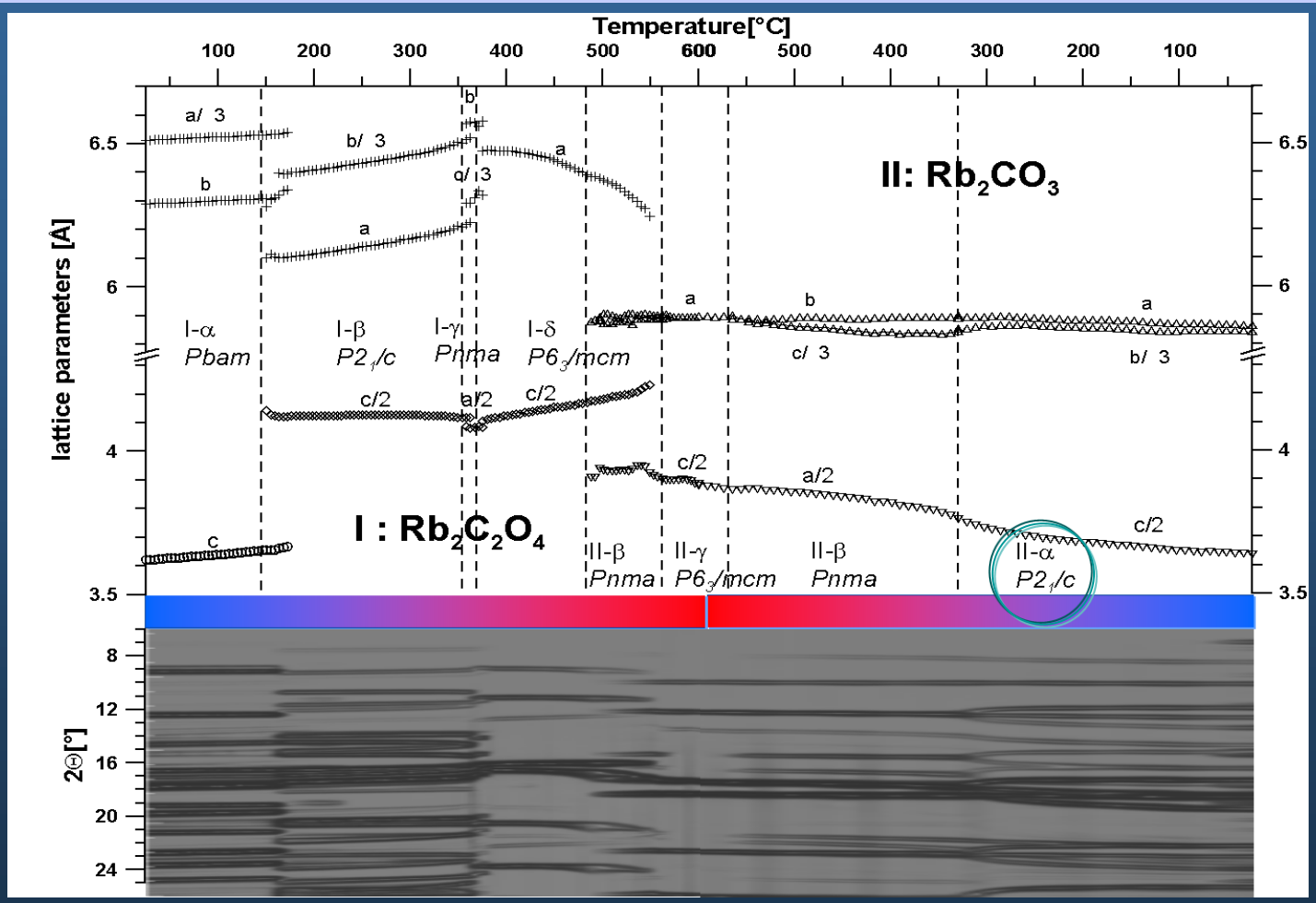

T: 25°-450°-25°

200 scans in 3½ hrs

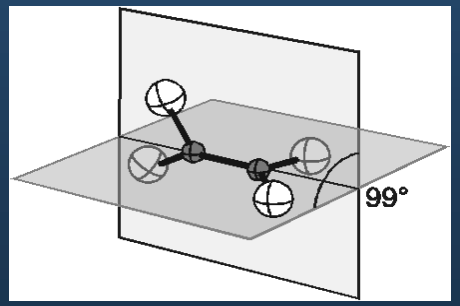

R. E. Dinnebier, S. Vensky, M. Jansen, and J. Hanson, Crystal Structures of and Topological Aspects on the High Temperature Phases and the Decomposition Products of the Alkali Oxalates $M_2[C_2O_4]$, M=(K, Rb,Cs), *2005, Chemistry, a European Journal, 11, 1119 – 1129.*

A. Samy, R. E. Dinnebier, S. van Smaalen, and M. Jansen, The Maximum Entropy Method and Charge Flipping, a powerful combination to visualize the true nature of structural disorder from *in situ* X-ray powder diffraction data. *(2010) Acta Cryt. B.*

Crystal structures of the different phases of $Rb_2C_2O_4$ and Rb_2CO_3

MAX PLANCK GESELLSCHAFT

$Rb_2C_2O_4$

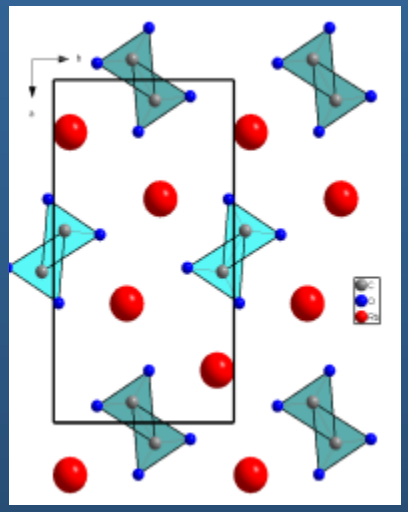

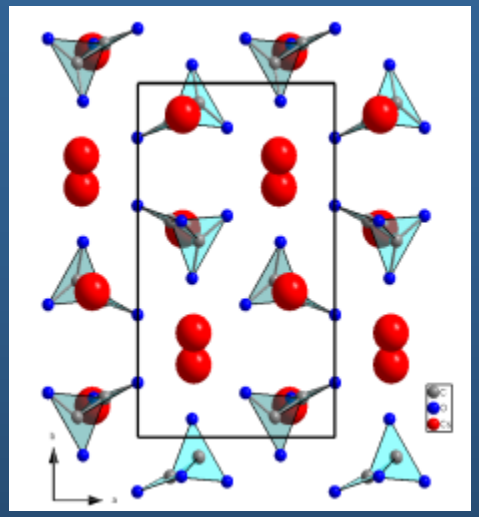

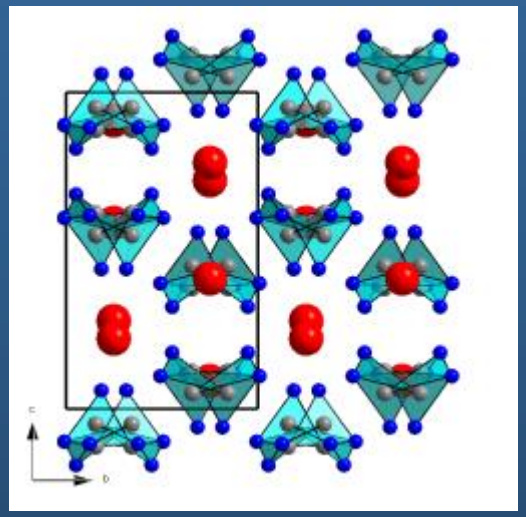

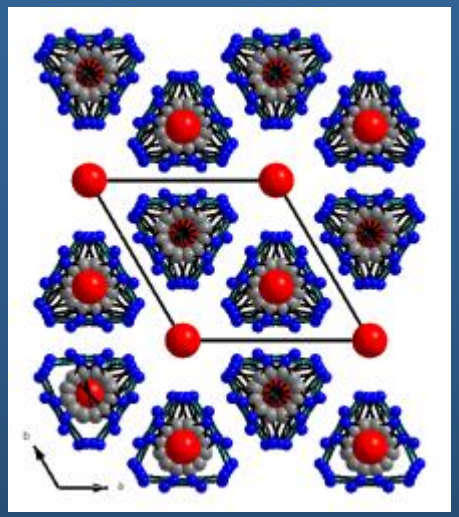

Pbam → *P21$_1$/c* ↔ *Pnma* ↔ *P6$_3$/mmc*

Rb_2CO_3

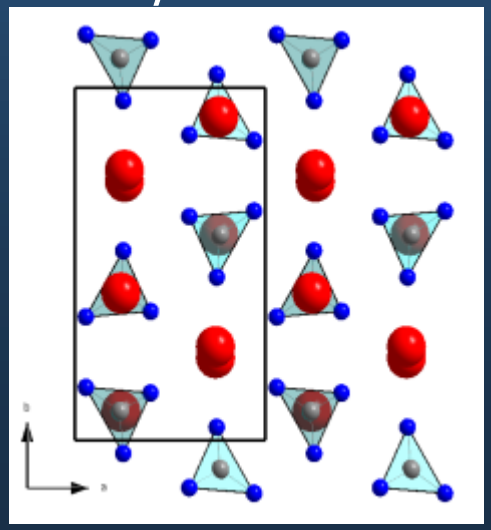

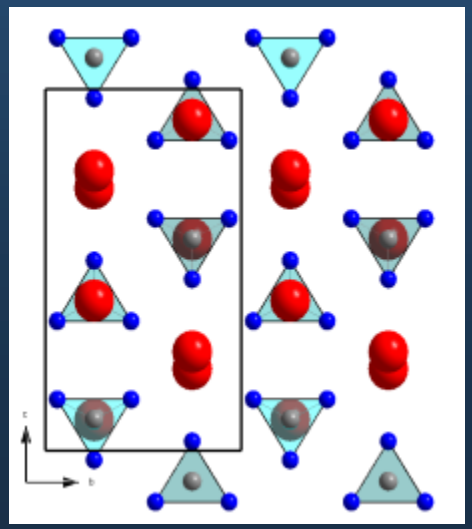

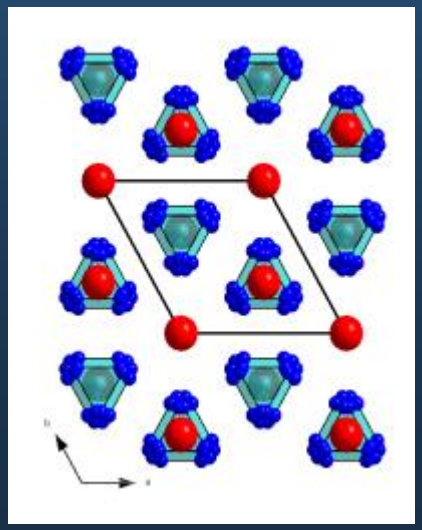

Example: Rietveld plot of α-$Rb_2C_2O_4$

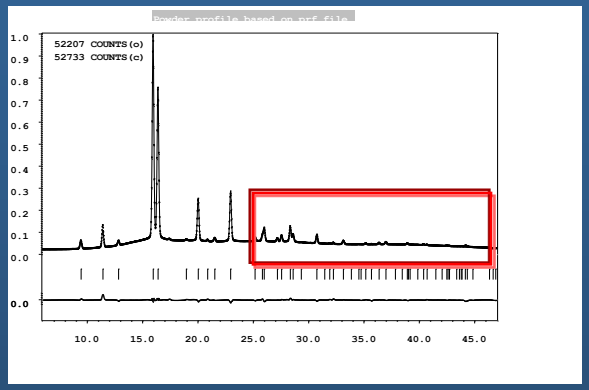

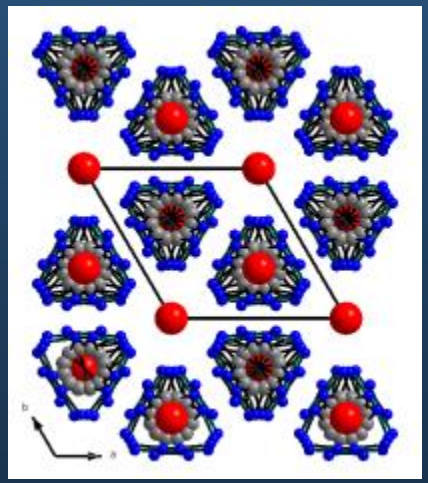

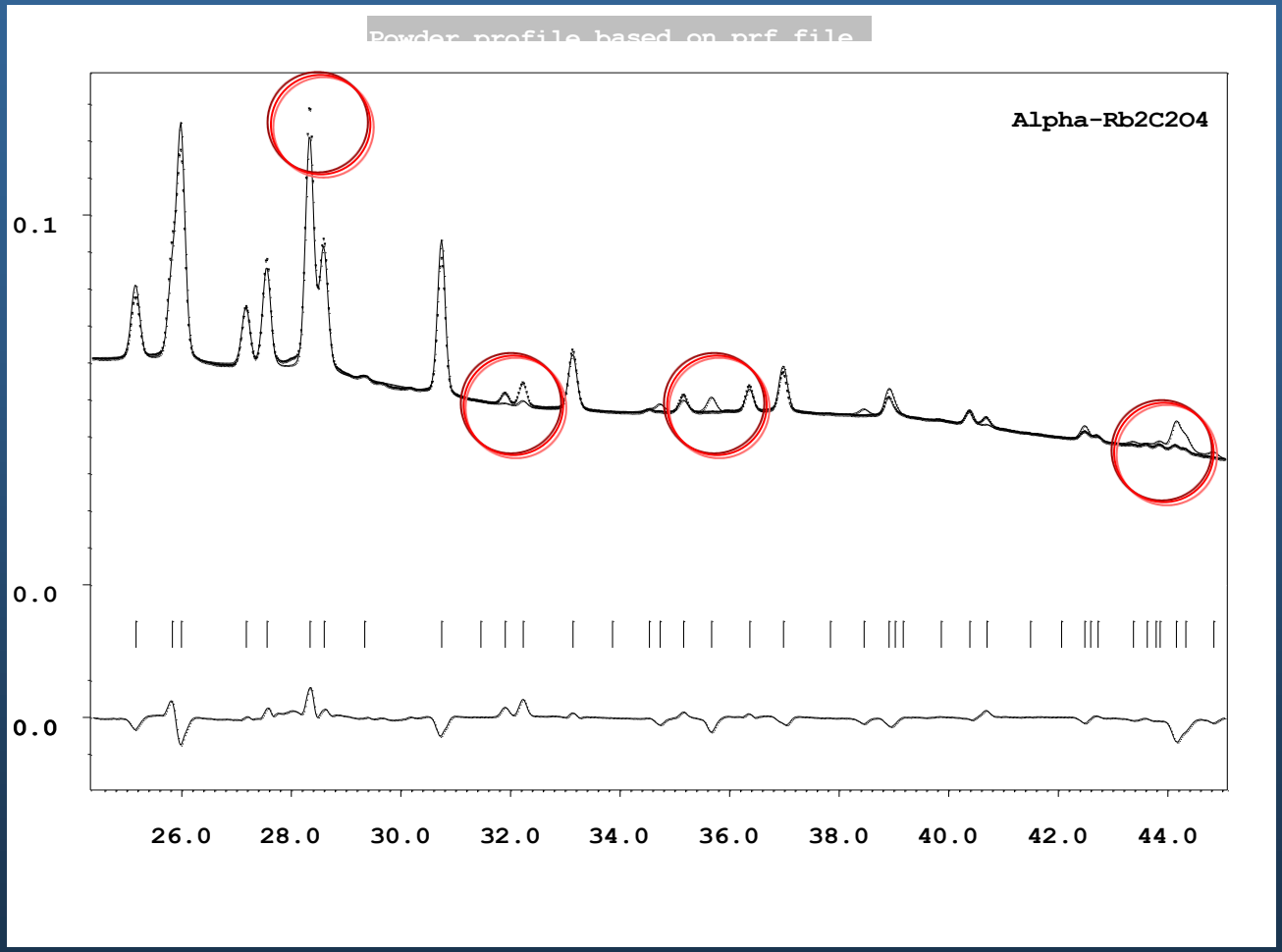

Rietveld refinement : GOF= 1.57, R_p=1.70, R_{wp}=2.77

Example: LeBail plot of α-$Rb_2C_2O_4$

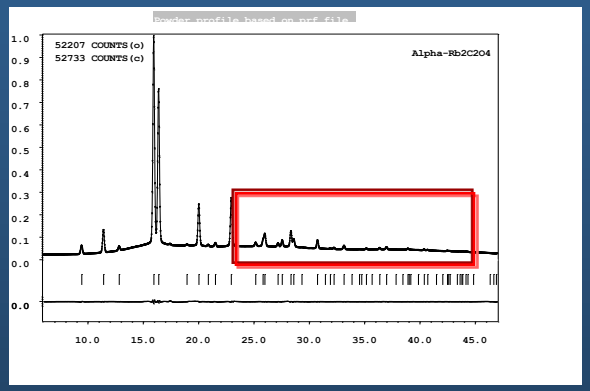

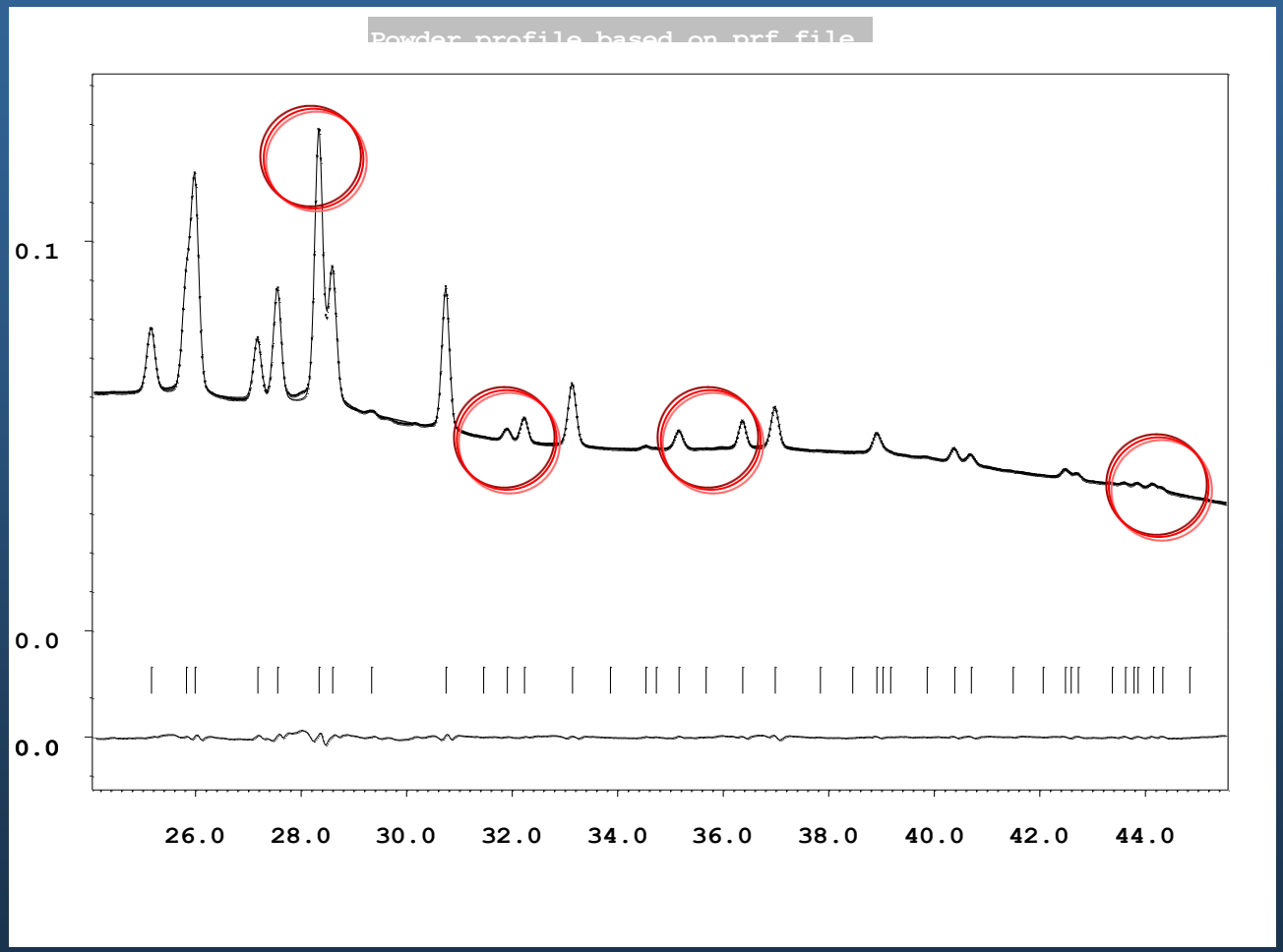

LeBail: GOF= 0.59, R_p=0.74, R_{wp}=1.03

Observed structure factors & model-biased effects

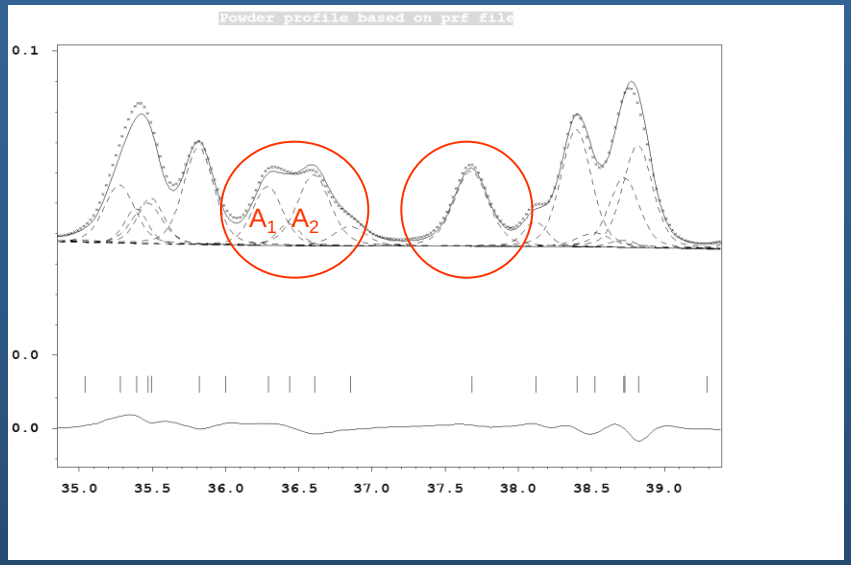

Rietveld refinement → F_{obs} -model-bias

$$A(obs)_1 = \sum_{i=1}^{n} \frac{A(calc)_1 \times q_1(i)}{A(calc)_1 \times q_1(i) + A(calc)_2 \times q_2(i)} (obs(i) - back(i))$$

$$A(obs)_2 = \sum_{i=1}^{n} \frac{A(calc)_2 \times q_2(i)}{A(calc)_1 \times q_1(i) + A(calc)_2 \times q_2(i)} (obs(i) - back(i))$$

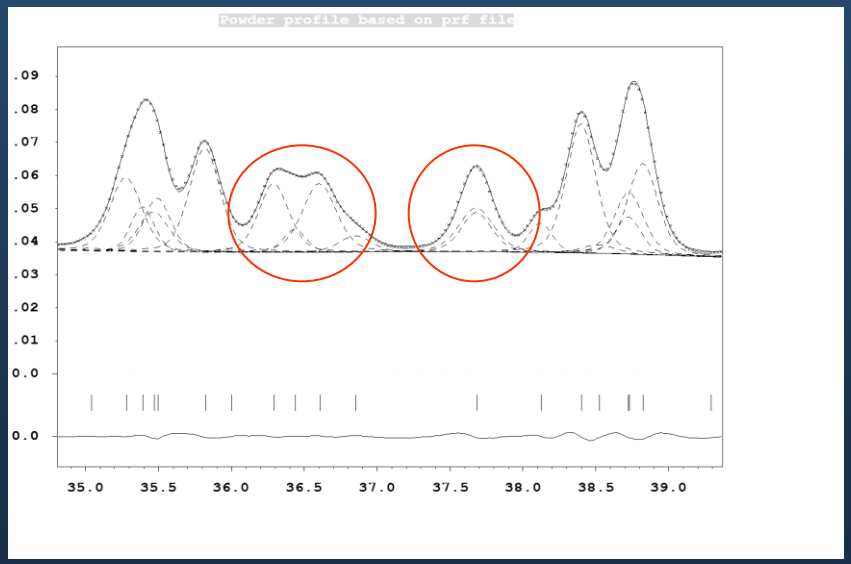

LeBail algorithm

$$A_m^{r+1}(obs) = \sum_{i=1} \frac{A^r{}_m(obs) \times q_m(i)}{\sum_{m=1}^{N} A^r{}_n(obs) \times q_n(i)} (obs(i) - back(i)), \text{ where, } A_m^{r=1} = 1, \text{ n=1,....N}$$

Ways of reconstructing the different types of electron density maps.

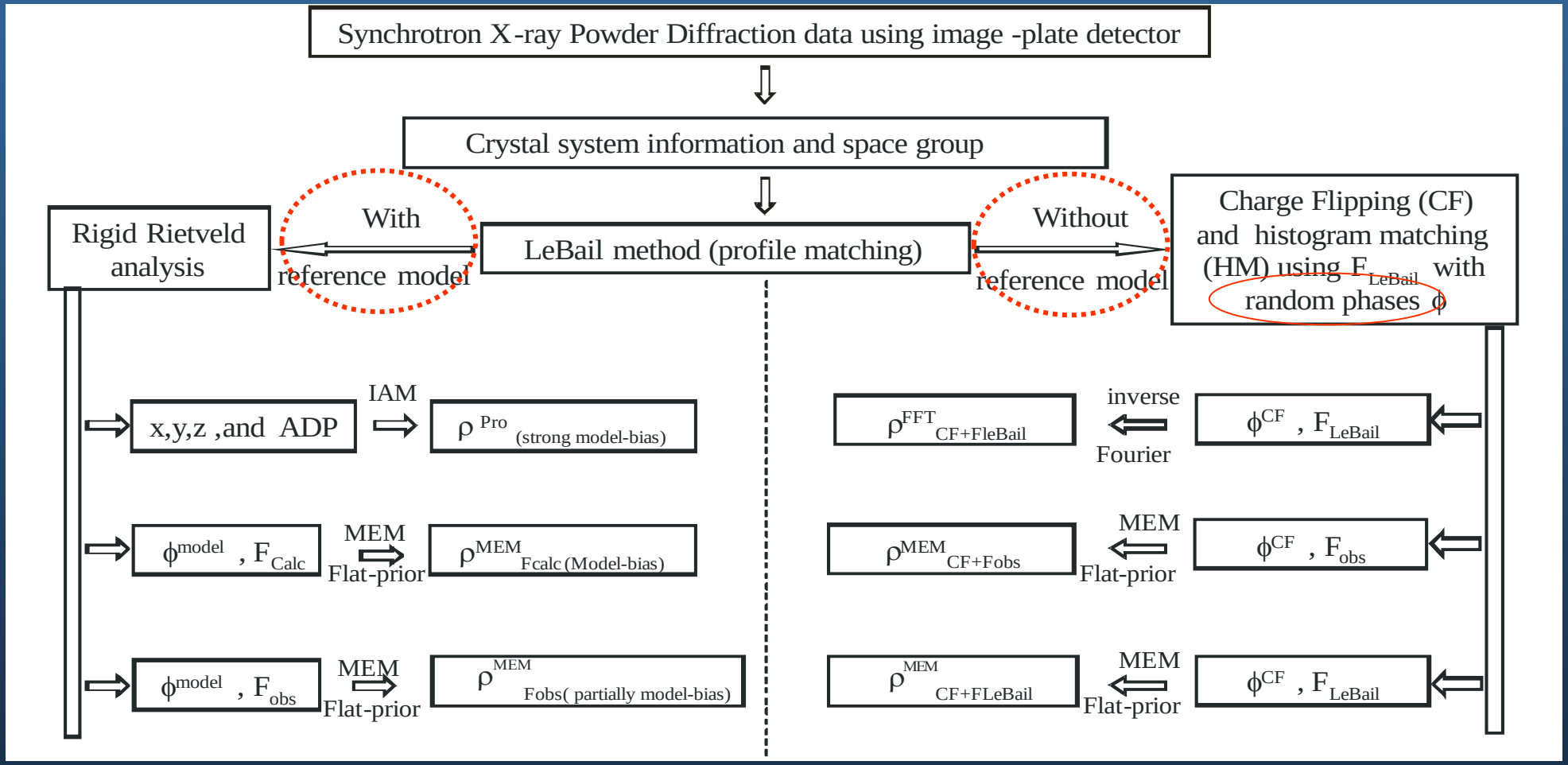

MEM algorithm: Sakata&Sato (1990); Computer programs: BayMEM, Jana, Superflip

Results of MEM-calculations based on model-Rietveld-refinement

MAX PLANCK GESELLSCHAFT

	Prior: IAM	MEM-Fcalc:	MEM-Fobs:	MEM-Fobs-G-constr.
	Strong-biased	All F biased	F_{obs} partially biased	Less biased
δ-$K_2C_2O_4$ (*Pbam*) ordered T = 295 K	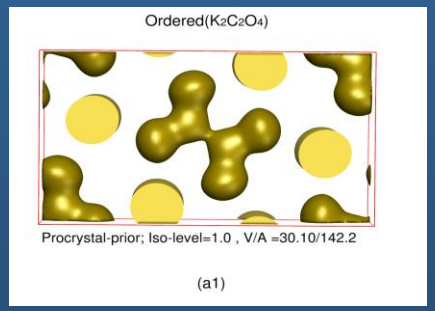	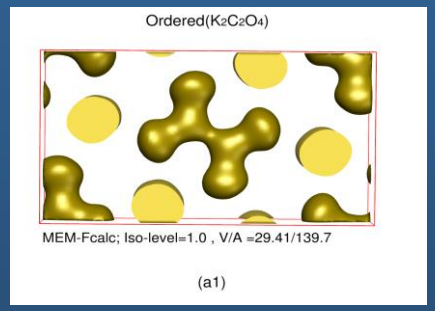	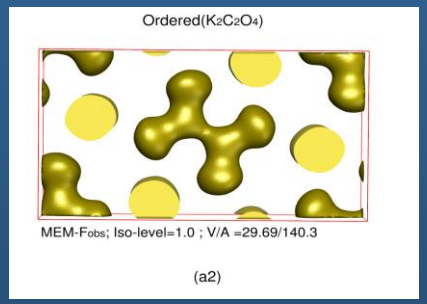	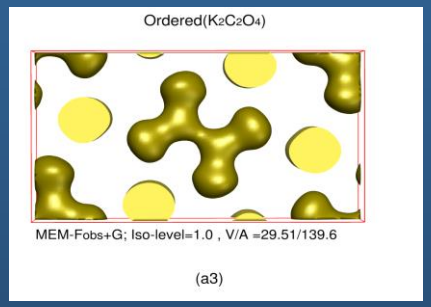
α-$Rb_2C_2O_4$ (*P6$_3$/mmc*) disordered T = 683 K	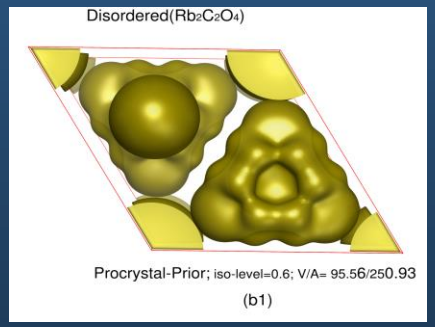	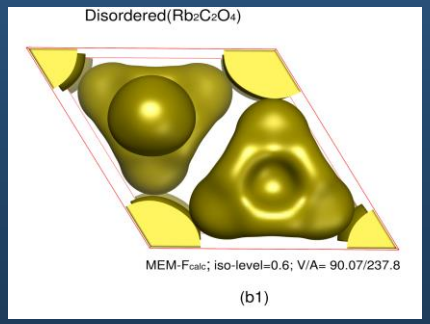	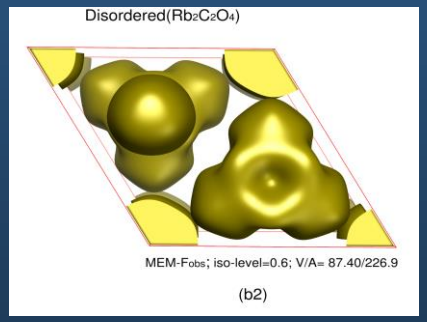	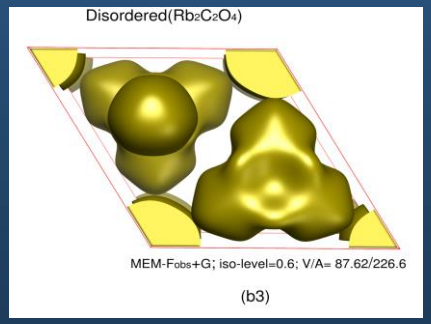
α-Rb_2CO_3 (*P6$_3$/mmc*) disordered T = 860 K	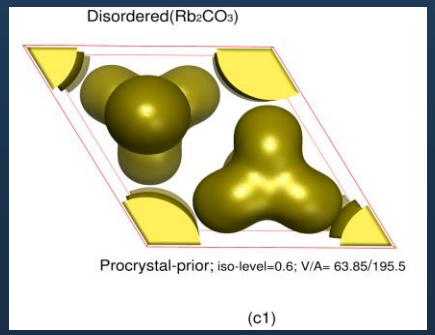	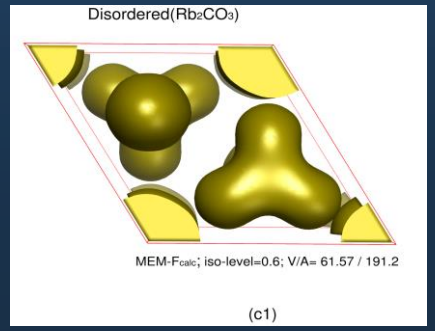	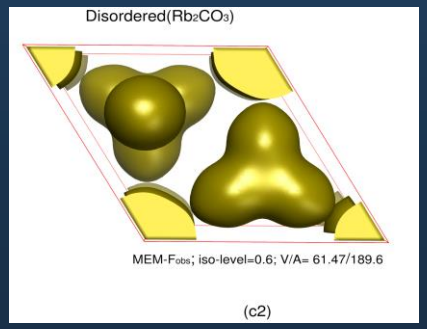	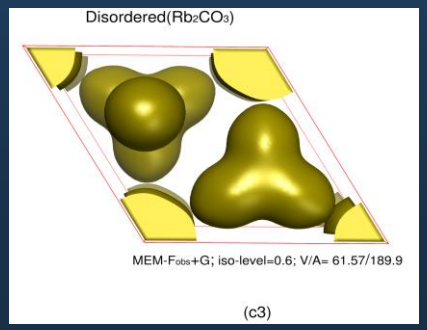

Results of the combination of MEM with phases of CF

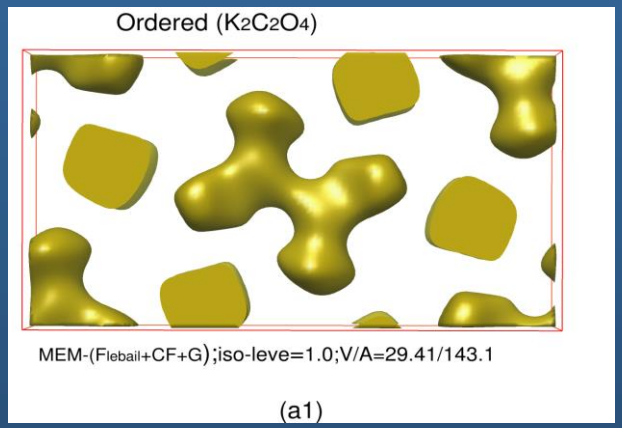

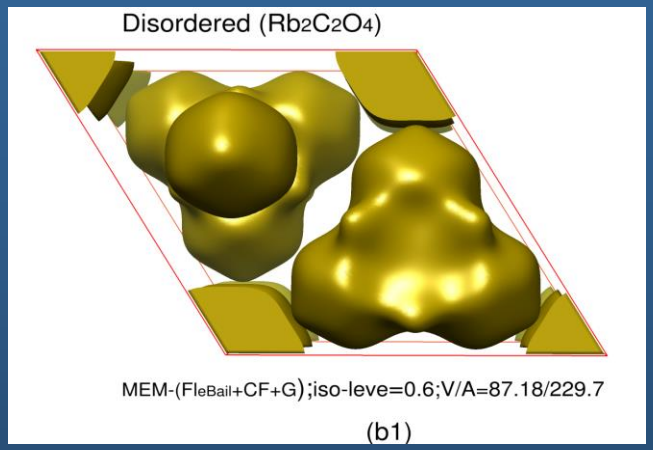

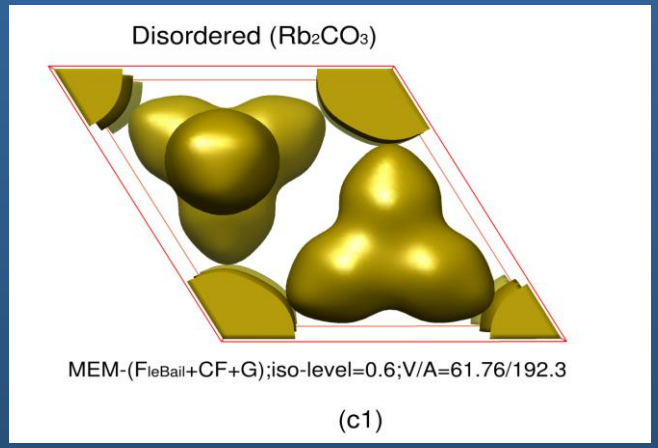

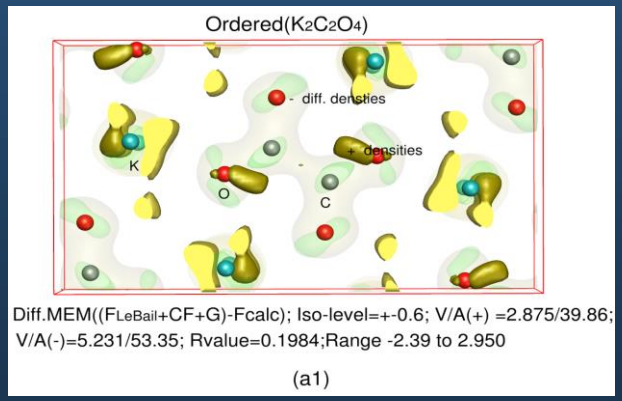

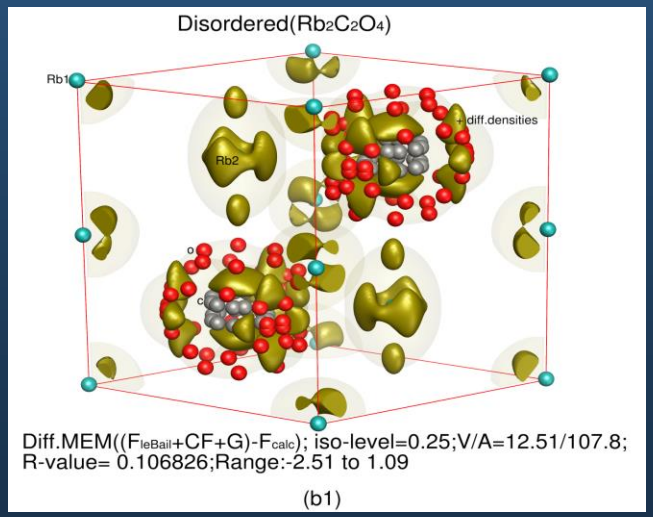

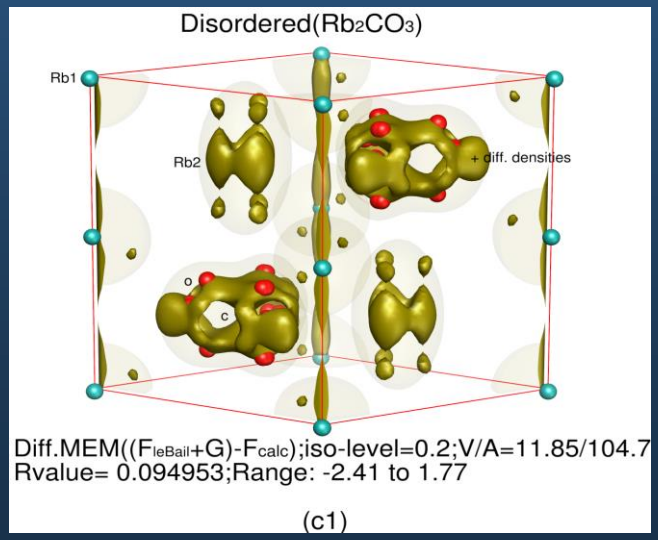

Not perfect, but a <u>powerful combination</u> to solve disordered crystal structures from powder data directly…

My view of the future
(it starts now…)

MAX PLANCK GESELLSCHAFT

- Many experiments which were only be possible at the synchrotron can now be done in the laboratory (e.g. Mo $K_{\alpha 1}$ in Debye-Scherrer geometry)
- Future Rietveld-programs: toolboxes, macros, self learning, user community
- Determination from powder data is becoming routine.
  (for small and medium sized structures).
- Parametric Rietveld refinement opens a new world
  (determination of non-structural parameters, e.g. kinetics, order parameters)
- Accurate electron density distributions using MEM method from XRPD
- Complex structure determination from powder data by the combination of CF and MEM.
- High speed (<1 s) + high resolution is now available at the synchrotron (ESRF, SLS, Petra III, Diamond, etc.)
- High pressure powder diffraction and PDF analysis in the laboratory….

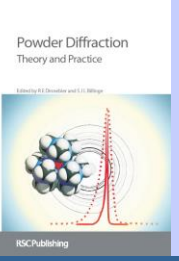

Acknowledgement

To where the money came from

MPG, FCI, BMFT

To the facilities providing beamtime

NSLS, ANKA, ESRF, APS

To collaborators

Peter Stephens (SUNY at Stony Brook), John Hanson (NSLS), Sander van Smaalen (Bayreuth), Bernd Hasse (Incoatec), Ralph Weigel (ANKA), Andy Fitch (ESRF), Haozhe Liu (APS), Branton Campbell (BYU) …

To current and former group members





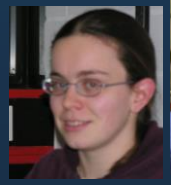






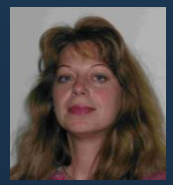
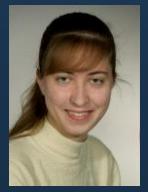

Constraints in MEM

1. Normalization of ρ to the expected number of electrons per unit cell volume (F_{000})

$$\int_V \rho dV - N_{el} = 0$$

2. F-constraints C_F with central moment *mn.* The resulting error distribution must be obeying the Gaussian distribution function

$$C_{F_n} = -1 + \frac{1}{m_n(Gauss)} \frac{1}{N_F} \sum_{i=1}^{N_F} \left(\frac{F_{obs}(\overrightarrow{H_i}) - F_{MEM}(\overrightarrow{H_i})}{\sigma(F_{obs}(\overrightarrow{H_i})} \right)^n$$

3. G-constraints, sometimes phases or even amplitudes of individual structure factors cannot be determined reliably. This is often the case for powder diffraction data, where systematic and/or accidential overlap of reflections is common.

$$G_G = -1 + \frac{1}{N_G} \sum_{i=1}^{N_G} \left(\frac{G^i{}_{obs} - G^i{}_{MEM}}{\sigma(G^i{}_{obs})} \right)^2$$

$$G^i = \sqrt{\sum_{j=1}^{N_g^i} \left[\frac{m_j}{\sum m_j} \left| F(\overrightarrow{H_j}) \right|^2 \right]}$$

Sakata & Takata, 1996

Basics of Maximum Entropy Methode (MEM)

MAX PLANCK GESELLSCHAFT

Maximize:

$$Q(\rho) = S(\rho) - \sum_{j=1}^{N_c} \lambda_j \, C_j(\rho), \quad \longrightarrow \quad \frac{\partial Q}{\partial \rho_i} = 0$$

$$\rho_i = \frac{N_{el} N_{pix}}{V} \tau_i \exp\left(-\lambda_F \frac{\partial C_F}{\partial \rho_i}\right) \Big/ \sum_{i=1}^{N_{pix}} \tau_i \exp\left(-\lambda_F \frac{\partial C_F}{\partial \rho_i}\right) \qquad (3)$$

Set of N_{pix} *nonlinear equations*

$$\tau_i^{n+1} \approx \rho_i^{n}$$

αππροξιματιονσ

ρ_i	Electron density
τ_i	Prior density
N_{pix}	no of pixels of cell volume V
N_{el}	no of electron/unit cell = F000
w	weight factor
$\sigma(H)$	standered error of F_{obs}
F_{obs}	observed structure factors
F_{MEM}	MEM structure factors
λ	Lagrange multipliers
Nc	no of constraints

Iteration:

$$\rho_i^{n+1} = \frac{N_{el} N_{pix}}{V} \rho_i^{(n)} \exp\left(-\lambda_F \frac{\partial C_F}{\partial \rho_i}\Big|_{\rho_i^{(n)}}\right) \Big/ \sum_i \rho_i^{(n)} \exp\left(-\lambda_F \frac{\partial C_F}{\partial \rho_i}\Big|_{\rho_i^{(n)}}\right)$$

Sakata & Sato algorithm (1990)

The iteration is started with $\rho_i^{(1)} = \tau_i$ and the new density $\rho_i^{(n+1)}$ is calculated from the prior density $\rho_i^{(n)}$, the value of the constraint decreases each cycle untile the condition of $C_F \leq 1$ is fulfilled

The parameters of MEM-calculations

Chemical formula	□-$K_2C_2O_4$	□-$Rb_2C_2O_4$	□-Rb_2CO_3
Number of voxels	108 □ 64 □ 36	96 □ 96 □ 108	54 □ 54 □ 72
Pixel size /Å	0.101□0.095□0.096	0.067□ 0.067 □0.076	0.109□0.109□0.108
Electrons per unit cell	164	236	208
Lagrange multiplier □	0.05	0.05	automated
Initial density	Flat-prior	Flat-prior	Flat-prior
F-constraints	86	46	42
G-constraints	9	6	4

Initial density (flat-prior)= N_{el} / N_{pix}

Algorithm: Sakata&Sato (1990)

Computer program: BayMEM (van Smaalen, 2003)

Simulated annealing and disorder

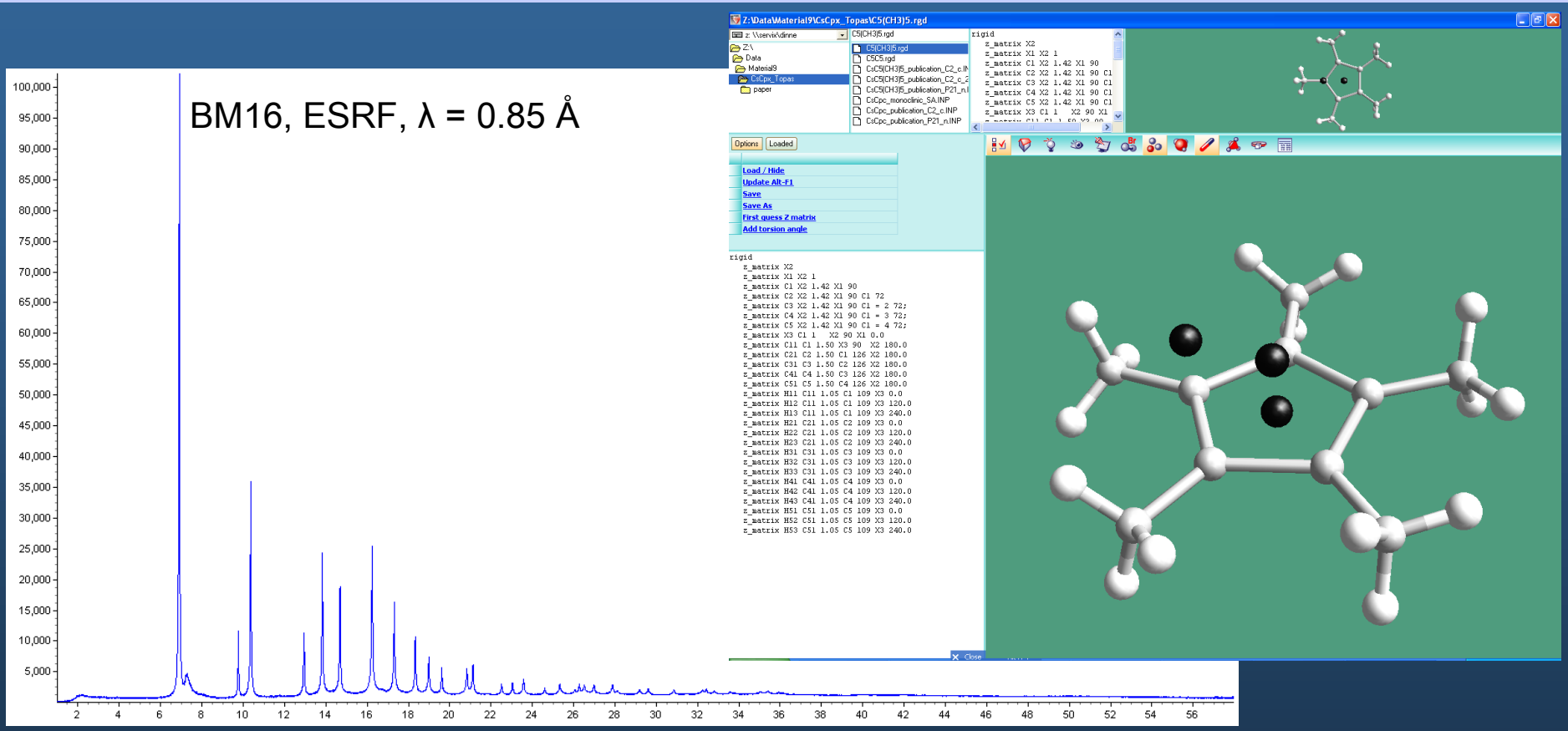

CsCp* : perfect fit in $I4_1/amd$ (a = 7.54Å, and c = 19.97 Å), but problems in solving the crystal structure (Cs at 0 0 0, Cp* (as pseudo atom) at 0 1/4 1/8 ???)

U. Behrens, R. E. Dinnebier, S. Neander, F. Olbrich, Solid State Structures of base free rubidium and cesium pentamethylcyclo-pentadienides. Determination by high Resolution Powder Diffraction, 2008, Organometallics. 27(20), 5398-5400.

10 years after the measurement ….

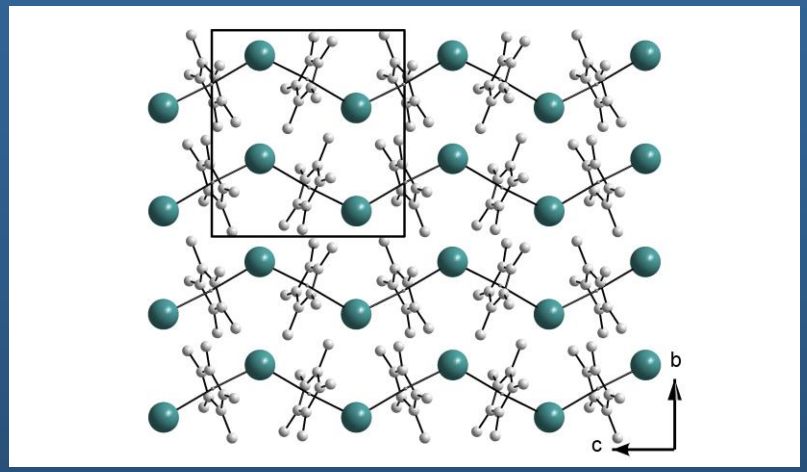

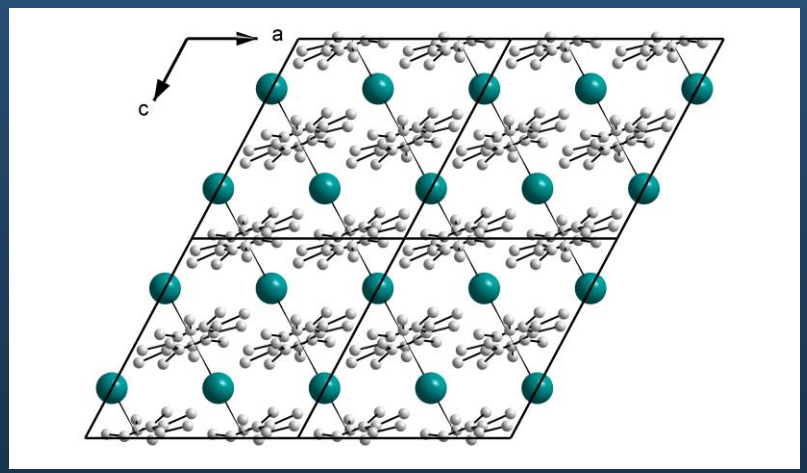

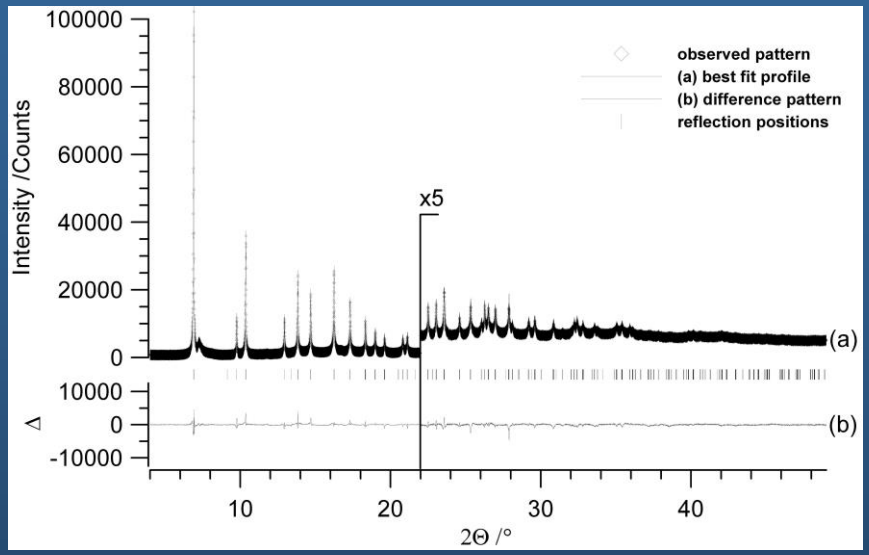

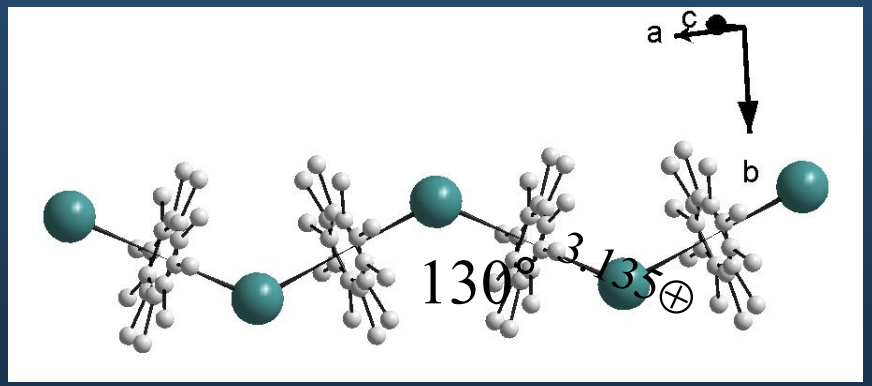

Structure determiantion „by hand“ in maximal translationengleiche subgroup *I*2/*d* (*C*2/*c*)

Optimum results for bent Cp*-Cs-Cp* chains with two-fold rotational disorder of the Cp* rings

Why tetragonal ?

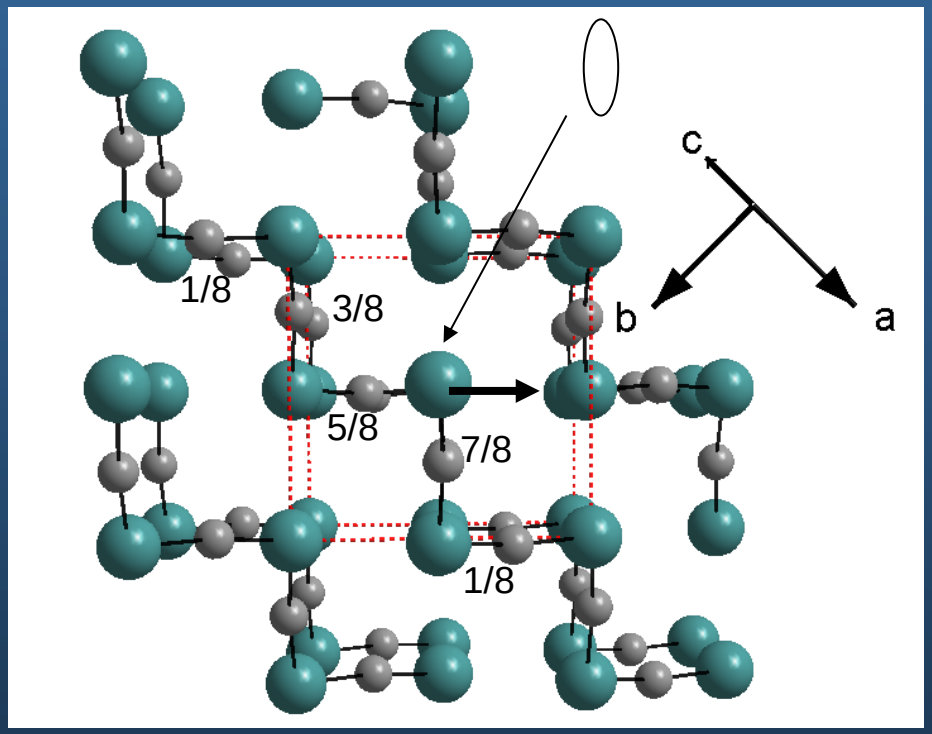

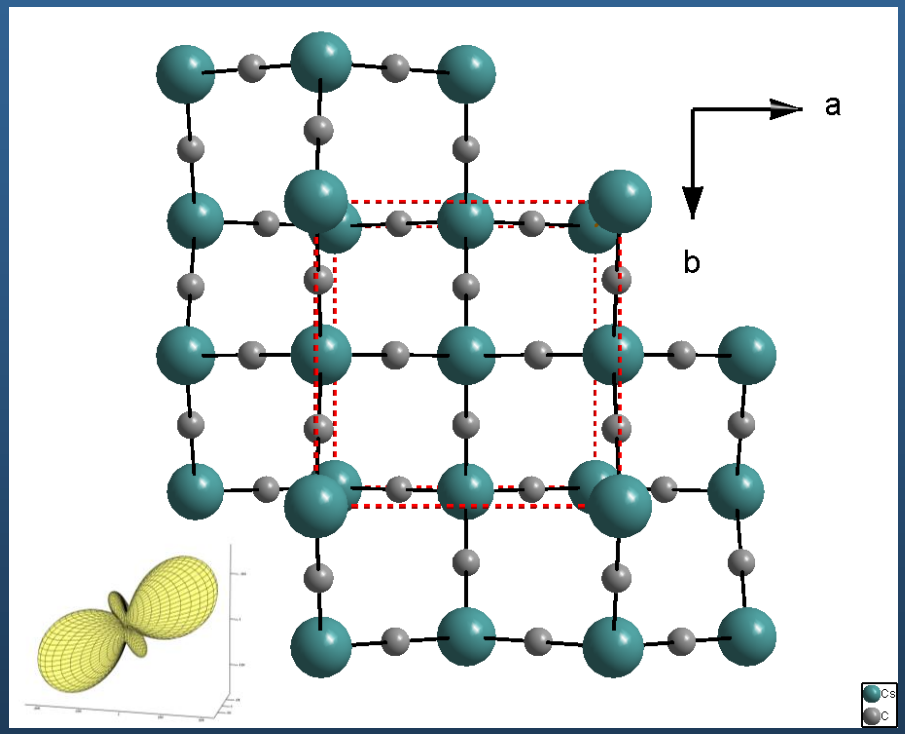

Most likely stacking faults perpendicular to the *ac*-plane lead to pseudotetragonal appearance
(supported by anisotropic microstrain broadening with the maximum “strain” occurring long the vector *a*±*c* and shape of thermal ellipsoids)

Temperature dependence of the order parameter for 2nd order phase transitions

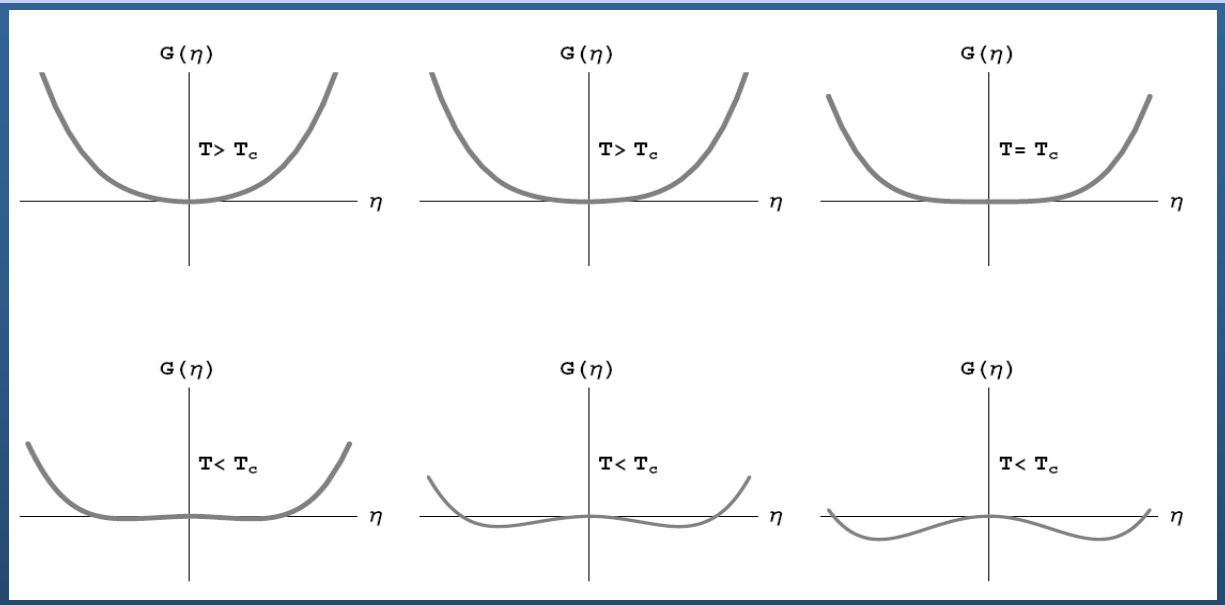

G is continuous at phase transition

→ ▪G/▪T has a kink at $T = T_c$

$T > T_c$: $\eta \rightarrow 0$ → Minimum of free energy at $\eta = 0$ → ▪ = 0; $A > 0$

$T < T_c$: $\eta > 0$ → Minimum of free energy at $\eta \neq 0$ → ▪ = 0; $A < 0$, $B(P,T) > 0$

Simplest choice: $A(P,T) = a\,(T-T_c)$

Assumption: $C = 0$

→ $G = G_0 + a(T-T_c)\eta^2 + B\eta^4$ (2-4 potential)

→ ▪G/▪η = 0 → $2a(T-T_c)\eta = -4B\eta^3$ → $\eta^2 = a/(2B)(T_c-T)$ → $\eta = c\,(T_c-T)^{1/2}$ $(T < T_c)$

→ $\eta = 0$

Temperature dependence of the order parameter for „weakly 1st order" phase transitions

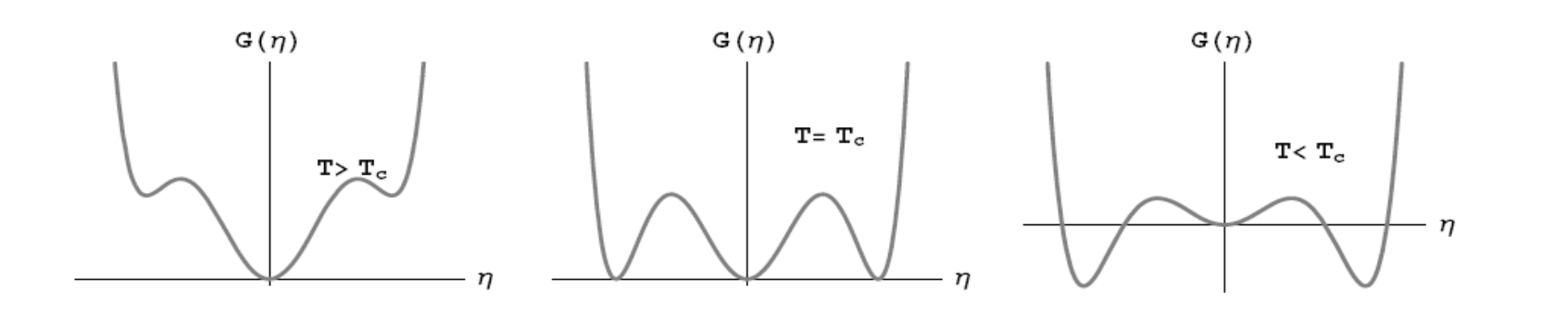

Assumption: $C = 0$ → $G(P,T) = A(P,T)\eta^2 + B(P,T)\eta^4$

Assumption: $B(P,T_c) < 0$ → higher order terms are necessary to allow for a minimum of the free energy at any finite value of η

$G = A\eta^2 + B\eta^4 + D\eta^6$ with $D > 0$

Assumption: $B = 0$

→ $G = G_0 + a(T-T_c)\eta^2 + D\eta^6$ (2-6 potential)

→ $\partial G/\partial \eta = 0$ → $2a(T-T_c)\eta = -6D\eta^5$ → $\eta^4 = a/(3D)(T_c-T)$ → $\eta = c\,(T_c-T)^{1/4}$ $(T < T_c)$

→ $\eta = 0$ $(T > T_c)$

<u>At the point where B(P,T) changes sign, a 2nd order phase transition goes over to a 1st order phase transition (tri-critical point)</u>